Analysis of acrylic polymers by MALDI-TOF mass spectrometry

Wyatt, Mark Francis

Analysis of Acrylic Polymers by MALDI-TOF Mass Spectrometry

Mark Francis Wyatt

Graduate Society

A thesis submitted in partial fulfilment of the requirements for the degree of Doctor of Philosophy

Department of Chemistry

University of Durham

2001

Analysis of Acrylic Polymers by MALDI-TOF Mass Spectrometry

Abstract

Poly(methyl methacrylate) (PMMA) homopolymers synthesised using '*classical*' anionic methods and subsequently studied by matrix-assisted laser desorption/ionisation time-of-flight mass spectrometry (MALDI-TOF-MS) are discussed. Specifically, the attempts at different end-group functionalisation reactions, their varying degrees of success, and the characterisation of these functionalised polymers via MALDI are reported. Extra peaks were observed in the spectra of samples containing a tertiary amine end-group. A mechanism for the *in situ* elimination of $H_2(g)$ involving these end-groups, which would fit the observations, is proposed.

Two alternative, *'non-classical'* routes to the desired materials were investigated, as difficulties in successfully performing capping reactions to give end-functionalised PMMA were noted. The first method was a variation of standard anionic polymerisation that involved the use of lithium silanolates, which could be performed at a higher temperature than normal. The second was a controlled free-radical technique known as Reversible Addition-Fragmentation Chain Transfer (RAFT). A lack of control of the polymerisation to the desired degree was observed with the former method. A well-defined RAFT sample was observed to undergo *in situ* elimination also, for which a mechanism involving the dithioester end-group is proposed, and which is supported by MALDI-collision induced dissociation (CID) evidence.

The synthesis of block copolymers of various compositions of MMA with *t*-butyl methacrylate (*t*-BMA) and hexyl methacrylate (HMA), along with their homopolymers, and their subsequent characterisation is reported. PHMA was analysed easily, in contrast to P*t*-BMA. Only copolymers with a high PMMA content were analysed successfully and this has been rationalised in terms of the factors that affect cationisation.

The characterisation of equimolar blends of various end-functionalised PMMA samples is reported also. Samples that favour the binding of a metal ion over protonation appear to have a higher ion yield. Once more, these observations are rationalised in terms of the factors that affect cationisation.

Memorandum

The work described in this thesis was carried out in the Interdisciplinary Research Centre in Polymer Science and Technology, the University of Durham, between October 1998 and July 2001. This work has not been submitted for any other degree and is the original work of the author, except where acknowledged by reference.

Aspects of this work have been presented by the author at the MacroGroup Young Researchers Meeting as part of the Royal Society of Chemistry Annual Conference, UMIST, Manchester, April 2000, and at the MacroGroup Young Researchers Meeting, University of Strathclyde, Glasgow, April 2001.

Statement of Copyright

Acknowledgments

First and foremost, I would like to thank my academic supervisor Prof. Randal Richards and my industrial supervisor Dr. Anthony Jackson for their support, help and guidance during my time here in Durham. I would also like to take this opportunity to express my thanks to EPSRC and ICI Technology for their financial support of this project.

I am grateful to my colleagues both in the IRC and the Chemistry Department for their advice, friendship and good humour. Special thanks go Dr. Lian Hutchings for his help in all matters concerning polymer synthesis and to the members of the Durham NMR service, Dr. Alan Kenwright, Ian McKeag and Catherine Heffernan. I would like to thank Douglas Carswell and Andrew Bosanko for recording SEC data, and to Richard Tyldsley at Micromass, UK, for collecting the MALDI-CID data. Many thanks must go also to Dr. Dave Parker, for many helpful discussions about MALDI and much humorous banter. Indeed, humorous banter has been enjoyed on many occasions during my time in Durham, particularly with Dr. Stuart 'shotgun humour' Reynolds, Simon Aldersley, Alison Stoddart, Dr. Wilfried Lövenich, Mark O'Halloran, Dr. Helen Birkett, Dr. Aline Miller, Alistair Reid, Lisa Wylie, Kelly Flook, Dr. Andreas Kilbinger, Dr. Oliver Henze, Dr. Richard Thompson, Dr. James Cook, Dr. Julian Bent, Dr. Zaijun Lu, Dr. Michelle Coote, Dr. Toine Biemans and all the members of GSAFC. An acknowledgements section of mine would not be complete without a mention of Gérard Houllier, for taking Liverpool F.C. to an unimaginable five trophies in six months, and his contribution to this work should not be underestimated.

I would like to thank my family for all their support and for allowing me the freedom to make my own choices in this world. Finally, I would like to express my warmest gratitude to my partner Suzy, for all the love, support, help and advice (and nagging!) that has seen me complete this project. There are no words to accurately describe the joy that she has brought to my life, but it is deeply appreciated.

Contents

Chapter 1

Introduction

1.1 Research Aims

The focus of this research project was the investigation of the matrix-assisted laser desorption/ionisation time-of-flight (MALDI-TOF) mass spectrometry technique, applied to low molecular weight, functionalised, polymers and copolymers of methyl methacrylate (MMA). The aim being to extend the range of acrylic polymers and copolymers that may be characterised, to provide end-group and molecular weight information.

Acrylic polymers are a very important class of commercial polymer, particularly poly(methyl methacrylate) (PMMA), *e.g.* paints, sheet plastic and surfactants, and polymers with chain-end functional groups can be extremely useful. Not only can these functional groups terminate a polymerisation to form a functional polymer, but they can also participate in several reactions, such as chain extension or branching with polyfunctional reagents, coupling and linking with reactive groups on other chains, and the initiation of polymerisation of other monomers. Thus, a greater understanding of the MALDI analytical technique, and its application to acrylic polymers, would be of great use to both industry and academia. Furthermore, there have been few investigations of copolymer systems by MALDI.

The remainder of this chapter provides background information on the MALDI technique, from its conception through to sample preparation issues, and an outline of the work to date concerning PMMA. Controlled anionic polymerisation and its application to PMMA will also be described.

1.2 Background to MALDI-TOF Mass Spectrometry

MALDI-TOF-MS, along with electrospray ionisation (ESI), has become a very important and highly investigated technique for polymer analysis in recent years. It was the work of Karas and Hillenkamp,[1] and later with Chait and Beavis,[2] in the late eighties that established the technique, initially for the analysis of biomolecules, and subsequently applied it to synthetic polymers.[3] This technique was developed because conventional forms of mass spectrometry were of little use for biomolecules with high molecular weights, due to the fact that their conversion to ions in the gas phase was difficult to achieve, because such large molecules are extremely non-volatile.

Following more than two decades of systematic attempts to generate ions of organic molecules with lasers, two principles evolved,[2] which are summarised below. The first was that efficient, controllable energy transfer to the sample required resonant absorption by the molecule at the laser wavelength. As a consequence, far-UV and far-IR radiation gave the best results, due to coupling to electronic and vibrational states respectively. Secondly, the energy must be transferred as fast as possible to avoid thermal decomposition of thermally labile molecules. With resonant desorption, mass limitation of ~1000 atomic mass units (amu) for biopolymers and ~9000 amu for synthetic polymers was encountered. This limit was thought to result primarily from the requirement that energy transfer to the analyte needed to be controllable and non-explosive, resulted in energy transfer into photodissociation channels. For non-resonant desorption, the necessary irradiation was very close to the onset of plasma generation, which also destroys large organic molecules. The breakthrough came when it was realised that the use of a matrix could circumvent this problem.[4]

The improved technique involves mixing the compound to be analysed with a matrix, usually a small, solid, organic compound, having a strong absorption at the laser wavelength.[1] In this way, efficient and controllable energy transfer is retained, while the analyte molecules are spared from excessive energy that would lead to their decomposition. The laser then irradiates the sample spot and this induces a large amount of energy accumulation in the condensed phase, through excitation of the matrix molecules. This then causes both matrix and analyte to be desorbed and ionised, with the ions being formed by either proton transfer from the photoexcited matrix (shown in Figure 1.2.1), or by cationisation via an added salt.

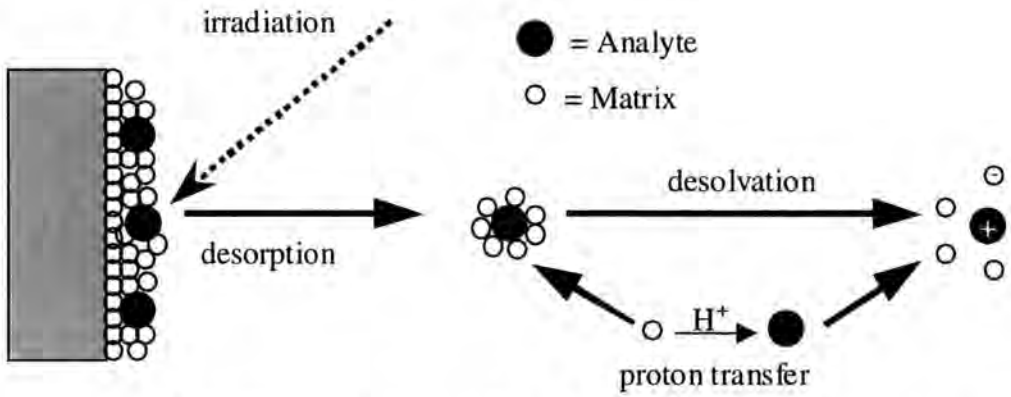

Figure 1.2.1. General scheme of the desorption/ionisation process.

Quite often for synthetic polymers, a salt is added to promote ionisation. Two modes of ionisation involving salts are possible; i) the direct cationisation of the analyte by metal cations from the salt, and ii) cationisation of the matrix by the metal cations, followed by transfer of charge to the analyte.

There are several advantages to this method:

a) The number of matrix molecules greatly exceeds those of the sample, thus separating the sample molecules and thereby preventing the formation of sample clusters, which inhibit the appearance of molecule ions.
b) It is no longer necessary to adjust the wavelength of the laser to match the absorption frequency of each analyte.
c) It is now possible for macromolecules with molecular masses up to 1.5 million amu[5] to be desorbed and ionised, since the process is independent of both the absorption properties and the size of the analyte.
d) The sensitivity is highly increased and there is little or no fragmentation.

A laser pulse width is in the 1-100 nanoseconds (ns) range, and is approximately 3 ns for the N_2 lasers that are typically used, due to their cheapness and relatively low maintenance. Given this short duration and the fact that laser beams can easily be focused to spot sizes, typically ~100 μm for a N_2 laser, that are small compared to the other dimensions of the source, the ions are generated at a point source in space and time. It is this pulse feature that makes MALDI ideally suited to be combined with TOF mass spectrometers, which are also pulsed. TOF mass analysis uses the velocity of an ion in order to determine its mass-to-charge ratio (m/z). A packet of ions is accelerated to a fixed kinetic energy by an electric potential. The ions are then allowed to pass through a field-free region (drift tube) where they separate into a series of spatially discrete ion packets, each travelling with a velocity characteristic of its mass-to-charge ratio.

The relationship between mass, charge, potential difference (V_0) and ion velocity (v) is shown below in Equation 1.2.1.

$$v = \sqrt{\frac{2zV_0}{m}} \qquad \textbf{Eqn 1.2.1}$$

When V_0 is constant with respect to all ions, the smaller the *m/z* value (lighter ions for a given value of *z*), the shorter the flight time, and the quicker they reach the detector. Conversely, the larger the *m/z* value (heavier ions for a given value of *z*), the longer the flight time. Due to the fact that the flight time (*t*) is equal to ratio of drift tube length-to-ion velocity (*L/v*), a relationship between *t* and *m/z* can be derived, as shown in Equation 1.2.2.

$$\frac{m}{z} = \frac{2V_0 t^2}{L^2} \qquad \textbf{Eqn 1.2.2}$$

Therefore, *m/z* can be calculated from t^2 and, in theory, there is no mass limit for a time-of-flight analyser.

Finally, how does a stream of ions become a spectrum? To begin with, once the ions are formed, they are accelerated and pass down a field-free region and are detected. Microchannel plate detectors (MCP), based on electron multipliers, are most frequently used in MALDI-TOF spectrometers. The high-mass ions are converted into low-mass ions or electrons at an electrode, and in order to keep a constant ion flight pathlength across the whole detector surface, the electrode should be relatively flat and mounted at exactly 90° to the ion trajectory. The yield of secondary charged particles from the conversion electrode is a function of the velocity of the ions to be detected.[6] The secondary charged particles are used to start an electron cascade in an electron multiplier, and the signal is further increased with an amplifier. High-fidelity of the detector signal is important for mass accuracy and the digitised data from successive laser shots can be summed, resulting in a TOF mass spectrum. Multiple shots are used to improve the signal-to-noise ratio and the peak shapes, thereby increasing the accuracy of the mass determination.

1.3 Linear and Reflectron Modes

MALDI-TOF-MS can be run in two modes, the first of these being linear mode,[7] which is illustrated in Figure 1.3.1. This instrumental configuration is the more basic in design, and therefore cheaper. Linear instruments are also lower in terms of mass accuracy and resolution, although higher in sensitivity, and it is these three important parameters that are used to evaluate and compare the performance of different

instrumental configurations. Mass accuracy is a measure of the error involved in assigning a mass to a given ion signal. It is expressed as the mass assignment error divided by the actual ion mass, and is often quoted as a percentage, but more commonly in ppm. Mass resolution ($m/\Delta m$) is a measure of the instrument's capability to produce separate signals from ions of similar mass. It is expressed as the mass (m) of a given ion signal divided by the full width at half height of that signal (Δm). In practical terms, mass resolution is the width of the signal observed for a single ion species. Contributions to signal width come from the production time for the ions, the initial velocity distribution, extraction time and space-charge effects.

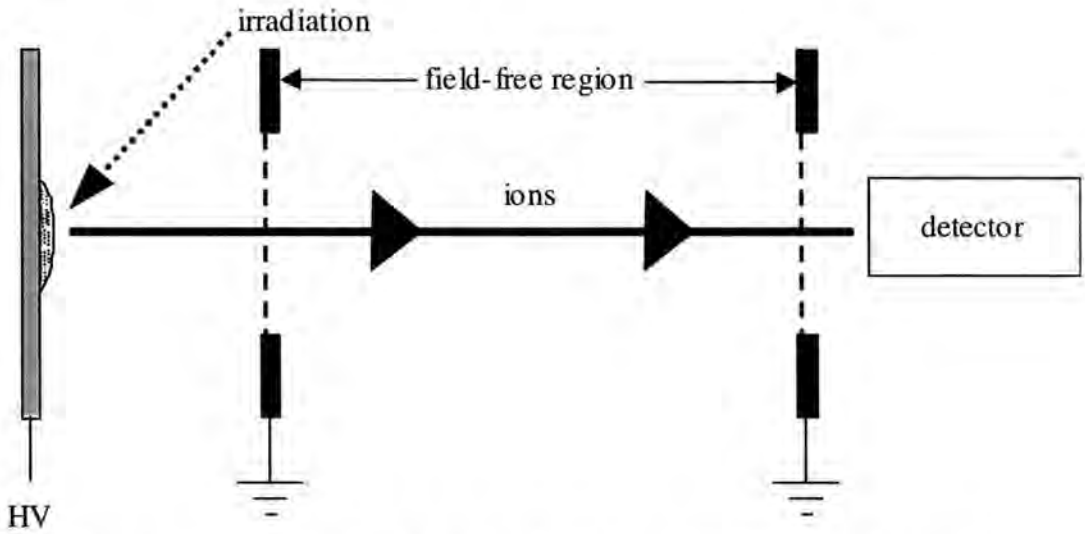

Figure 1.3.1. General scheme for the linear MALDI operating mode.

Running MALDI-TOF-MS in its other mode, known as reflectron mode can reduce the broadening caused by the initial velocity distribution, though not all instruments have this capability. A reflectron is the common term for an ion mirror and was first proposed by Mamyrin and co-workers.[8] The mirror is placed in the path of the ion packets, as shown in Figure 1.3.2. Some instruments have a linear ion path for reflectron mode, so ions are reflected through ~180° towards the detector. Providing that the mirror electrode voltages are arranged appropriately, the peak width contribution from the initial velocity distribution can be largely corrected for at the plane of the detector. The correction leads to an increase in resolution for all stable ions in the spectrum, *i.e.* those ions that do not dissociate in flight. Mass accuracy is also increased, but sensitivity is lowered, hence there is a trade-off between the two modes of operation with regard to the three main parameters.

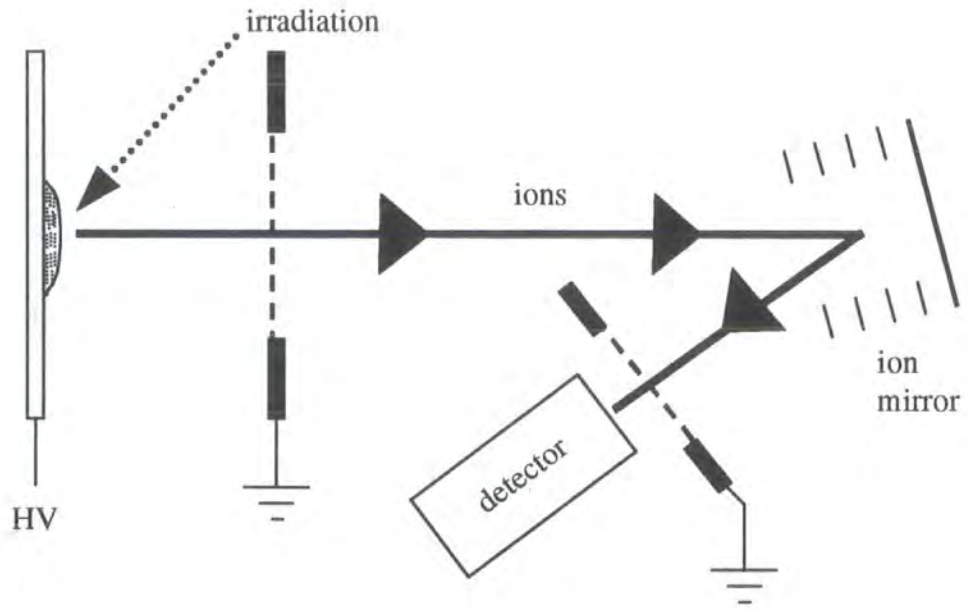

Figure 1.3.2. General scheme for the linear MALDI reflectron mode.

A full simple schematic of a MALDI instrumentation set-up is shown below in Figure 1.3.3.

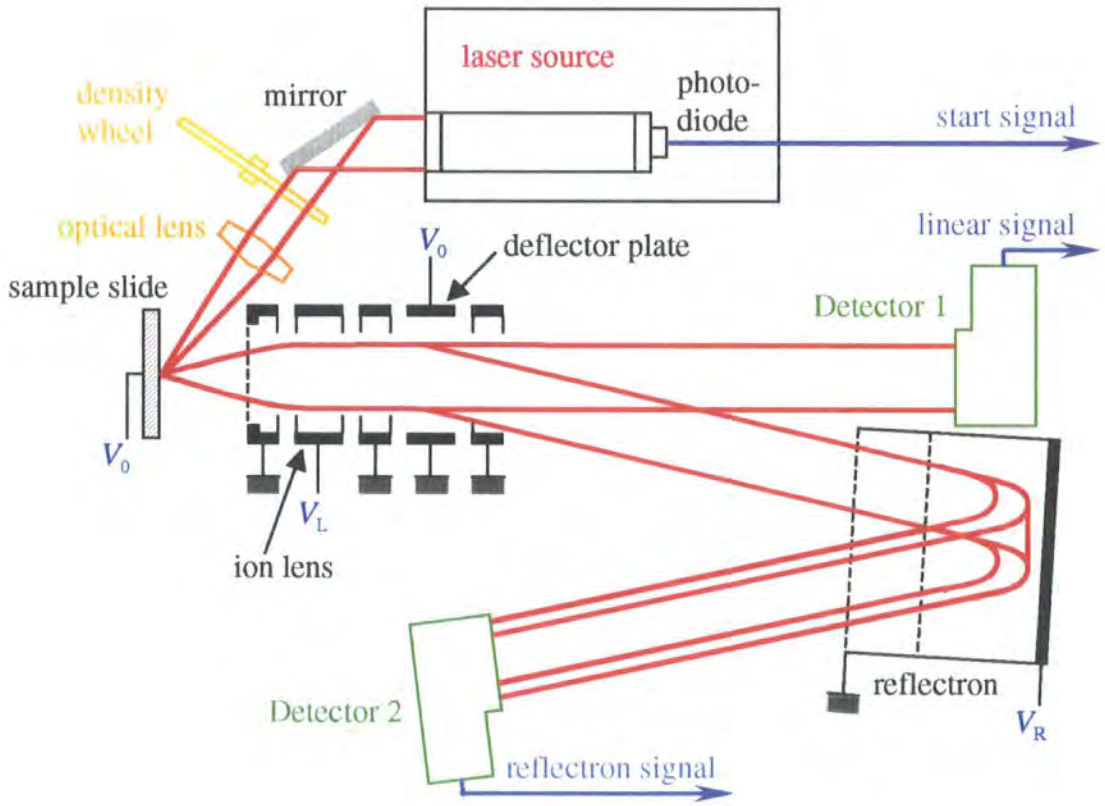

Figure 1.3.3. General schematic of a MALDI mass spectrometer.

1.4 Technical Advances

One of the most important technical advances, along with the reflectron, was the incorporation of pulsed extraction into the instrumental set-up. Pulsed extraction is a combination of two techniques, time-lag focusing, otherwise known as delayed extraction, and two-stage extraction. It essentially corrects for the initial kinetic energy and spatial distributions that ions of the same mass have upon their formation.

The principles behind time-lag focusing were originally proposed by Wiley and McLaren in 1955[9] and were applied to MALDI-MS in 1990.[10] A time delay, usually in the order of a few hundred nanoseconds, is introduced between the formation and extraction of the ions. During the delay, the ions rearrange themselves according to their initial kinetic energies, while retaining their spatial distribution. When the ions are extracted, those that have higher kinetic energies will gain less energy from the extraction field, with the result being kinetic energy focusing. Two-stage extraction compensates for the spatial distribution, by the application of a low voltage pulse that focuses ions before they are extracted.[11]

The overall result of pulsed extraction is to provide much greater resolution, mass accuracy and signal-to-noise ratio for the data acquired. As a result, resolution became so good that different species of low molecular weight polymer could be differentiated, meaning that end-group structure could be inferred from the mass values. Isotopic resolution at very low molecular weights (typically < 5000 amu) meant that polymer end-groups could be determined with reasonable accuracy, especially when used in a complimentary fashion to NMR.

Another important advance, which has become particularly useful in determining polymer end-groups and backbone architecture, was the introduction of MALDI collision-induced dissociation (MALDI-CID). MALDI-CID is basically tandem mass spectrometry (MS-MS) with a MALDI source, usually with a quadrupole[12] or an EBE (electrostatic-magnetic-electrostatic geometry) triple sector[13] as the first mass analyser and a TOF analyser as the second. Ions are selected by the first mass analyser and focussed into a collision cell, where they collide with an inert gas, i.e. xenon. Fragmentation occurs and the fragment ions that leave the collision cell are focussed into the TOF analyser, which records the full product ion spectrum. Detailed information about individual end-groups was now available because the fragment series

observed were derived from either end of the chain. Specific references with regard to the analysis of PMMA via MALDI-CID are given later in Section 1.6.

1.5 Matrices and Sample Preparation

The choices of matrix and sample preparation method are extremely important in the acquisition of good quality spectra. The most commonly used matrices are sinapinic acid, 2,5-dihydroxybenzoic acid (DHB), *trans*-3-indoleacrylic acid (IAA), *all-trans*-retinoic acid, α-cyano-4-hydroxy-cinnamic acid and 1,8,9-trihydroxyanthracene (dithranol).

The most commonly employed method of sample deposition onto the sample target is the dried droplet technique. This is summarised in Figure 1.5.1 and involves mixing together solutions of analyte, matrix and salt, such as an alkali metal halide, silver trifluoroacetate, or copper (II) nitrate, and then a small amount is deposited onto the target well via pipette. The solvent is evaporated so that the sample and matrix can co-crystallise, so for synthetic polymers it is advantageous if both are soluble in the same solvent. It is also advantageous to use volatile solvents, as rapid evaporation increases the homogeneity of the co-crystallised sample. These considerations are not so important for peptides and proteins.

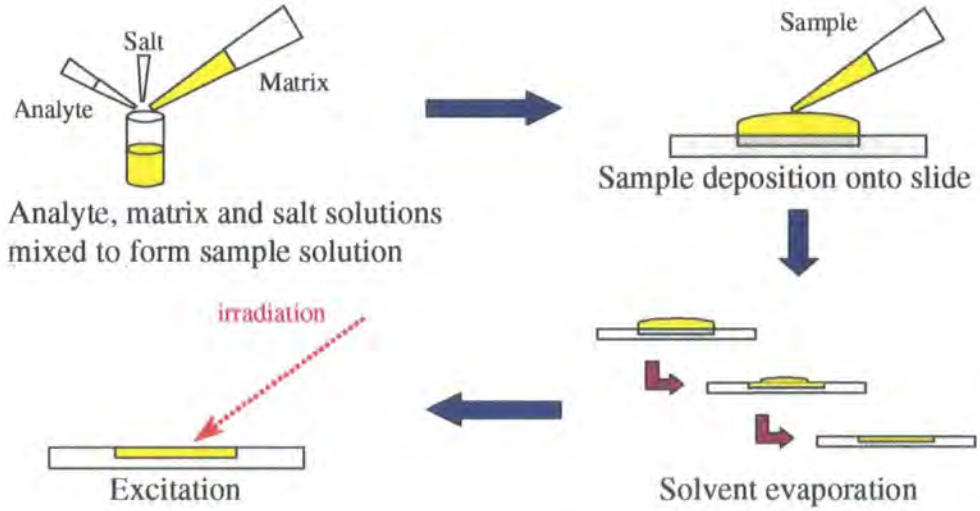

Figure 1.5.1. Illustration of the mixed dried droplet sample preparation method.

The choice of metal, counter-ion, solvent and the ratio of matrix-to-analyte-to-salt have all been shown to have an effect upon the spectra acquired.[14-19] Several other

preparation methodologies have been proposed in order to increase the homogeneity of the prepared sample, such as the layer technique, were components are deposited individually, electrospray[20] and solventless approaches.[21]

1.6 MALDI-TOF-MS of PMMA

Most of the research to date has concentrated on low molecular weight or oligomeric samples because of constraints in resolution. The majority of the work has also been undertaken with narrow polydispersity samples, as the results from more polydisperse samples have been shown to suffer from mass discrimination effects.[22,23] Due to the fact that polymers are synthesised with a distribution in the number of repeat units (n) per molecule, we expect the mass spectrum to have a distribution, or a series, of peaks. Each peak in a series should be separated by a mass-to-charge ratio equal to the mass of the monomer or repeat unit, which conveniently equals 100 amu for MMA. The exact mass value of a peak depends upon the masses of the groups at either end of the chain, and also the mass of the cation.

Several different groups have performed MALDI-TOF-MS experiments with PMMA from various synthetic routes, with different combinations of matrix and cation, and with respect to a number of aspects. For example, samples of PMMA synthesised by group transfer polymerisation (GTP),[24,25] anionic polymerisation[26] and atom transfer radical polymerisation (ATRP),[27] have been analysed. Polymer end-groups have been investigated,[24,26] more recently employing MALDI-CID.[25,27] Several groups have compared and contrasted molecular weight distribution data obtained via MALDI and the more conventional technique of size exclusion chromatography (SEC).[28-30] MALDI analysis has also been performed with regard to the backbone architecture of PMMA copolymers, for example, an alternating copolymer with methyl α-phenylacrylate[31] and a block copolymer with *n*-butyl methacrylate.[32]

1.7 Background to Controlled Polymerisations

It has already been mentioned that the MALDI analysis of more polydisperse samples are prone to mass discrimination effects, and that, due to constraints in

resolution, more useful information is derived from low molecular weight samples. The method by which such polymers are synthesised should therefore exercise control over their molecular weight and polydispersity, if MALDI-TOF-MS is to be used to characterise the full sample without fractionation. The concept of control has many different aspects:[33]

1. Molecular weight (chain length and polydispersity)
2. Stereospecificity
3. Rate
4. Chain architecture, *e.g.* block, comb, *etc.*
5. Functionality introduction

These are achieved to the best extent via anionic polymerisation. Anionic-initiated polymerisations are generally specific, since the formation and stabilisation of a carbanion depends largely upon the nature of the R-groups in the vinyl monomer $CH_2=CR'R''$. For this reason, anionic initiators require monomers with electron withdrawing substituents (–CN, –COOR, $-CH=CH_2$, *etc.*) to promote the formation of a stable carbanion. The stability of the carbanion is greatly enhanced when there is a combination of both mesomeric and inductive effects. The counter-ion can influence both the rate and stereochemical nature of the reaction.

An important aspect of monomer reactivity in anionic polymerisation is the relationship between monomer reactivity, the stability of the corresponding propagating species, and the appropriate initiating species. The general relationship can be deduced from the pK_a values for the conjugate acids of the anions being formed. Thus, monomers that form the least stable anions (*i.e.* have the largest pK_a values for the corresponding conjugate acids) are the most unreactive for anionic polymerisation. Therefore, these less reactive monomers require the most reactive initiators, in order to polymerise. Generally, an appropriate initiator is an anionic species, which possesses a similar reactivity to that of the propagating carbanionic species. Too reactive an initiator will promote side reactions, whereas too unreactive an initiator will lead to a slow or inefficient reaction.

Initiation of anionic polymerisations can occur in one of two ways, involving essentially the gain of an electron by the monomer to produce either i) an anion or ii) a radical anion. Organolithium compounds and Grignard reagents are common initiators.

Once initiation is complete, the only reaction that gives rise to the growth of the polymer molecule is between the active polymer species and monomer and the choice of solvent will have a profound influence on the propagation process. The separation of the initiator and counter-ion pair is directly related to the solvent, and chain propagation depends significantly on ion pair separation. This separation will also control the mode of entry of an adding monomer. The increasing polarity of the solvent increases the ion pair separation from an intimate pair, through a solvent separated pair, to a state of complete dissociation, as shown below in Figure 1.7.1.

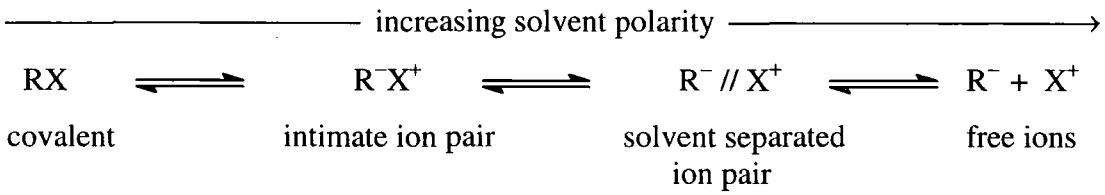

Figure 1.7.1. Illustration of the effect of solvent polarity on ion pair separation.

Free ions propagate faster than a tight ion pair, which is reflected in an increase in the rate constant for polymerisation (k_p). The separation of the ions also lowers the steric restrictions to the incoming monomer, so that free ions exert little stereo-regulation on the propagation. If the separation is too great, reactions, which are assisted by co-ordination of the monomer with the counter-ion, may be hindered.

Propagation ends with consumption of all the monomer since in anionic polymerisation there is no inherent termination step. The recombination of a chain with its counter-ion or the transfer of a hydrogen to give terminal unsaturation, frequent in other polymerisations, is unlikely in anionic mechanisms. However, anionic polymerisation reactions are extremely sensitive to traces of impurities, and because carbanions are rapidly neutralised by compounds with labile hydrogens, carbon dioxide and oxygen, these become effective terminating agents. Thus, there is a great need for stringent experimental procedures to exclude impurities when carrying out anionic polymerisations. Since the termination step usually involves transfer to some species not involved in the actual reaction, anionic polymerisation with carefully purified reagents should lead to systems in which termination is absent, resulting in so-called 'living' polymers.[34] These polymers can have extremely narrow polydispersity, the essential requirement for this is the absence of termination routes, including chain transfer, and not necessarily a rapid initiation rate compared to propagation.[35]

There are several criteria[36] that can be used to describe whether a polymerisation is living or not. Criterion 1 is that polymerisation proceeds until the consumption of all the monomer present, and that all chains will continue to grow upon the further addition of monomer. The second criterion is that the molecular weight increases linearly with conversion. A theoretical value for the number average molecular weight ($\overline{M}_n$) for complete conversion can be calculated using Equation 1.7.1.

$$\overline{M}_n = \text{g of monomer/moles of initiator} \qquad \textbf{Eqn. 1.7.1}$$

The third criterion is that the number of polymer chains is constant, and independent of monomer conversion. Criterion 4 states that the number average molecular weight should be a simple function of the degree of monomer conversion, and that it is controlled by the stoichiometry of the reaction, so there must be complete utilisation of the initiator before full monomer consumption. Criterion 5 is that polymerisations should have a low polydispersity ($\overline{M}_w/\overline{M}_n \leq 1.1$), also known as a narrow or monodisperse molecular weight distribution. There are some essential requirements for this:

1. Polymer molecule growth proceeds exclusively by consecutive monomer addition to an active terminal group.
2. At all times during the polymerisation, the active terminal of each molecule must be equally susceptible to reaction with monomer.
3. All active termini must be created at the start of the polymerisation.
4. Chain transfer or termination must be absent.
5. Propagation must be irreversible (*i.e.* rate of depropagation is minute).

The sixth criterion is that block copolymers can be formed by sequential monomer addition and this can be used as a diagnostic test in a similar fashion to Criterion 1. Along the same lines, Criterion 7 states that controlled termination of living polymerisations can conclude with chain-end functionalised polymers.

All these experimental criteria can be used to determine the living nature of a polymerisation, though generally, they should be used collectively, as no single criterion can prove whether or not a polymerisation is living.

1.8 Controlled Anionic Synthesis of PMMA

For a MMA monomer, the desired Michael addition reaction with the initiator is shown in Figure 1.8.1, so the choice of initiator is of critical importance in obtaining polymers with predictable, well-defined structures.

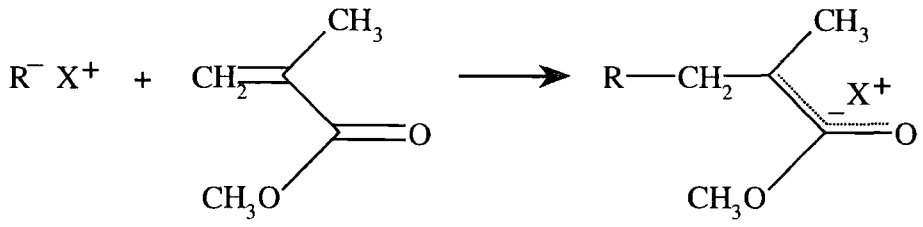

Figure 1.8.1. Michael Addition reaction of initiator with MMA.

Anionic polymerisation of methacrylate monomers is often complicated by side reactions of the monomer with both the initiator and the propagating chain ends, as well as termination and chain transfer reactions. The main side reaction involving the initiator, *e.g.* for *n*-butyllithium, results in the formation of a ketone and an alkoxide (see Figure 1.8.2), and a similar reaction can occur between the propagating chain end and the monomer.

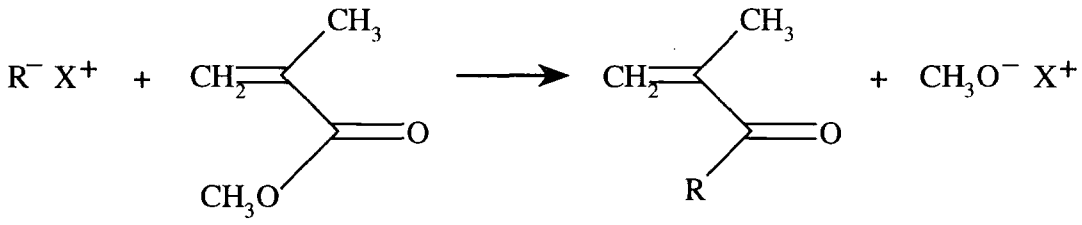

Figure 1.8.2. Side-reaction of initiator with MMA to form a ketone.

The other main termination reaction is the unimolecular backbiting reaction between the living ester enolate anion and the penultimate non-living ester group, forming a six-member, β-ketoester end-group, as depicted in Figure 1.8.3. This reaction is considered to be the major mechanism for termination, but it is known to be less likely to occur with increasing chain length, due to steric hindrance. Performing polymerisations at low temperatures, *e.g.* –78°C, and employing bulky initiators can, for the most part, circumvent these reactions. To achieve fine-control mechanisms for methacrylate

polymerisations, factors, including counter-ion, solvent, temperature, Lewis base additives and inorganic salts, have been investigated.

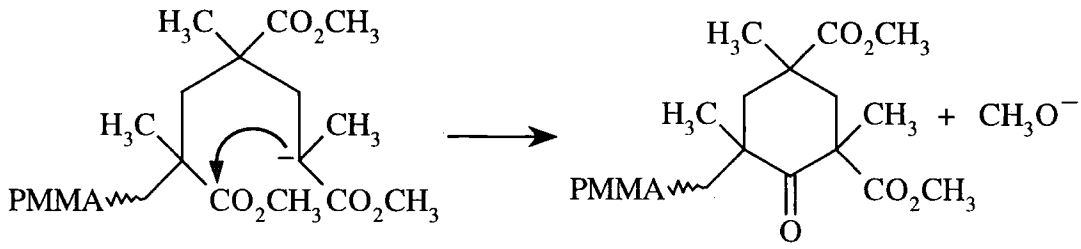

Figure 1.8.3. Self-termination reaction of anionic PMMA chains.

One of the most widely utilised initiators for methacrylates and related monomers is diphenylhexyllithium (DPHLi),[37] prepared by the stoichiometric nucleophilic addition of *n*-butyllithium (*n*-BuLi) to 1,1-diphenylethylene (DPE), as shown in Figure 1.8.4.

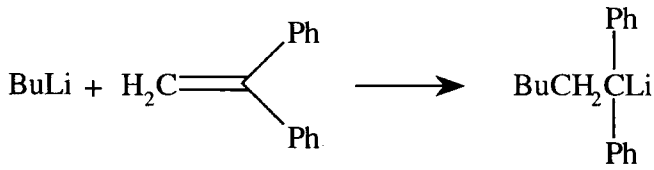

Figure 1.8.4. Reaction of *n*-BuLi and DPE to form DPHLi initiator.

It is easily prepared in most solvents, and is a useful route for functional initiators, by using substituted or protected diphenylethylenes. DPHLi is a bulky initiator and so reduces the likelihood of termination by attack on the carbonyl of the monomer. Initiator efficiency (*f*) is defined as the concentration of growing chains divided by the initiator concentration, and is frequently quoted as a percentage. Polymerisations initiated with DPHLi gave an average value for *f* of 0.93 and an average polydispersity of 1.14.[38]

Lithium diisopropylamide (LDA) is the most effective initiator of the alkylamide class,[39,40] showing an initiator efficiency (*f*) = 75% in THF at –78°C. Ester enolate anions should be ideal initiators, as they are models for the propagating enolate in the methacrylate polymerisation. Ethyl α-lithioisobutyrate (LiEIB) has been shown to give 100% conversion, $f = 0.91$, and a polydispersity of 1.04 for the polymerisation of MMA, in THF at –78°C.[41] Soluble and stable in most solvents, they show high degrees

of aggregation, though they show limited stability in THF at room temperature because of self-condensation reactions. LiEIB is easily prepared from ethyl isobutyrate and LDA.

Other alkyl lithium reagents are generally considered to be too reactive on a pK_a basis, though oligomeric α-methylstyryllithium (pK_a = 43 for toluene) is a surprisingly effective initiator. Very reasonable polymerisations have been achieved using this initiator at –78°C in THF, giving 99% conversion, f = 85%, and a polydispersity of 1.10.[38] Many more initiating systems, far too many to mention in this text, have also been demonstrated to be effective for the controlled initiation of MMA.

In controlled anionic synthesis, the nature of the propagating chain end is very important, and it should be emphasised that for MMA this is an enolate, rather than a simple carbanion.[33] Therefore, the charge is delocalised across three atoms, as can be seen in Figure 1.8.5. Propagation relies on a stabilised chain-end that is protected from termination reactions and selected reaction conditions, in order to allow monomer insertion.

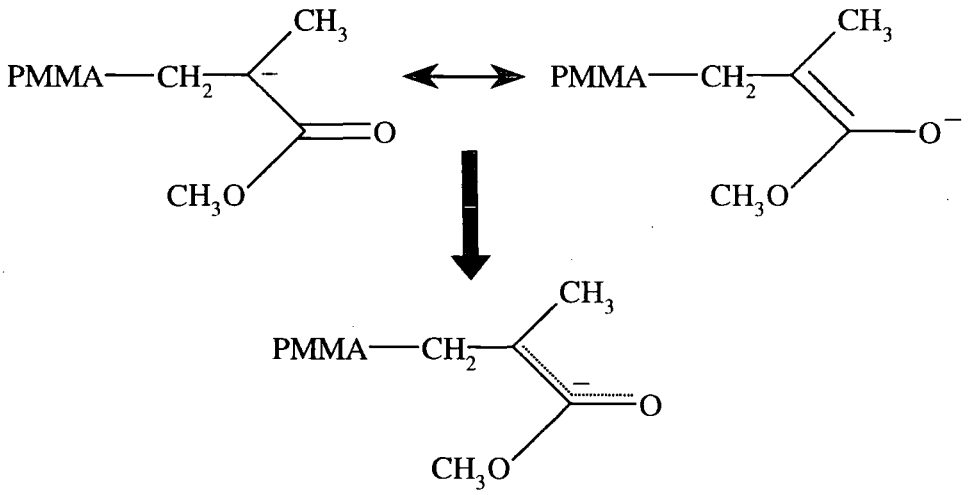

Figure 1.8.5. Delocalisation of negative charge in propagating PMMA chains.

Several aspects of control in anionic polymerisations have been increased recently with the development of ligated anionic polymerisation (LAP).[42] Suitable ligands are used to co-ordinate with the active initiating and propagating ion pairs, and this fulfils three major functions:

a) Promotion of complexation equilibrium among ion pairs and/or aggregates, hopefully leading to a single, stable active species.

b) Modulation of the stability and reactivity of the ion pair.

c) Protection of the ion pair by an increased steric effect, so that self-termination via backbiting of the growing anion is minimised.

Two groups of efficient ligated systems have come to the fore, those being with i) μ-type ligands such as inorganic lithium salts, or ii) μ/σ-type dual ligands such as lithium 2-(2-methoxyethoxy) ethoxide. The addition of lithium chloride (LiCl), lithium *t*-butoxide (LiO*t*-Bu), or LiOEEM can lead to low polydispersities as well as increased stability of the active species. DPHLi was shown to give slightly improved values for polydispersity and initiator efficiency with the added presence of LiCl[38] with MMA. LiCl increases the efficiency of LDA with MMA to 94%,[40,41] while at the same time lowering the polydispersity from 1.35 to 1.05. This is thought to be due to the formation of a mixed dimer complex of LDA and LiCl (see Figure 1.8.6), with complexation increasing the reactivity of LDA, but leaving the selectivity of the reaction with MMA monomer unaffected.

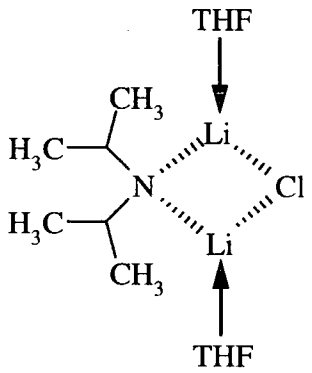

Figure 1.8.6. Mixed dimer complex of LDA and LiCl in THF.

The fact that controlled anionic polymerisation leads to stable anionic species upon completion opens up a multitude of possibilities for ω-end functionalisation and copolymer formation. In the literature, there are far more numerous examples of functionalisations for polystyrene and polybutadiene, but, in an analogous fashion, many of these reactions can be applied to PMMA. Reagents that can be utilised for this purpose include electrophilic compounds, *i.e.* alkyl[43,44] or silyl halides, carbon dioxide, ethylene oxide and protected amines. As there are monomers that do not polymerise under anionic conditions, these to can be used as functionalisation reagents.[45]

Functionalised initiators can also be used to produce functionalised polymers, *i.e.* those employing ring substituted 1,1-diphenylethylenes,[46-48] though care must be taken that the functionality does not affect the controlling properties of the initiator. Copolymerisation is also possible with these systems. Indeed, one of the uses of this technology is in the facile synthesis of block copolymers via sequential monomer addition, as well as the more unusual star and comb-shaped structures. Again, the stability of the ester enolate anion is critical to the success of these copolymerisations. Polystyryl[49] and polydienyl[50] anions can initiate copolymerisation of MMA, but the resultant ester enolate anions are too stable to reinitiate styrene or diene monomers. In principle, PMMA anions will initiate other acrylic monomers,[41,51,52] epoxides, siloxanes and lactones to give even more stable anions. Where anion stability is unfavourable towards copolymerisation, coupling reactions between blocks with terminal functionalised units can be utilised. These blocks may be prepared by adding a compound that both terminates the chain and incorporates itself as a useful end group, at the end of a reaction. This method is also useful for triblock copolymer synthesis. The synthesis of alternating[53] and random[52,54,55] copolymers is not as simple, but these can still be prepared with certain monomers and conditions. Pseudo-random copolymers can be prepared by alternated addition of various small amounts of monomer repeatedly.

1.9 References

1. Karas, M.; Hillenkamp, F. *Anal. Chem.* **1988**, *60*, 2299-2301.
2. Hillenkamp, F.; Karas, M.; Beavis, R. C.; Chait, B. T. *Anal. Chem.* **1991**, *63*, A1193-A1202.
3. Bahr, U.; Deppe, A.; Karas, M.; Hillenkamp, F.; Giessmann, U. *Anal. Chem.* **1992**, *64*, 2866-2869.
4. Karas, M.; Bachmann, D.; Bahr, U.; Hillenkamp, F. *Int. J. Mass Spectrom. Ion Process.* **1987**, *78*, 53-68.
5. Schriemer, D. C.; Li, L. *Anal. Chem.* **1996**, *68*, 2721-2725.
6. Beuhler, R. J. *Journal of Applied Physics* **1983**, *54*, 4118-4126.
7. Macfarlane, R. D.; Torgerson, D. F. *Science* **1976**, *191*, 920-925.

8. Mamyrin, B. A.; Karataev, V. I.; Shmikk, D. V.; Zagulin, V. A. *Sov. Phys. JETP* **1973**, *37*, 45-48.
9. Wiley, W. C.; McLaren, I. H. *Rev. Sci. Instr.* **1955**, *26*, 1150.
10. Spengler, B.; Cotter, R. J. *Anal. Chem.* **1990**, *62*, 793-796.
11. Cotter, R. J. *Anal. Chem.* **1999**, *71*, 445A-451A.
12. Jennings, K. R. *International Journal of Mass Spectrometry* **2000**, *200*, 479-493.
13. Bateman, R. H.; Green, M. R.; Scott, G.; Clayton, E. *Rapid Commun. Mass Spectrom.* **1995**, *9*, 1227-1233.
14. Danis, P. O.; Karr, D. E. *Org. Mass Spectrom.* **1993**, *28*, 923-925.
15. Belu, A. M.; DeSimone, J. M.; Linton, R. W.; Lange, G. W.; Friedman, R. M. *J. Am. Soc. Mass Spectrom.* **1996**, *7*, 11-24.
16. Dogruel, D.; Nelson, R. W.; Williams, P. *Rapid Commun. Mass Spectrom.* **1996**, *10*, 801-804.
17. Jackson, A. T.; Yates, H. T.; MacDonald, W. A.; Scrivens, J. H.; Critchley, G.; Brown, J.; Deery, M. J.; Jennings, K. R.; Brookes, C. *J. Am. Soc. Mass Spectrom.* **1997**, *8*, 132-139.
18. Hoberg, A. M.; Haddleton, D. M.; Derrick, P. J.; Jackson, A. T.; Scrivens, J. H. *Eur. Mass Spectrom.* **1998**, *4*, 435-440.
19. Yalcin, T.; Dai, Y. Q.; Li, L. *J. Am. Soc. Mass Spectrom.* **1998**, *9*, 1303-1310.
20. Axelsson, J.; Hoberg, A. M.; Waterson, C.; Myatt, P.; Shield, G. L.; Varney, J.; Haddleton, D. M.; Derrick, P. J. *Rapid Commun. Mass Spectrom.* **1997**, *11*, 209-213.
21. Marie, A.; Fournier, F.; Tabet, J. C. *Anal. Chem.* **2000**, *72*, 5106-5114.
22. Schriemer, D. C.; Li, L. A. *Anal. Chem.* **1997**, *69*, 4169-4175.
23. Schriemer, D. C.; Li, L. A. *Anal. Chem.* **1997**, *69*, 4176-4183.
24. Pasch, H.; Gores, F. *Polymer* **1995**, *36*, 1999-2005.
25. Jackson, A. T.; Yates, H. T.; Scrivens, J. H.; Critchley, G.; Brown, J.; Green, M. R.; Bateman, R. H. *Rapid Commun. Mass Spectrom.* **1996**, *10*, 1668-1674.
26. Jackson, A. T.; Yates, H. T.; Lindsay, C. I.; Didier, Y.; Segal, J. A.; Scrivens, J. H.; Critchley, G.; Brown, J. *Rapid Commun. Mass Spectrom.* **1997**, *11*, 520-526.
27. Borman, C. D.; Jackson, A. T.; Bunn, A.; Cutter, A. L.; Irvine, D. J. *Polymer* **2000**, *41*, 6015-6020.
28. Montaudo, G.; Montaudo, M. S.; Puglisi, C.; Samperi, F. *Rapid Commun. Mass Spectrom.* **1995**, *9*, 453-460.

29. Lloyd, P. M.; Suddaby, K. G.; Varney, J. E.; Scrivener, E.; Derrick, P. J.; Haddleton, D. M. *Eur. Mass Spectrom.* **1995**, *1*, 293-300.
30. Jackson, C.; Larsen, B.; McEwen, C. *Anal. Chem.* **1996**, *68*, 1303-1308.
31. Mormann, W.; Walter, J.; Pasch, H.; Rode, K. *Macromolecules* **1998**, *31*, 249-255.
32. Jackson, A. T.; Scrivens, J. H.; Simonsick, W. J.; Green, M. R.; Bateman, R. H. *Abstr. Pap. Am. Chem. Soc.* **2000**, *219*, 50-POLY.
33. Davis, T. P.; Haddleton, D. M.; Richards, S. N. *J. Macromol. Sci.-Rev. Macromol. Chem. Phys.* **1994**, *C34*, 243-324.
34. Szwarc, M. *Nature* **1956**, *178*, 1168-1169.
35. Gold, L. *J. Chem. Phys.* **1958**, *28*, 91-99.
36. Quirk, R. P.; Lee, B. *Polym. Int.* **1992**, *27*, 359-367.
37. Wiles, D. M.; Bywater, S. *Trans. Faraday Soc.* **1965**, *61*, 150-158.
38. Varshney, S. K.; Hautekeer, J. P.; Fayt, R.; Jérôme, R.; Teyssié, P. *Macromolecules* **1990**, *23*, 2618-2622.
39. Long, T. E.; Guistina, R. A.; Schell, B. A.; McGrath, J. E. *J. Polym. Sci. Pol. Chem.* **1994**, *32*, 2425-2430.
40. Antoun, S.; Teyssié, P.; Jérôme, R. *J. Polym. Sci. Pol. Chem.* **1997**, *35*, 3637-3644.
41. Antoun, S.; Teyssié, P.; Jérôme, R. *Macromolecules* **1997**, *30*, 1556-1561.
42. Wang, J. S.; Jérôme, R.; Teyssié, P. *J. Phys. Organ. Chem.* **1995**, *8*, 208-221.
43. Altakrity, E. T. B.; Jenkins, A. D.; Walton, D. R. M. *Makromol. Chem.* **1990**, *191*, 3069-3072.
44. Altakrity, E. T. B.; Jenkins, A. D.; Walton, D. R. M. *Makromol. Chem.* **1990**, *191*, 3073-3076.
45. Cernohous, J. J.; Macosko, C. W.; Hoye, T. R. *Macromolecules* **1997**, *30*, 5213-5219.
46. Altakrity, E. T. B.; Jenkins, A. D.; Walton, D. R. M. *Makromol. Chem.* **1990**, *191*, 3059-3067.
47. Hirao, A.; Haraguchi, N.; Sugiyama, K. *Macromolecules* **1999**, *32*, 48-54.
48. Moon, B.; Hoye, T. R.; Macosko, C. W. *J. Polym. Sci. Pol. Chem.* **2000**, *38*, 2177-2185.
49. Ohnuma, H.; Kotaka, T.; Inagaki, H. *Polymer* **1969**, *10*, 501-516.

50. Yu, J. M.; Dubois, P.; Teyssié, P.; Jérôme, R. *Macromolecules* **1996**, *29*, 6090-6099.

51. Graham, R. K.; Panchak, J. R.; Kampf, M. J. *J. Polymer Sci.* **1960**, *44*, 411-419.

52. Hatada, K.; Kitayama, T.; Ute, K. *Makromol. Chem., Makromol. Symp.* **1993**, *70-1*, 57-66.

53. Hirabayashi, T.; Yamamoto, H.; Kojima, T.; Takasu, A.; Inai, Y. *Macromolecules* **2000**, *33*, 4304-4306.

54. Wang, J. S.; Jérôme, R.; Bayard, P.; Baylac, L.; Patin, M.; Teyssié, P. *Macromolecules* **1994**, *27*, 4615-4620.

55. Zune, C.; Archambeau, C.; Dubois, P.; Jérôme, R. *J. Polym. Sci. Pol. Chem.* **2001**, *39*, 1774-1785.

Chapter 2

Synthesis and Characterisation of End-Functionalised PMMA

2.1 Introduction

PMMA homopolymers synthesised using classical anionic methods and subsequently studied by MALDI-TOF-MS are discussed. Specifically, the attempts at different end-group functionalisation reactions, their varying degrees of success, and the characterisation of these functionalised polymers via MALDI are reported. The need for very low polydispersity, well-defined polymers has already been described in the previous chapter, thus LDA[1,2] and DPHLi[3] initiating systems, proven to exert great control over the polymerisation process, were used to synthesise all these polymers. In addition, the initiator-derived end-groups are interesting from a MALDI perspective, as nitrogen has a strong affinity for protons, whereas phenyl rings are known to bind metal cations. These systems are dealt with in the following section.

2.2 Proton and Self-Terminated Polymers

Sample *1* was initiated with LDA and terminated with a proton via methanol (CH_3OH). Sample *2* was initiated with DPHLi and terminated likewise. Sample *3* was initiated with LDA and allowed to self-terminate by warming to room temperature from the reaction temperature of –78°C. The SEC data for these polymers are given in Table 2.2.1.

Sample	$\overline{M}_n$	$\overline{M}_w$	$\overline{M}_w/\overline{M}_n$
1	1390	1520	1.09
2	2650	2840	1.07
3	1940	2080	1.07

Table 2.2.1. SEC molecular weight data for *1-3*.

The SEC trace for *1* (see Figure 2.2.1) shows that this polymer is monomodal, hence initiation was by a single species and all chains were initiated at the same time. The narrow peak-width is also a characteristic of all chains being initiated coincidentally and the polymer having a low polydispersity index, which is confirmed by the calculated figures.

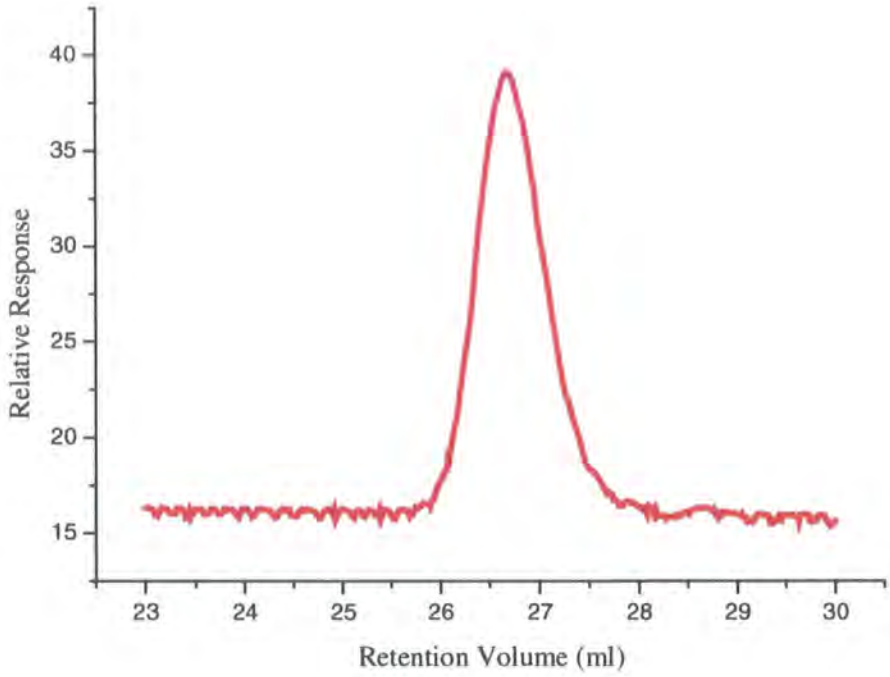

Figure 2.2.1. SEC trace of *1*.

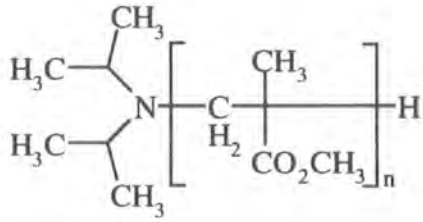

Figure 2.2.2. Stoichiometric formula of *1*.

The stoichiometric formula of *1* is shown in Figure 2.2.2. The proton NMR spectrum (Figure 2.2.3) has three main peaks due to groups in the polymer repeat units, which can be assigned as follows.[4] The peaks occurring between δ = 0.8-1.4 ppm corresponds to the pendant methyl group of the repeat unit. The complicated splitting pattern is derived from the many slightly different environments and couplings that this group has. The doublet at δ = 1.1 ppm is due to the methyl group of the ultimate repeat unit, due to coupling to the single terminating methine proton, which is given credence by the measured coupling constant J_{HH} = 7 Hz. The next set of peaks occur between δ = 1.6-2.3 ppm and also has a complicated splitting pattern, again due to different environments and couplings. These peaks correspond to the methylene groups in the backbone of the chain. The third peak is a singlet at δ = 3.6 ppm. This peak

corresponds to the methyl group of the pendant ester and is not split because each group is isolated from other protons, so they are essentially all in the same environment.

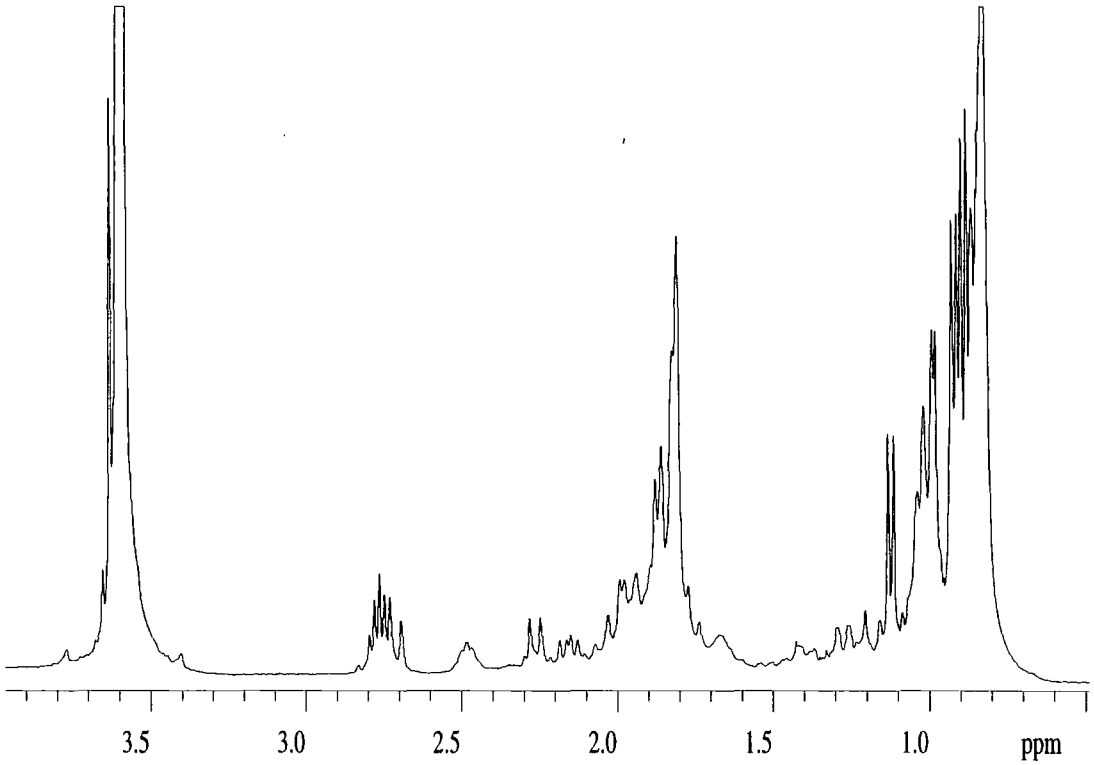

Figure 2.2.3. Proton NMR spectrum of *1*.

The peak at δ = 2.5 ppm corresponds to the sextet expected for the terminating methine proton, but as the signal only comes from a single proton it appears to be poorly resolved. The peak at δ = 2.8 ppm appears to be a septet, which is the splitting pattern one would expect for the methine proton of an isopropyl group. This peak must be due to end-group protons from the initiator and its occurrence at lower field supports this conclusion, since this group is bonded to a more electronegative nitrogen atom. The ratio of the sextet-to-septet peak integrations is 1:2, and confirms the assignment. The remaining doublet expected for the methyl groups of the initiator is hidden under the more intense peak of the pendant methyl groups at roughly 1 ppm. By comparing the integration of the peak due to the initiator methines with that for the methyl ester peak, the average ratio of repeat unit-to-initiator can be calculated. The number of protons from which each signal is derived must be accounted for, *i.e.* 3 for the methyl ester, multiplied by n repeat units, and 2 for the equivalent methines. In this case, the ratio was roughly 8.5:1, giving an average molecular weight for the polymer of

950 g mol^{-1}, a value that does not agree with that obtained via SEC. Due to the fact that the signal intensities of end-group protons will be come steadily weaker as we go to higher molecular weights, it is clear that this is not the best method for obtaining reliable molecular weight information, but it serves well as an approximation.

The carbon NMR spectrum (Figure 2.2.4) shows five signals due to carbons in the polymer repeat units, which can be assigned as follows.[5,6] The peaks around δ = 177 ppm are due to the carbonyl of the pendant ester groups. The peak at δ = 52 ppm corresponds to the methyl group of the pendant ester. The peaks occurring between δ = 16-20 ppm correspond to the pendant methyl group of the repeat unit. The other two peaks, due to the backbone carbons, occur between δ = 53-55 ppm corresponding to the methylene groups, and between δ = 44-46 ppm corresponding to the quaternary carbons. The peak at δ = 59 ppm is most likely attributable to the methylene of the first repeat unit is bonded directly to the nitrogen of the initiator.

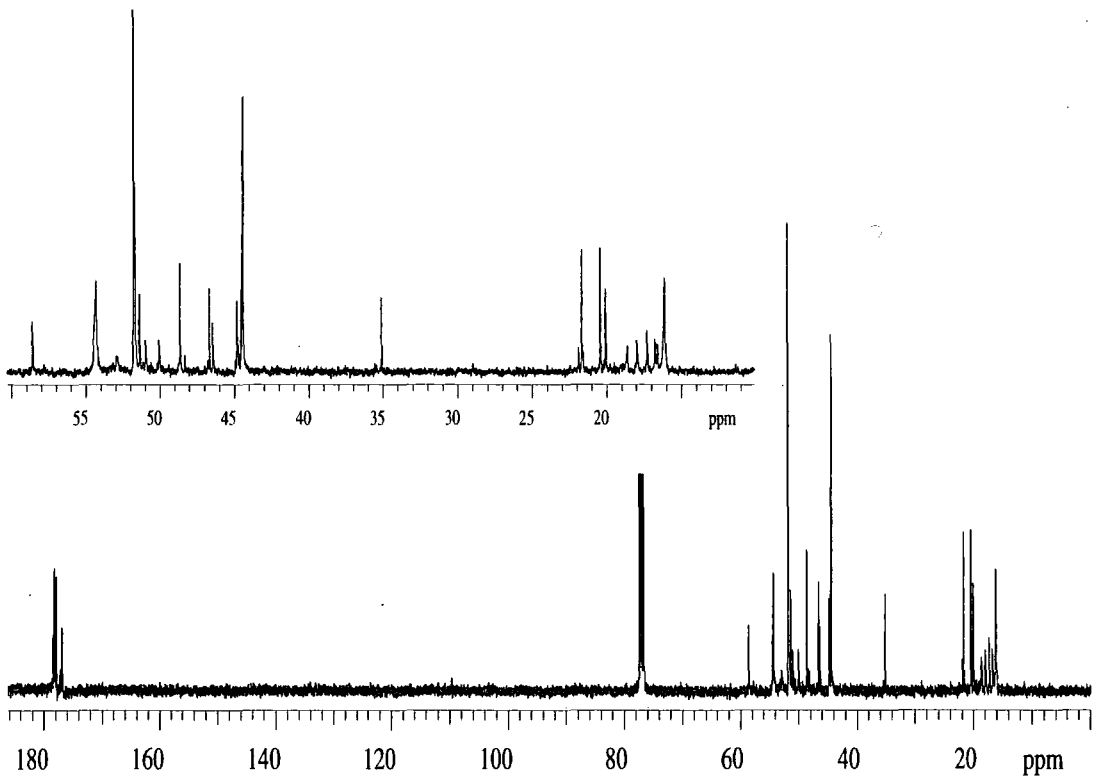

Figure 2.2.4. Carbon NMR spectrum of *1* with expanded higher field region.

The peak at δ = 35 ppm corresponds to the tertiary carbon associated with the terminating methine proton, and that at δ = 48 ppm is due to the tertiary carbon of the isopropyl group of the initiator. The remaining signal expected for the methyl groups of the initiator are at δ = 22 ppm. Both proton and carbon NMR give credence to the stoichiometric formula given in Figure 2.2.2.

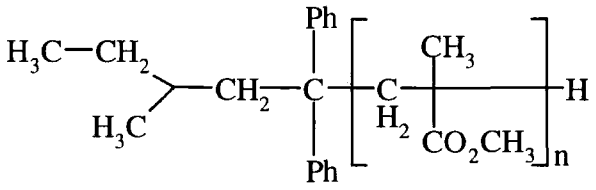

Figure 2.2.5. Stoichiometric formula of *2*.

The stoichiometric formula of *2* is shown in Figure 2.2.5. The proton NMR (Figure 2.2.6 below) shows the same resonances assigned earlier to the polymer repeat unit. There is also a peak at δ = 3.3 ppm that can be attributed to the methoxy group of the repeat unit adjacent to the initiator. Additionally, there are other peaks due to the end-groups of the polymer, those immediately obvious being the broad peaks between δ = 7.1-7.3 ppm due to the phenyl rings of the initiator. The other peaks due to the alkyl groups of initiator are difficult to assign because of overlap with signals derived from the polymer chain. There are several peaks between δ = 0.2-0.8 ppm, which are most likely initiator derived since they did not appear in the proton spectrum for *1*. Of these, the triplet at δ = 0.6 ppm may be due to terminal methyl group, and the small doublet at δ = 0.2 ppm may be attributable to the methylene group betwixt the methine and quaternary groups. The peak corresponding to the terminating methine proton is at δ = 2.5 ppm as expected, confirming the anticipated chain termination mode. A notable absence is a septet peak at δ = 2.8 ppm assigned to the methines of the isopropyl groups for *1*, thus giving credence to the original assignment.

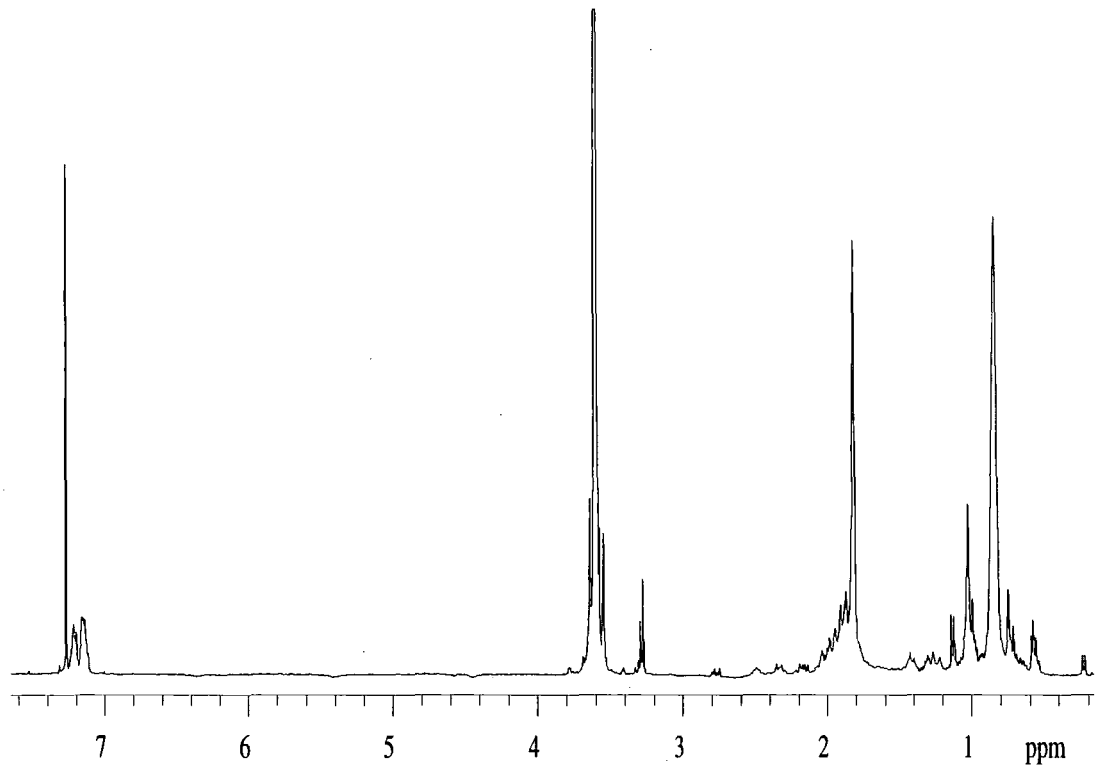

Figure 2.2.6. Proton NMR spectrum of *2*.

The carbon NMR (Figure 2.2.7) also shows the same resonances previously assigned to the polymer repeat unit. The peaks previously assigned to groups of the LDA initiator for *1* (δ = 22 and 48 ppm) are not observed here, thus confirming their original assignments. The easiest peaks to assign are those pertaining to the phenyl rings of the initiator, which are observed at δ = 147-149 ppm for the quaternary carbons and at δ = 126-129 ppm for the methines. The peak at δ = 50 ppm is probably due to the similarly shifted methylene groups either side of the diphenyl quaternary carbon, the latter having a peak at δ = 36 ppm. The peaks at δ = 30, 29, 21 and 11 ppm correspond to the remaining methylene, methine, pendant methyl and terminal methyl groups of the initiator respectively. Again there is a peak at δ = 35 ppm corresponding to the tertiary carbon at the ω-end of each chain. Hence, both proton and carbon NMR confirm the stoichiometric formula given in Figure 2.2.5.

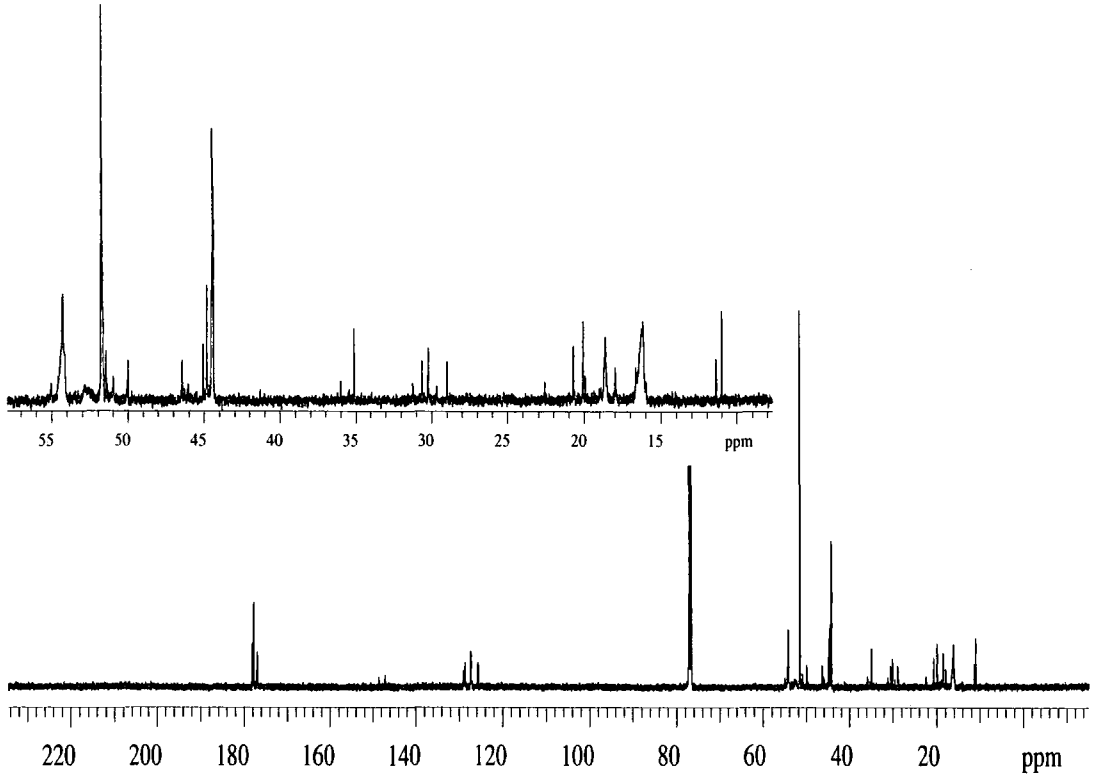

Figure 2.2.7. Carbon NMR spectrum of *2* with expanded higher field region.

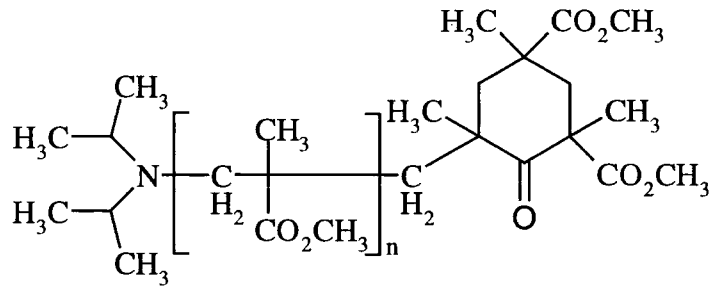

Figure 2.2.8. Stoichiometric formula of *3*.

The stoichiometric formula of *3* is shown in Figure 2.2.8. The proton NMR (Figure 2.2.9) shows the same resonances previously assigned to groups of the polymer repeat unit and the LDA initiator. However, the doublet at δ = 1.1 ppm, assigned previously to the methyl group of the ultimate repeat unit, is missing, and as we would not expect to see that peak for the cyclic ketone end-group, it can be concluded that the original assignment was correct. Absent also is a peak at δ = 2.5 ppm corresponding to the terminating methine proton. The end-group essentially consists of the same groups that are found in the polymer backbone, except that their environments differ by varying degrees. Therefore, we would expect to see additional peaks in the spectrum for each of the repeat unit peaks signals, as observed. The most notable difference observed

comparing both cyclic end-group and in-chain methylene groups, with protons of the latter being completely magnetically inequivalent. The very small peaks between δ = 2.4-2.6 ppm can be assigned to these particular protons.

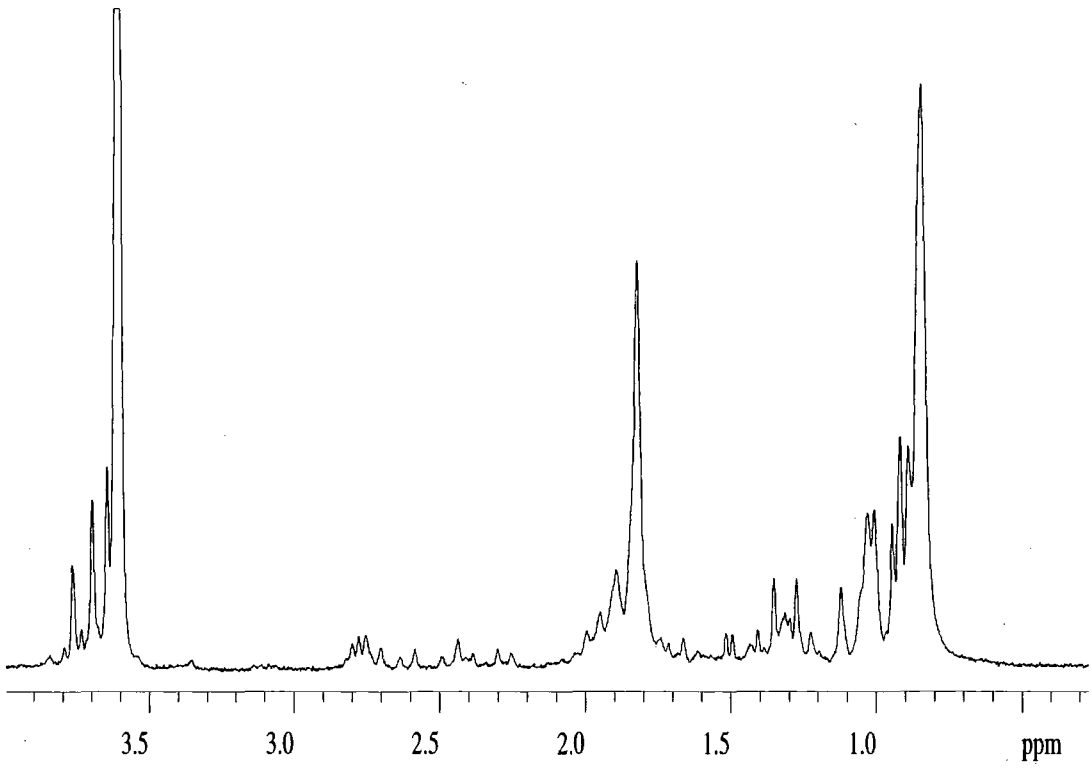

Figure 2.2.9. Proton NMR spectrum of *3*.

The carbon NMR (Figure 2.2.10) also shows the same resonances previously assigned to groups of the polymer repeat unit and the LDA initiator. Again the spectrum appears more complicated as signals due to the cyclic ketone are very similar to those of the polymer backbone. The spectrum has no peak at δ = 35 ppm corresponding to the tertiary carbon of the ultimate repeat unit, as observed previously for both *1* and *2*. The final evidence for the predicted end-group is the peak for a ketone carbonyl found at δ = 212 ppm. Hence, both proton and carbon NMR verify the stoichiometric formula given in Figure 2.2.8.

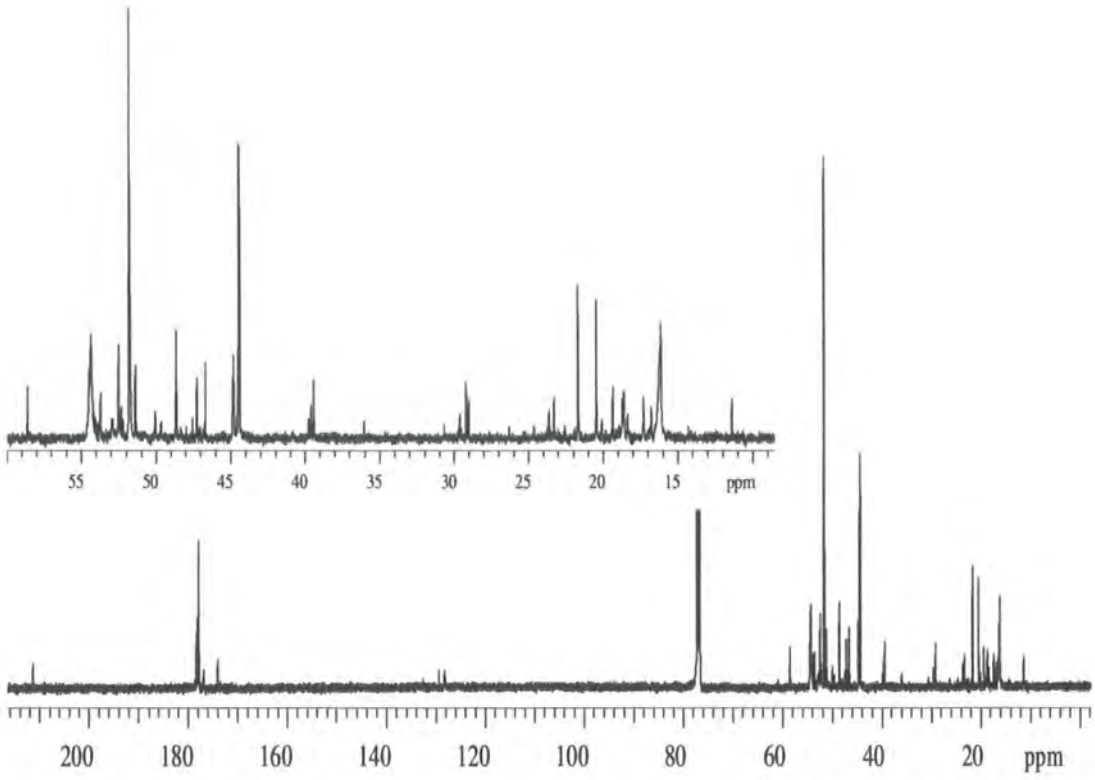

Figure 2.2.10. Carbon NMR spectrum of *3* with expanded higher field region.

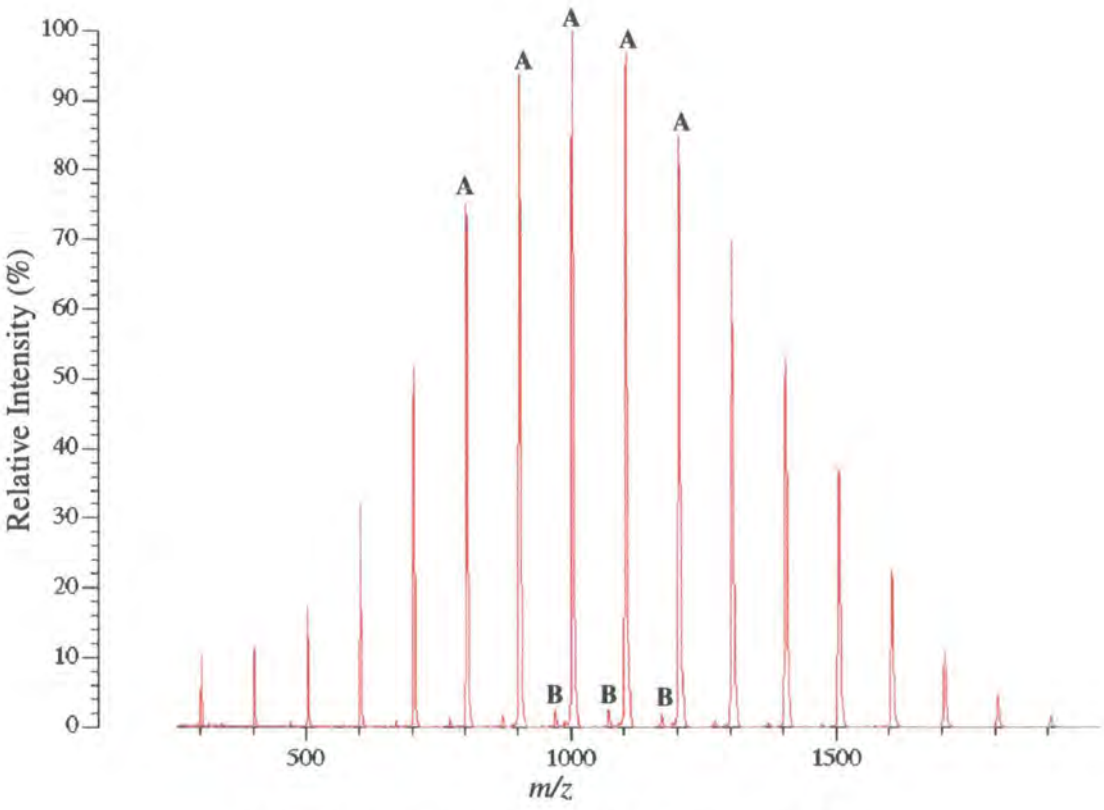

Figure 2.2.11. Linear MALDI spectrum of *1*.

The linear MALDI spectrum for *1* is shown in Figure 2.2.11 and two series are visible, one (**A**) much more intense than the other (**B**). These series are due to either two different species being present in the sample or the same species being ionised by different cations. The sample was analysed without the addition of a salt, therefore protons or impurity derived sodium or potassium ions are most likely to cationise the sample. The separation of the peaks within each series has an integer value of 100 amu, which verifies that the sample is indeed PMMA. In order to identify each series of peaks, the observed and theoretical mass values had to be compared. The theoretical mass values, for normally encountered singly charged species, were calculated using Equation 2.2.1 below.

$$m/z = (\text{repeat unit mass} \times \text{n}) + \text{end-group masses} + \text{cation mass} \qquad \textbf{Eqn 2.2.1}$$

Average atomic masses were used in these calculations to give average molecule ion masses. The comparison of mass values, taken from around the centre of the distribution, for the observed series **A** and the calculated series for stoichiometric formula *1* cationised by a proton ($[1+H]^+$) is given for in Table 2.2.2. These values are in very good agreement, confirming both stoichiometric formula and mode of cationisation. The separation of peaks between **A** and **B** has values of roughly 32 or 68 amu, depending on which direction the measurement is taken from, *i.e.* a loss or a gain. For cationisation of *1* by either sodium of potassium ions, the interseries separation would only be 22 or 38 amu respectively, therefore **B** is due to a species that is 32 amu lower in mass than $[1+H]^+$. With direct fragmentation not usually occurring in MALDI analysis, it is highly unlikely that this difference is due to a loss from **A**. The difference does correspond to the mass of CH_3OH, so it can be inferred that **B** originates from a small amount of polymer anion self-termination during the synthesis. In short, **B** corresponds to $[3+H]^+$ molecule ions. Analysis of a sample with added LiCl showed that $[1+H]^+$ was still the major species, therefore, *1* has a greater binding affinity for protons than for lithium ions. The nitrogen of the amine end-group derived from the initiator is considered an ideal binding site for a proton, so explaining these observations.

1 (**A** and $[1+H]^+$)			*2* (**A** and $[2+Li]^+$)			*3* (**A** and $[3+H]^+$)		
n	Obs.	Calc.	n	Obs.	Calc.	n	Obs.	Calc.
7	802.76	803.03	18	2050.61	2047.45	9	1271.36	1271.58
8	902.92	903.15	19	2150.14	2147.56	10	1371.47	1371.70
9	1003.28	1003.26	20	2250.17	2247.68	11	1471.50	1471.81
10	1103.40	1103.38	21	2350.40	2347.80	12	1571.61	1571.93
11	1203.61	1203.50	22	2450.57	2447.92	13	1671.66	1672.05
12	1303.96	1303.62	23	2550.81	2548.04	14	1771.81	1772.17
13	1404.22	1403.74	24	2650.87	2648.15	15	1872.08	1872.28
14	1504.44	1503.86	25	2751.22	2748.27	16	1971.90	1972.41

Table 2.2.2. Average observed and calculated mass comparisons for *1-3*.

A spectrum for *2* could not be obtained without the addition of a salt. The linear MALDI spectrum for *2* with the addition of LiCl is shown in Figure 2.2.11. There are four series, clearly visible in the expansion, two (**A** and **B**) being much more intense than the others (**C** and **D**).

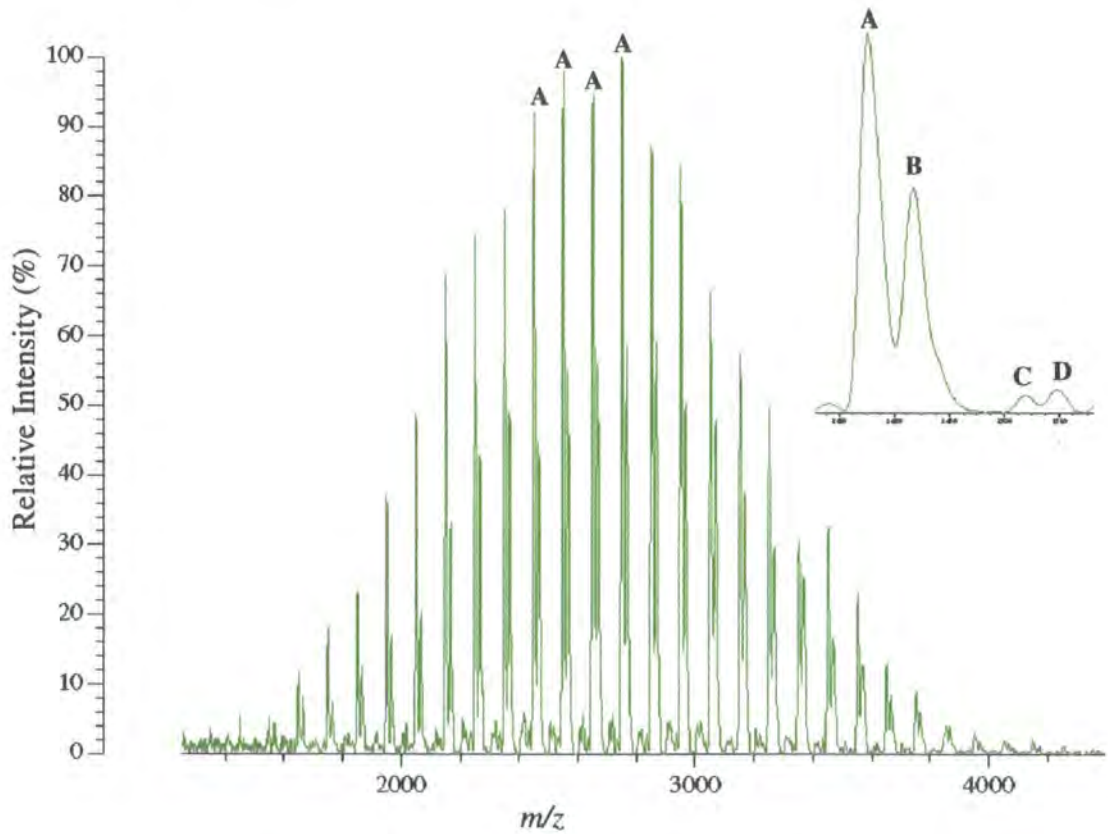

Figure 2.2.12. Linear MALDI spectrum of *2*.

As LiCl has been added, $[2+Li]^+$ molecule ions would be expected to concur with the major series in the spectrum, and a comparison of calculated and observed mass values for series **A** testify to this (see Table 2.2.2). Series **B** is observed 16 amu higher than **A**, and it is reasonable to conclude that this is due to $[2+Na]^+$ molecule ions. Both **A** and **B** confirm the polymer stoichiometric formula given in Figure 2.2.5. Series **C** and **D** are 32 amu less than series **A** and **B** respectively, thus we can conclude as before, that these correspond to synthetically derived self-terminated species, cationised by both lithium and sodium.

The linear spectrum of *3* without added salt gave just a single series of peaks, which corresponded to $[3+H]^+$ molecule ions, proven by good agreement between observed and calculated mass values. Further comparison of the observed masses with series **B** of *1* was also in good agreement. Analysis of a sample containing LiCl again showed that protonated molecule ions were the major species. This observation leads us to believe that the amine end-group may be highly influential in proton binding, as this is the only structural difference between the two samples.

The reflectron MALDI spectrum for *1* is pictured in Figure 2.2.13. Two series of peaks, **A** ($[1+H]^+$ species) and **B** ($[3+H]^+$ species), are observed as with the linear spectrum. The greater mass accuracy and resolution of reflectron mode provided more detailed information about these series, and the end-groups of the polymer.

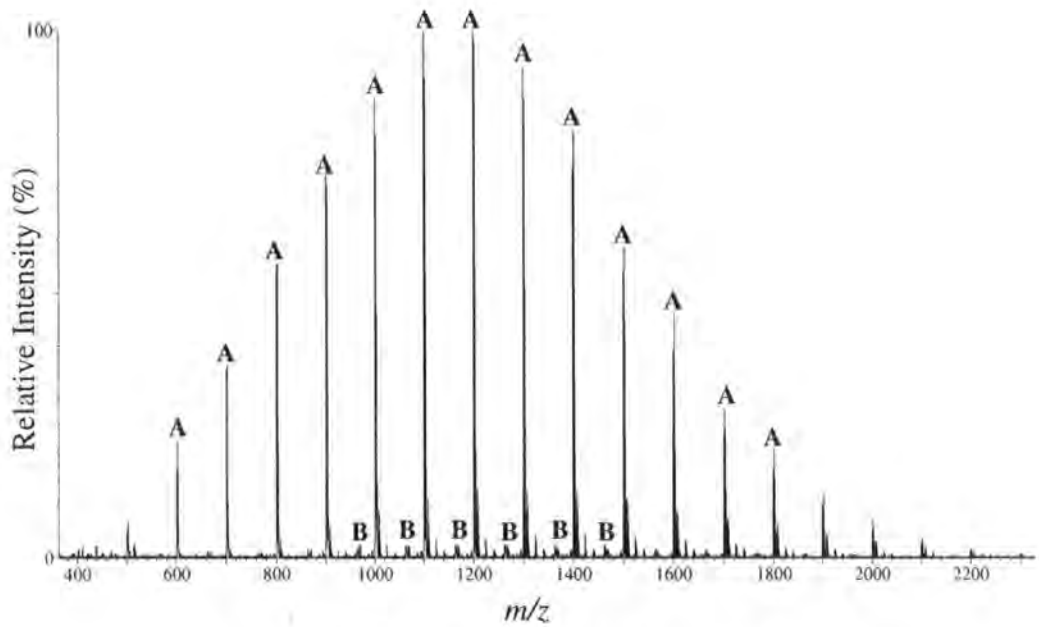

Figure 2.2.13. Reflectron MALDI spectrum of *1*.

For lower molecular weight oligomers, isotopic resolution of the peak due to a particular species was achieved. In an analogous fashion to the comparison of observed and calculated mass values for the entire distribution, isotopically resolved peaks can be used as a '*fingerprint*' for sample stoichiometric formula confirmation, when compared with the theoretical isotope distribution for that particular oligomeric species. Such a comparison for series **A** revealed some very interesting and surprising data. When considering the peak for the decamer, as shown in Figure 2.2.14, both distributions match, in terms of both mass value and relative intensity, from the 100% ^{12}C peak at 1102.23 amu, the peak for species containing one ^{13}C at 1103.16 amu, and so on for higher masses. However, two extra peaks are visible in the observed spectrum, occurring approximately 1 and 2 amu less than the ^{12}C peak (labelled *). It is highly unlikely that these peaks are due to the cationisation of *1* by a different ion, as there are no singly charged ions that would draw a parallel with these mass values. It is also not possible for these peaks to correspond to multiply charged species of higher mass oligomers, as the peaks are not separated by 0.5 amu. Therefore, these extra peaks must be the product of some mass loss from the $[1+H]^+$ molecule ions, either by fragmentation or elimination. As the difference is only 2 amu (we can safely assume that the peak betwixt these two is the one ^{13}C containing species of the loss product) and fragmentation is rarely observed within the MALDI experiment, the loss most likely corresponds to the elimination of molecular hydrogen ($H_2(g)$). The question arises as to the source of this elimination?

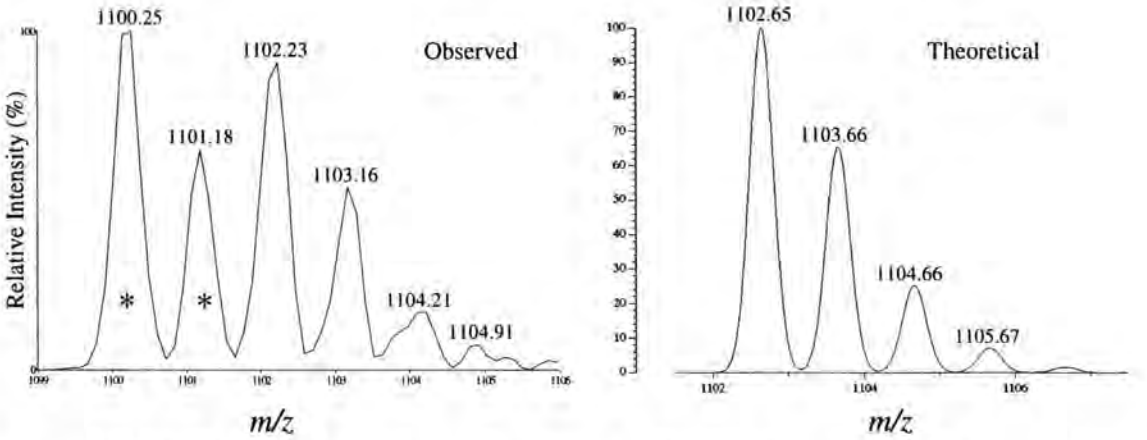

Figure 2.2.14. Observed and theoretical isotope distributions for the decamer of *1*.

To help answer this question, another may be asked. Are similar peaks observed in the reflectron spectrum for *2*? The reflectron MALDI spectrum for *2* is pictured in Figure 2.2.15, and contains two series of peaks, **A** and **B**, corresponding to the $[2+Li]^+$ species and the self-terminated analogue respectively.

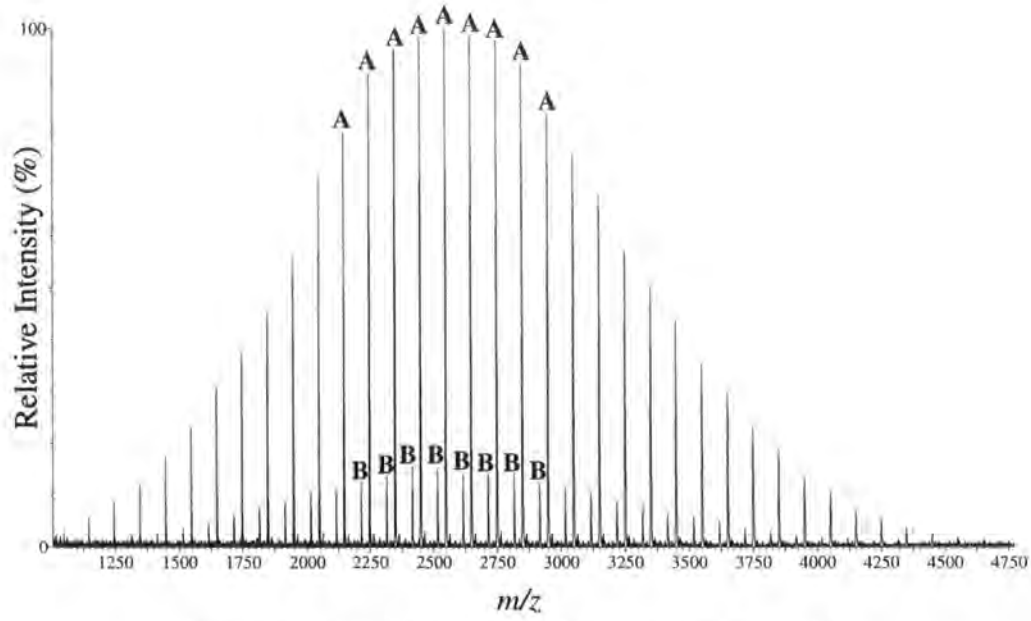

Figure 2.2.15. Reflectron MALDI spectrum of *2*.

A comparison of the series **A** peaks for the n = 13 oligomer with the relevant theoretical isotope distribution is shown in Figure 2.2.16. Both distributions clearly match each other, with the small peak at 1544.76 amu corresponding to *2* being cationised by ^6Li, the next peak at 1545.87 amu corresponding to a mixture of the species containing one ^{13}C being cationised by ^6Li and the 100% ^{12}C species being cationised by ^7Li, and so on for higher masses. There was no sign of the extra peaks that were observed in the spectrum of *1*. This observation strongly suggests that the amine end-group is involved in the elimination of H_2 from *1*, as the initiator end-group is the only difference between *1* and *2*. As a proton cannot cationise *2*, and protonation is the major form of cationisation for *1*, both the cation and the mode of cationisation are most probably connected with the elimination.

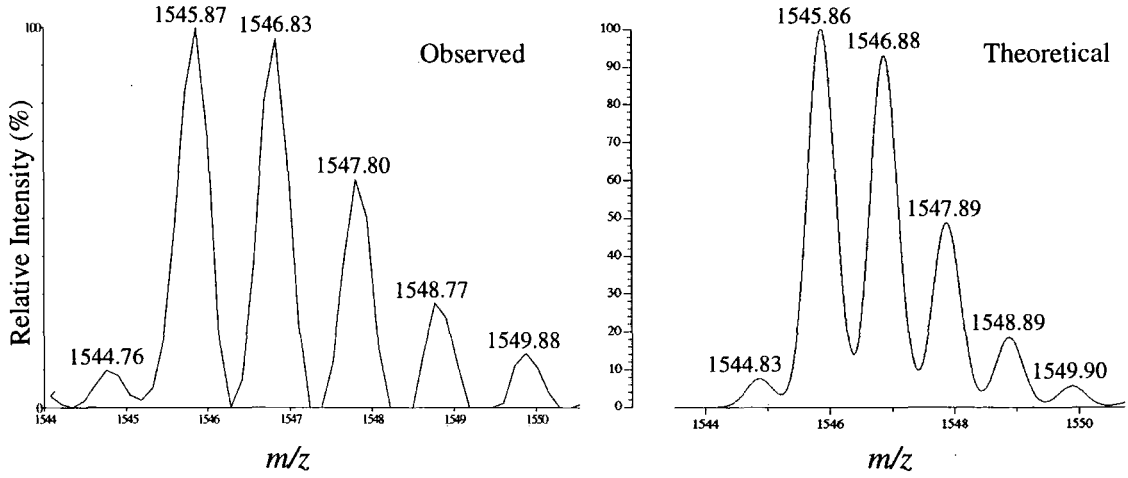

Figure 2.2.16. Observed and theoretical isotope distributions for *2* (n = 13).

The elimination may not be solely due the amine end-group. Gas-phase conformation studies of PMMA cationised by Na^+, using ion chromatography instrumentation, have shown that the polymer adopts a U-shaped, horseshoe conformation, with the metal ion interacting with multiple carbonyl oxygen atoms at both ends of the chain.[7] Even though it is believed that the cationising proton is binding to the nitrogen of the initiator, the other terminating end-group and the backbone structure may be involved in the mechanism of the elimination. A comparison of the observed peak for the n = 12 oligomer of *3*, with the relevant theoretical isotope distribution, is shown in Figure 2.2.17. Once more, the two extra peaks were recorded; hence the process that results in their formation appears to be independent of the nature of the terminating end-group.

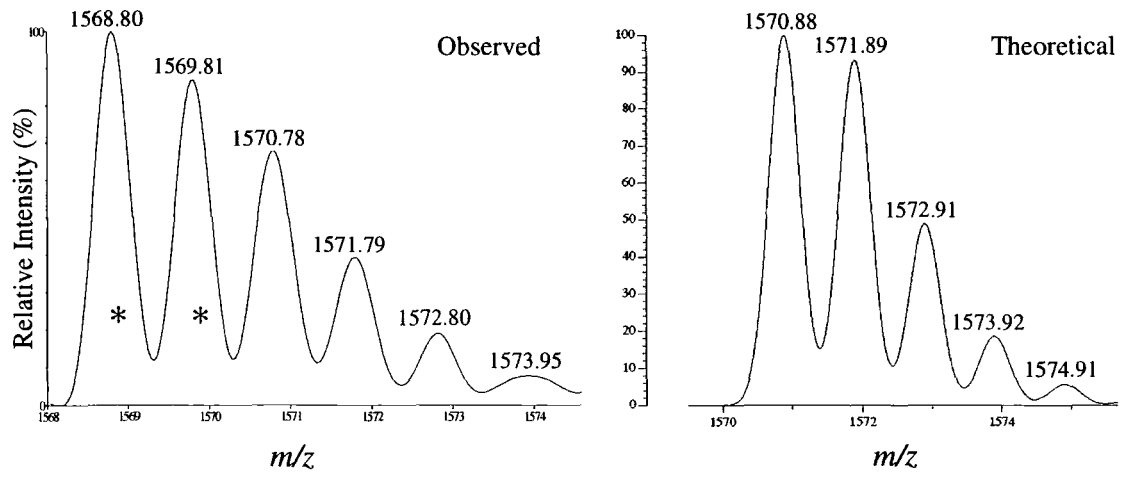

Figure 2.2.17. Observed and theoretical isotope distributions for *3* (n = 12).

In order to assess the influence of backbone structure on this elimination, attempts were made at initiating styrene with LDA, but without success. However, styrene has been successfully polymerised by other amine containing initiators and these samples have subsequently been analysed via MALDI.[8] While straightforward MALDI data showed proton and Cu^+ cationisation without any extra peaks being visibly obvious, MALDI-CID-MS spectra gave peaks for products of eliminations involving Cu^+ and the amine moiety. In this case, it was proposed that Cu^+, bound to a phenyl ring of the polymer backbone, interacted with the amine end-group, so eliminating copper (I) hydride (CuH) and transferring the positive charge to the nitrogen, which results in a immonium ion end-group. The ability of the nitrogen to hold the positive charge stable lends further weight to this elimination mechanism. A similar phenomenon may occur with LDA initiated samples, although the charge is already located on the nitrogen. If this has high stability, then why is elimination observed?

MALDI-CID data was gathered for *1*, to consider the amine end-group individually, and possibly explain the origins of the extra peaks observed. The peak at 1000.62 amu, which corresponds to the 100% ^{12}C nonamer elimination species, was selected for MALDI-CID analysis. The resulting fragmentation spectrum is shown in Figure 2.2.18. The spectrum was expected to give us several peak series, **A-G**, due to main chain bond scissions from either chain-end (series **A** and **B**), as well as mid-chain rearrangement processes (series **C-G**), the mechanisms for which are given elsewhere.[9] Unfortunately, even though several peak series were observed, none corresponded to **A-G** series. The initial loss from the base peak to the peak at 958.60 amu equals a C_3H_6 fragment, which could correspond to the elimination of a propene group from the amine end-group. The peak at 926.57 amu corresponds to a further loss from the peak at 958.60 amu of CH_3OH, due a hydrogen rearrangement process. The peak at 898.56 amu is also due to a further loss from the peak at 926.57 amu, this time corresponding to methyl methanoate (HCO_2CH_3). All other major peaks in the spectrum correspond to consecutive losses of either CH_3OH or HCO_2CH_3. These data fit with being derived from a sample of PMMA, but reveal nothing about the nature of the end-groups.

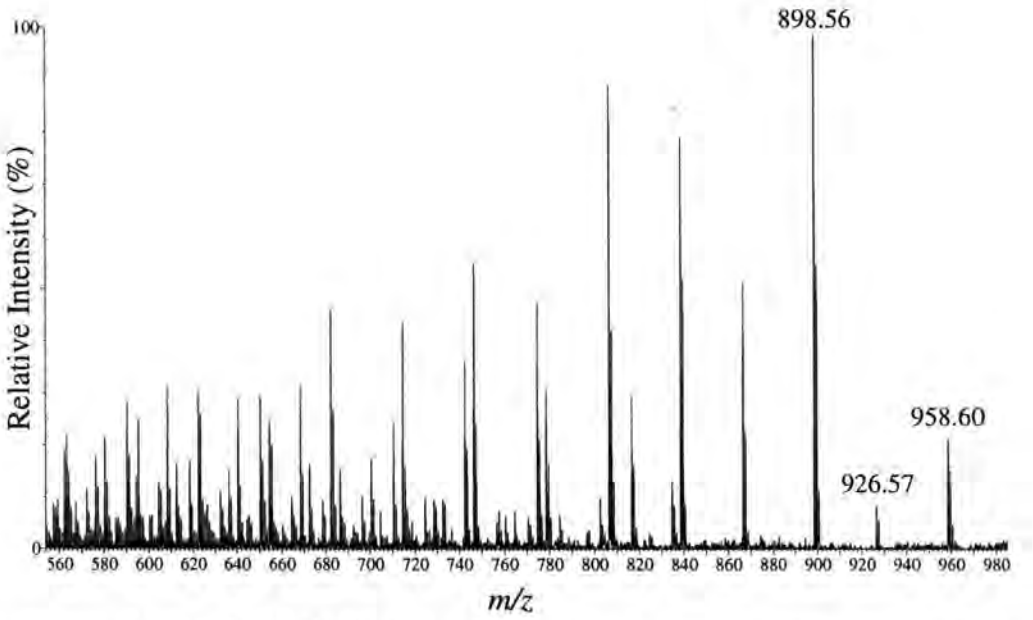

Figure 2.2.18. MALDI-CID spectrum of post-elimination nonamer of *1*.

Assuming that the charge is localised upon the nitrogen atom, how might the elimination of H_2 be accounted for? According to the literature,[10] cationised amines in the gas phase generally eliminate in one of two ways: a) loss of an alkene, and b) loss of ammonia or an alkyl amine. Neither of these pathways can explain a 2 amu loss, but what about the loss of 102 amu? The alkene elimination mechanism, involving proton transfer from a β-carbon with the formation of an ammonium ion, would explain the observed loss of propene in the MALDI-CID spectrum of *1*, but cannot be used to rationalise a loss of 102 amu. To lose the entire end-group as diisopropylamine leaving a primary carbocation not only leaves the least stable cation, but is also a loss of only 100 amu. The resultant peaks in the spectrum would overlap with those of the original species. 1,2-elimination of protonated amines tends to result in the formation of CH_4, or a higher alkane, and an immonium ion species. Given the stoichiometric formula of *1*, a loss of CH_4 would be expected. A 1,2-elimination resulting in H_2(g) is usually only observed with the $CH_3NH_3^+$ species. Therefore, in order to rationalise the extra peaks observed, a mechanism for a 1,2-elimination of H_2(g) is proposed. This mechanism also enables the subsequent elimination of propene, fitting with the recorded CID data. The proposed mechanism is illustrated below, in Figure 2.2.19.

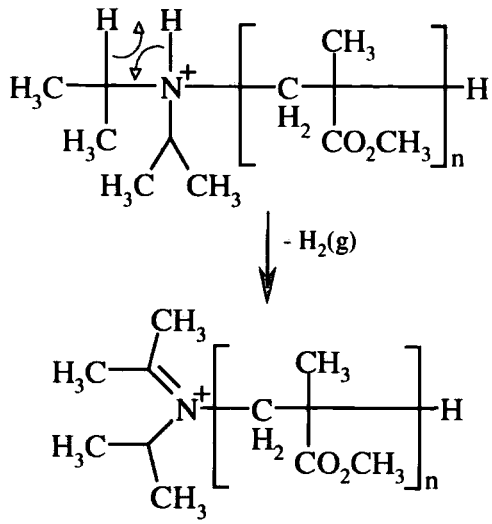

Figure 2.2.19. Proposed mechanism for H_2(g) elimination from *1*.

More recently, this sample was revisited and MALDI data collected with *all-trans*-retinoic acid being employed as the matrix. An expansion of the reflectron spectrum showing the peaks of the n = 10 oligomer, for both proton and Li^+ cationised species, is given in Figure 2.2.20. Although the peaks due to the elimination product are visible, they are not the major species, as was observed when dithranol was used as the matrix. With the change of matrix, cationisation of the sample was obtained with a lower, and therefore less energetic, laser power. Due to this '*softer*' form of ionisation, the elimination reaction appears to have been suppressed to some extent. Additionally, there is a further remarkable aspect to this spectrum, when the whole distribution is viewed. For a lithiated sample, the $[1+H]^+$ species dominates the $[1+Li]^+$ species. However, as we proceed to higher masses the relative intensities of each species start to equilibrate, with the peaks of each species for the n = 10 oligomer being approximately equal, as shown in Figure 2.2.20. As we proceed to even higher masses, $[1+Li]^+$ molecule ions become the dominant species. This observation may be explained by considering that smaller oligomers may not easily adopt a U-shaped, horseshoe configuration required for the binding of Li^+, so protonation prevails. Conversely, larger chains can more readily adopt this configuration, so cationisation via Li^+ prevails.

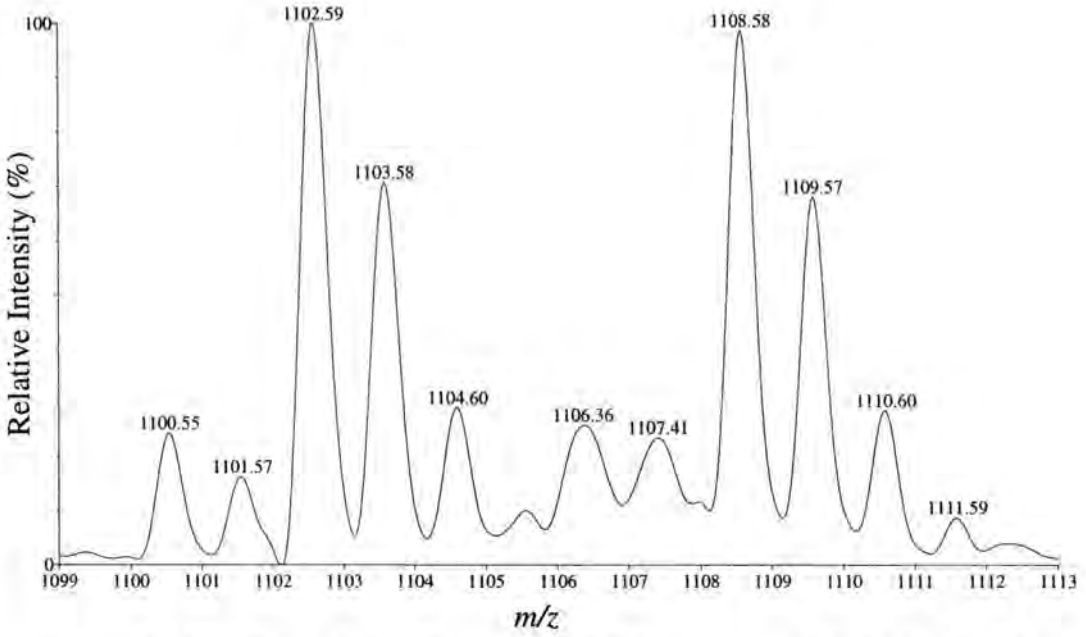

Figure 2.2.20. Expanded relfectron MALDI spectrum of *1* obtained with *all-trans*-retinoic acid.

In conclusion, two proton-terminated PMMA samples were synthesised using LDA and DPHLi initiators (*1* and *2*), while a third sample (*3*), initiated by LDA, was allowed to self-terminate. MALDI results further confirmed the stoichiometric formulas of all three samples, already proven by other analytical techniques. The spectra for LDA initiated samples were found to contain extra peaks as the dominant species, which could not be readily accounted for, but which were suspected to be the result of an elimination process associated with the amine end-group of the initiator. MALDI-CID data failed to reveal more information regarding the origin of these extra peaks. A mechanism was proposed as to their origin, based upon what could be fitted to the observations. Analysis with a different matrix at lower laser energies produced a spectrum that mostly contained peaks of intact species, which indicates that the elimination is an effect of the MALDI analysis.

2.3 Capping Reactions Involving DPE

The synthesis of each individual polymer, gives that polymer unique characteristics in terms of molecular weight and polydispersity. This makes the comparison of end-group data from MALDI analysis for different polymers more complicated, as these variables must be taken into account. In order to make direct

comparisons, the strategy focussed on splitting a living polymer solution into aliquots and end-capping each aliquot with a different functionality, providing polymers with identical values of molecular weight and polydispersity, but different end-groups. Three aliquots of the same polymerisation were to be capped with DPE + CO_2(g) (Sample *4a*), DPE (Sample *4b*), and CO_2(g) (Sample *4c*), to give the stoichiometric formulas shown in Figures 2.3.1-3 respectively.

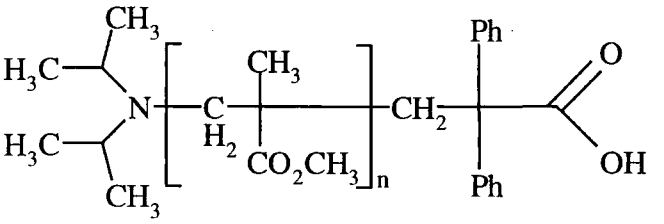

Figure 2.3.1. Stoichiometric formula of *4a*.

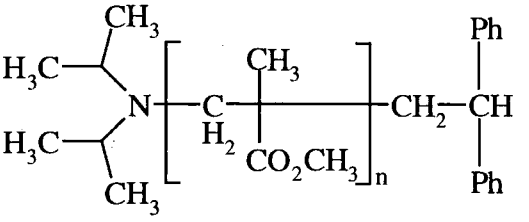

Figure 2.3.2. Stoichiometric formula of *4b*.

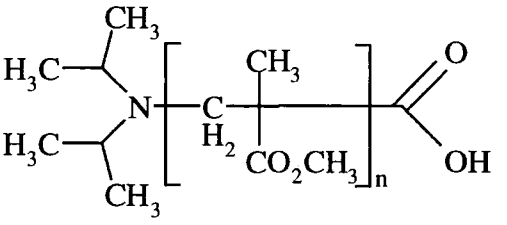

Figure 2.3.3. Stoichiometric formula of *4c*.

Although the diphenylmethyl anion is an efficient initiator of MMA, its reactivity is comparable with that of the methacrylic anion. It was considered possible that the active chains would react with DPE to give the diphenylmethyl anion, and thus the chains could remain active at a higher temperature with the steric bulkiness of the phenyl rings preventing self-termination. This would then permit a wider range of additional functionalisations to be explored.

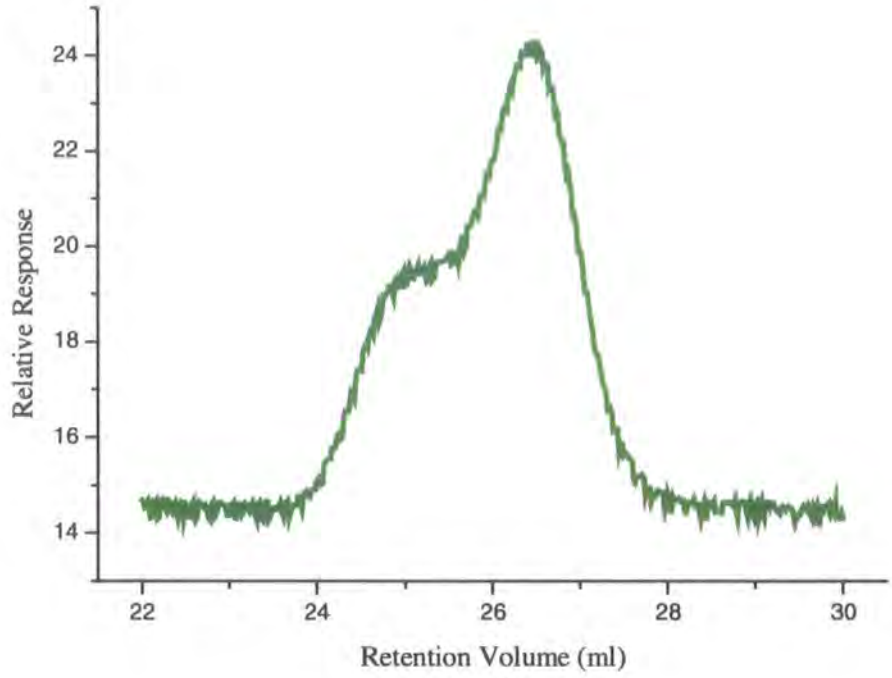

Figure 2.3.4. SEC trace of *4a*.

The SEC trace for *4a* (see Figure 2.3.4) has a shoulder towards lower retention volumes and shows that this polymer is not monomodal. The initiator is definitely a single species, so this observation means that all chains were not initiated at the same time. This result can be explained by considering the actual action of initiation for this polymerisation. The polymerisation was performed on a larger scale than normal as the resultant polymer was to be divided. For such a low target molecular weight, 7.29 ml of initiator was required, which meant using a 10 ml capacity syringe. The gas-tight seal on this particular syringe is tighter than that for lower capacity syringes, which are used more frequently. Hence, injection of the initiator required a substantial amount of strength, and so it is entirely possible that the initial grip of the syringe was not ideal and it was necessary to pause and re-grip the syringe. Therefore, injection was not one continuous process and the pause was long enough to allow active chains to grow substantially, before the remainder of the chains could be initiated. The result would be a proportion of chains with a slightly higher molecular weight than rest, which would show as a shoulder towards lower retention volumes on a SEC trace. This spread of chain size naturally increases the polydispersity of the sample. Similar shoulders were noted on the traces for *4b* and *4c*, indicating that this result is a product of the

polymerisation process and not related to any of the functionalisations. The molecular weight data for these samples is given in Table 2.3.1.

Sample	$\overline{M}_n$	$\overline{M}_w$	$\overline{M}_w / \overline{M}_n$
4a	2190	3360	1.53
4b	2370	3620	1.53
4c	2110	3420	1.62
5	3220	3460	1.07
6	2440	2820	1.16

Table 2.3.1. SEC molecular weight data for *4a-6*.

The absence of a deep-red colouration, typical of the diphenylmethyl anion, was noted during the synthesis. In the proton NMR spectrum for *4a*, we would expect to see peaks between δ = 7.1-7.3 ppm due to the phenyl rings of the terminal end-group, in addition to peaks from the initiator and polymer chain. However, these peaks were not present in the spectrum, indicating that the reaction of methacrylic anions with DPE was unsuccessful. Absent also is the peak for the carboxylic acid proton at very low field, though this signal may not be observable, due to chemical exchange. In fact, the spectrum very closely resembles that for *3* (see Figure 2.2.9), hence the most likely scenario is that when the polymerisation was allowed to warm to room temperature prior to the addition of CO_2(g), the chains self-terminated via the backbiting reaction. Had the DPE reacted, the backbiting reaction would have been prevented, and the CO_2(g) would have been able to add to the chain.

As the splitting of the polymerisation into aliquots *4a* and *4b* was subsequent to the supposed reaction with DPE, the proton NMR for *4b* is also very similar to that for *3*, as anticipated. The major differences expected between the proton NMR for *4c* and that for *1* are the lack of a peak at δ = 2.5 ppm corresponding to the terminating methine proton, and a peak for the carboxylic acid proton, which has already been discussed. Neither signal was observed and the spectrum also looks like that of a self-terminated polymer. This result is not easily explainable, as this portion of the polymerisation was not allowed to warm up until after the reaction with CO_2(g) and subsequent addition of N_2-sparged CH_3OH. Even if the methacrylic anions had not reacted with the gas, proton termination should have been the more prevalent termination mechanism.

Carbon NMR is of little use in this case, as the signal for the acid carbonyl would be found in a very similar position to those of the pendant ester carbonyls. Thus, the NMR evidence indicates that none of these samples has its anticipated stoichiometric formula.

MALDI analysis was performed on samples *4a-4c* without the addition of a salt. The reflectron spectrum of *4a*, shown in Figure 2.3.5 below, contained only one series. A comparison of the observed masses with those calculated for $[4a+H]^+$ can be found in Table 2.3.2 and these strongly contradict each other. This result was not surprising, given the evidence for non-reaction previously gleaned from NMR. The observed values correlate with $[3+H]^+$ molecule ions, confirming the earlier conclusion drawn from the NMR spectra, *i.e.* the backbiting reaction was the major form of termination. Similarly, the spectrum for *4b* also showed a single series and the comparison of observed and theoretical masses, for $[4b+H]^+$ molecule ions, strongly disagreed (see Table 2.3.2). Again, the observed values correlate with $[3+H]^+$ molecule ions, and the same conclusions can be drawn as for *4a*.

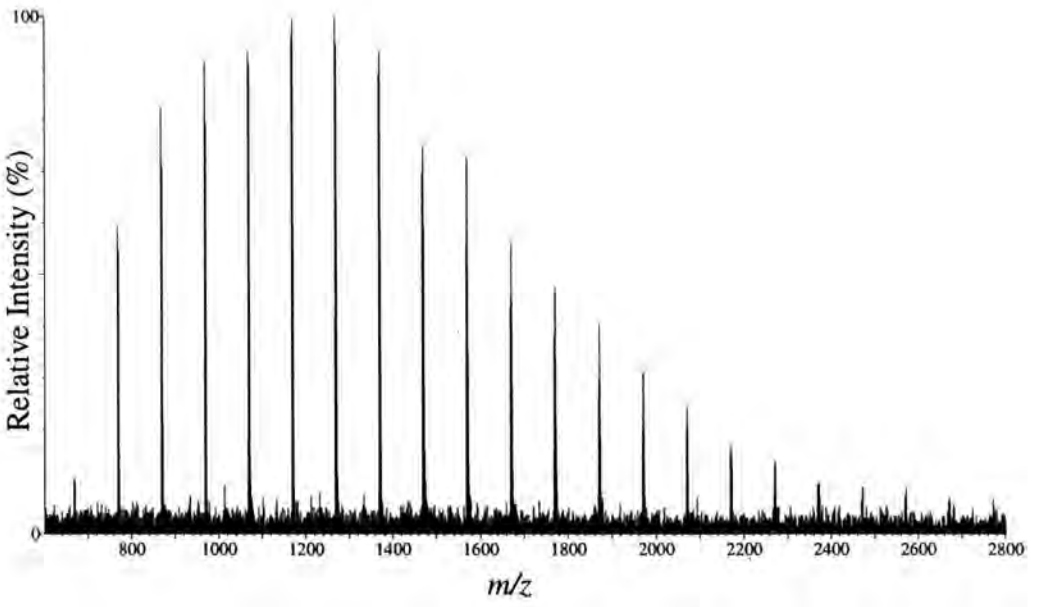

Figure 2.3.5. Reflectron MALDI spectrum of *4a*.

4a and $[4a+H]^+$			*4b* and $[4b+H]^+$			*4c* (**C** and $[4c+H]^+$)		
n	Obs.	Calc.	n	Obs.	Calc.	n	Obs.	Calc.
4	771.91	726.94	5	872.89	783.04	4	546.90	546.68
5	871.96	827.05	6	973.06	883.16	5	647.57	646.80
6	972.24	927.17	7	1073.43	983.28	6	747.99	746.92
7	1072.45	1027.29	8	1173.68	1083.40	7	848.32	847.04
8	1172.73	1127.41	9	1273.91	1183.52	8	948.41	947.16
9	1272.99	1227.53	10	1374.20	1283.64	9	1048.81	1047.28
10	1373.18	1327.65	11	1474.26	1383.75	10	1149.20	1147.40
11	1473.12	1427.76	12	1574.56	1483.87	11	1249.36	1247.51

Table 2.3.2. Average observed and calculated mass comparisons for *4a-4c*.

The reflectron spectrum for *4c* is shown in Figure 2.3.6 and contains three series, **A-C**. From NMR, we expect the major species to be the product of self-termination, indeed **A** was found to correspond to $[3+H]^+$ molecule ions following mass value comparisons. Similar mass comparisons revealed that **B** was due to the presence of $[1+H]^+$ species within the sample, most likely termination via CH_3OH added after the CO_2(g). Therefore, active chains were present, and so were at least available for reaction, when CO_2(g) was introduced. Did **C** correspond to a carboxylated species? Mass comparisons between **C** and $[4c+H]^+$ molecule ions, given in Table 2.3.2, were indeed found to be in very close agreement, thus indicating partial functionalisation had occurred. The presence of both $[1+H]^+$ and $[4c+H]^+$ species suggests that not enough time was allowed for the capping reaction to proceed. The fact that the major species is self-terminated polymer highlights the difficulties encountered during the synthesis in keeping '*alive*' each of the living polymer aliquots. Efforts were made to try to ensure that the intervening glassware between the main vessel and side-bulb was kept as cold as possible with the application of N_2(liq) and dry ice, which subsequently proved insufficient. An alternative might be to submerge the entire vessel in a dry ice/acetone bath, though this is not practical, as septa would become brittle and may crack causing leaks and therefore disadvantageous termination, and Young's taps would shrink with similar consequences. Nevertheless, it is possible to cap PMMA with CO_2(g) and to identify the product easily via MALDI, which is explored further in Section 2.5.

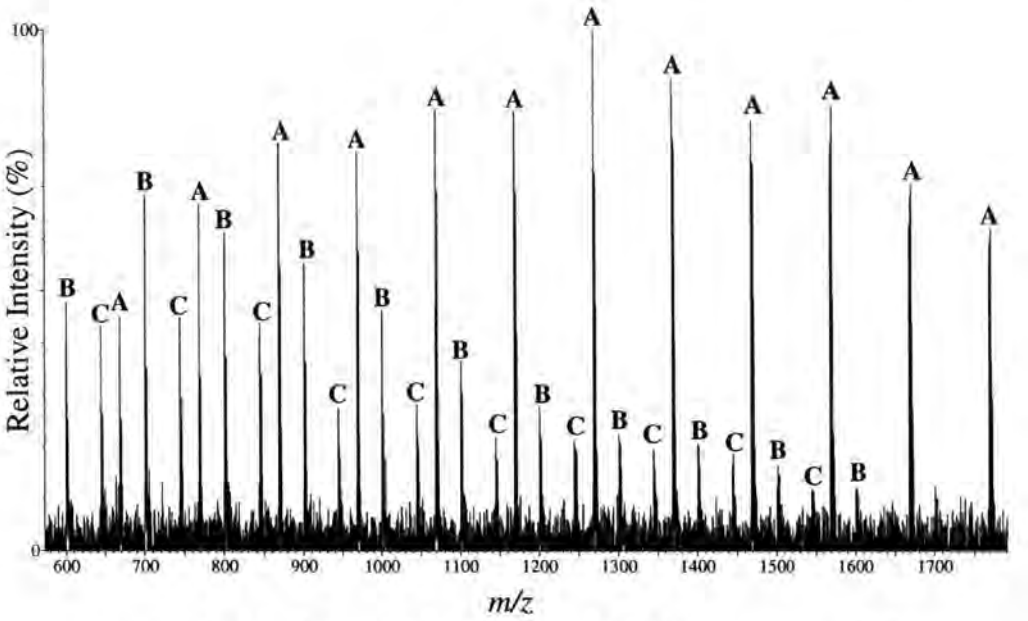

Figure 2.3.6. Expanded reflectron MALDI spectrum of *4c*.

A number of potential factors can be cited for the failure of the DPE capping reaction: i) the rate of the capping reaction might be very slow; ii) the polymerisation temperature was too low for the capping reaction; iii) the reaction simply does not proceed. The functionalisation with DPE alone was reattempted with a longer capping reaction time (Sample *5*). Again the lack of deep-red colouration was noted and both proton NMR and MALDI spectra gave identical results to that for *4b*, *i.e.* no reaction with DPE had occurred. The same functionalisation was attempted with an even longer capping reaction time and the living solution was only allowed to warm to room temperature at an extremely slow rate (Sample *6*). This was done to allow for the dual possibilities that the rate of reaction could be slow, and the initial reaction temperature was too low. A balance temperature was being sought, high enough to allow the capping reaction, low enough to suppress the backbiting termination reaction effectively. Once more the same results were obtained, the functionalisation being unsuccessful. The molecular weight data derived from SEC analysis for *5* and *6* are given in Table 2.3.1.

To summarise, a PMMA polymerisation was divided into three aliquots, with the capping of each aliquot with a different end-group, DPE + CO_2(g), DPE, and CO_2(g), being attempted. NMR and MALDI analysis proved that the first two of these reactions were unsuccessful, the third being only partially successful. Difficulties involving the division of the living solution were highlighted and these plus other

factors are given to explain the failure of these reactions. The capping reactions with DPE were attempted further, but without success.

2.4 Attempted Quaternisation and Sulphonation Reactions

Other members of the group have recently been working on the end-group analysis of α,ω-macrozwitterionic polystyrenes (PS) via SEC.[11] The synthesis of these polymers involves using an amine containing organolithium initiator, 2-[(dimethylamino)methyl]phenyllithium (DMPLi), and 1,3-propanesultone as the capping reagent, which gives a lithium sulphonate end-group.[12] The amino group of the initiator is subsequently quaternised with methyl bromide (CH_3Br). Differences in peak elution volume were noted between the SEC trace for functionalised and unfunctionalised samples of the same polymerisation, due to the interaction of the end-groups with the packing material of the SEC columns. This interaction caused the peak for the functionalised polymer to be shifted to a greater elution volume, *i.e.* lower molecular weight, and made it possible to determine the degree of functionalisation. Our aim was the transfer of these functionalisation reactions to a methacrylate system, which could be observed via SEC, and then undertake MALDI analysis of the samples. The lithium sulphonate end-group could also be converted to the sulphonic acid and the MALDI results from this compared with those for carboxylic acid terminated PMMA. MALDI data had already been successfully collected for the PS/polyisoprene samples.[12]

The DMPLi initiator used for the PS samples was considered too reactive to use for PMMA, giving rise to unwanted side reactions and lack of control of the polymerisation to the desired degree. Instead, the LDA initiator could be used, giving a tertiary amine end-group that could be quaternised afterwards. A sample of *1* was used to try out the quaternisation reaction using CH_3Br to give Sample *7* (stoichiometric formula given in Figure 2.4.1).

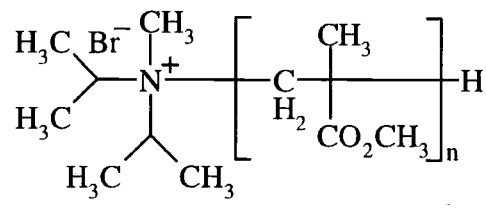

Figure 2.4.1. Stoichiometric formula of *7*.

Figure 2.4.2 shows the SEC traces of both *1* (red) and *7* (blue) for the purposes of comparison. We would expect the quaternary salt to interact with the column packing material in much the same way as the sulphonate salt. Therefore we would expect the peak for *7* to have a shifted to a higher retention volume compared to the peak for *1*. However, both traces give a peak at a retention volume of roughly 26.7 ml, which indicates that the quaternisation has not take place, though this evidence is far from conclusive. The molecular weight data for *7* are given in Table 2.4.1, and though these values differ slightly from those for *1* (see Table 2.2.1), they are well within the accuracy error range of the equipment, which is approximately 5%.

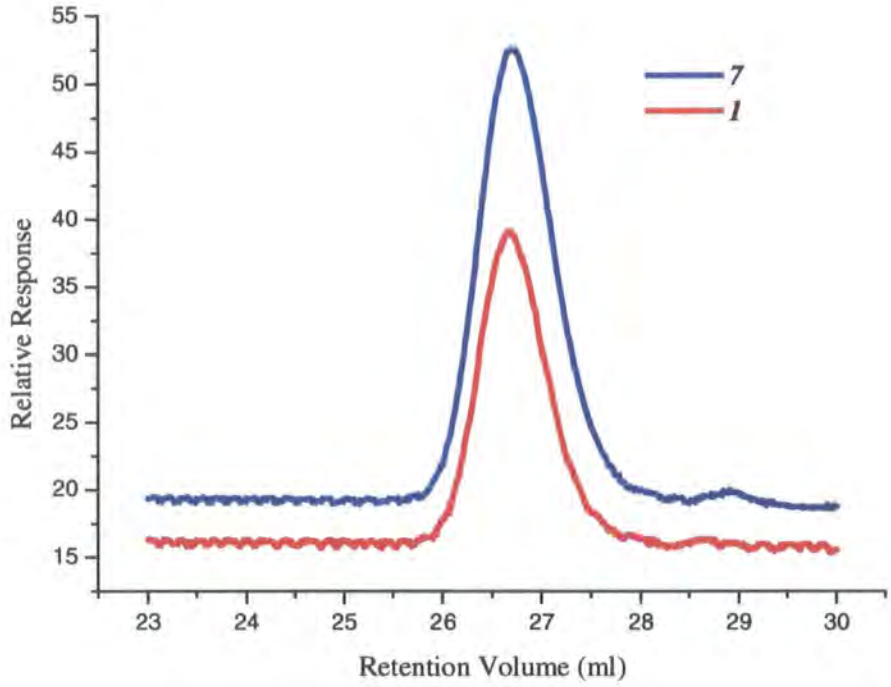

Figure 2.4.2. SEC traces of *1* and *7*.

Sample	$\overline{M}_n$	$\overline{M}_w$	$\overline{M}_w/\overline{M}_n$
7	1330	1510	1.14
8	3650	3670	1.01

Table 2.4.1. SEC molecular weight data for *7* and *8*.

The proton NMR spectrum for *7* would obviously be very similar to that for *1*, but we might anticipate seeing a peak between δ = 2.2-2.3 ppm for the ammonium

methyl group. Upon comparing the two spectra, no discernible difference could be noted. It is possible that this peak is hidden under the methylene backbone signals. The carbon NMR should also contain an extra peak for this group at around $\delta = 39$ ppm, but this is also missing. Elemental analysis of the sample revealed that bromide was not present in any quantity, and so all evidence thus far points to an unsuccessful quaternisation reaction. For completeness, MALDI analysis was run on the sample. Mass comparisons of the major series observed with values for both $[1+H]^+$ and $[7+H]^+$ molecule ions revealed a strong correlation with the former, as was expected following the results obtained via NMR and SEC. As the quaternary nitrogen of the end-group of *7* would no longer be available to bind a proton, a sample to which LiCl had been added was analysed, but the results continued to show $[1+H]^+$ molecule ions as the major species, along with $[1+Li]^+$ peaks of lower intensity. Hence, MALDI analysis further confirms that the quaternisation of the amine end-group was unsuccessful.

Therefore macrozwitterions of PMMA are not feasible using LDA as the initiator, but PMMA with a lithium sulphonate or sulphonic acid end-group, could still be investigated. Sultones are regarded as the classic reagents for the simple and direct sulphonation of polymeric organolithium compounds, with 1,3-propanesultone offering the highest functionalisation yields.[13] PS anions are capped with DPE prior to capping with the sultone, as this lowers the nucleophilicity of the anion, and, along with the increased steric bulk, prevents the unwanted competing sultone metalation reaction. We have already established that DPE will not cap PMMA anions, but as these ions already have a lower nucleophilicity than PS, this step of the procedure could be omitted. Hence, the sultone was added directly to a polymerisation after propagation to give the stoichiometric formula in Figure 2.2.3 (Sample *8*).

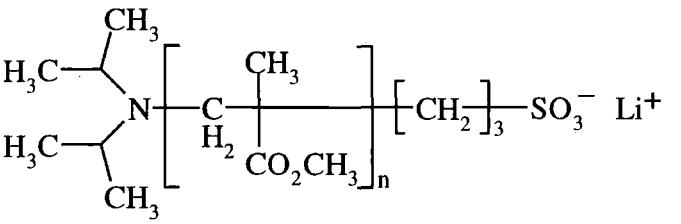

Figure 2.4.3. Stoichiometric formula of *8*.

The SEC trace for *8* showed only one peak, so either all or none of the polymer was functionalised. The value for molecular weight, given in Table 2.4.1, was not lower but higher than the target value, which is generally the case. This end-group

should just be detectable by NMR. The second and third methylene groups from the sulphur should appear at δ = 1.6 and 1.8 ppm respectively, and so would probably be masked by peaks from the backbone methylene groups. The first methylene group however, being directly bonded to the sulphur, will be shifted downfield, and should be found in a clear region of the spectrum at δ = 3.4 ppm or thereabouts. However, no such peak was recorded in the actual proton spectrum. Conversely, there is a peak at δ = 2.5 ppm, which would lead us to believe that the polymer is simply proton terminated. Three extra peaks for the methylene groups are also lacking in the carbon NMR spectrum. Elemental analysis of the sample revealed that no sulphur was present in any quantity, and so all evidence thus far points to an unsuccessful sulphonation reaction. MALDI analysis gave a peak series that again corresponded to $[1+H]^+$ molecule ions and not those for $[8+H]^+$, or even $[8+Li]^+$ for lithiated samples. No spectrum was observed when this sample was analysed with the spectrometer running in negative ion mode. All the evidence points towards an unsuccessful capping reaction.

In conclusion, the analytical evidence of MALDI and other techniques confirms that neither quaternisation nor sulphonation reactions were completed. When considering the quaternisation reaction, the reason for failure may be that the nitrogen is too sterically hindered, due not only to the amine being tertiary, but also because the amine substituents themselves have substituents. The amine group of the DMPLi initiator used with PS was primary. Reaction temperature, as with previously considered reactions, may also not be high enough to encourage the reaction. This could also be true for the reaction with 1,3-propanesultone. Additionally, although methacrylic anions are comparable in reactivity to diphenylmethyl anions, as with the reaction with DPE seen previously, their reactivity may not be sufficient to ring-open the sultone.

2.5 Capping Reactions Involving CO_2(g)

As the capping reaction with CO_2(g) alone was shown to work in part for Sample *4c*, this reaction was revisited. This was for several reasons: a) to determine if the capping reaction was quantitative, b) to determine if both the lithium salt and acid forms of the end-group could be isolated, and c) to investigate interconversion reactions of the carboxyl group as a strategy for extending the range of PMMA end-groups. The latter point was doubly interesting, as success would not only give samples with

different end-groups, but also these samples would have identical molecular weight characteristics, thus allowing direct end-group comparisons via MALDI.

Following the capping reaction with CO_2(g), N_2-sparged dilute HCl(aq), CH_3OH and glacial acetic acid was added to Samples *9-11* respectively. The molecular weight data for *9-11* is given in Table 2.5.1.

Sample	$\overline{M}_n$	$\overline{M}_w$	$\overline{M}_w/\overline{M}_n$
9	1580	1910	1.21
10	2400	2550	1.06
11	1630	1820	1.12
12	2410	2600	1.08
13	2440	2830	1.16
14	2480	2630	1.06
15	1970	2110	1.07
16	2020	2150	1.06

Table 2.5.1. SEC molecular weight data for *9-16*.

As mentioned earlier, neither proton nor carbon NMR provides strong evidence for the presence of the carboxylate end-group. Elemental analysis for lithium, in order to provide evidence for the salt form of the end-group, was marred by the presence of residual lithium salts from the synthesis. However, evidence for the presence of an acid end-group was gained by titration with base solution using phenolphthalein as the end-point indicator. Functionalisation was $\geq 95\%$ for all three samples.

The end-groups were confirmed as carboxylic acids in each case by MALDI analysis. For example, an expansion of the reflectron spectrum for *11*, showing the peak of the decamer, is featured in Figure 2.5.1. Comparisons between observed and calculated peak masses revealed that all three samples consisted of acid end-groups, and no peaks due to the lithium carboxylate salt were recorded. Peak masses accurately corresponded to the $[4c+H]^+$ species, so each sample has the same stoichiometric formula as that given previously for *4c* in Figure 2.3.3. This result proves that HCl(aq), CH_3OH and glacial acetic acid are all capable of protonating the carboxylate anion. The extra peaks associated with polymers initiated with LDA are also observed. No

spectrum was observed when these samples were analysed with the spectrometer running in negative ion mode.

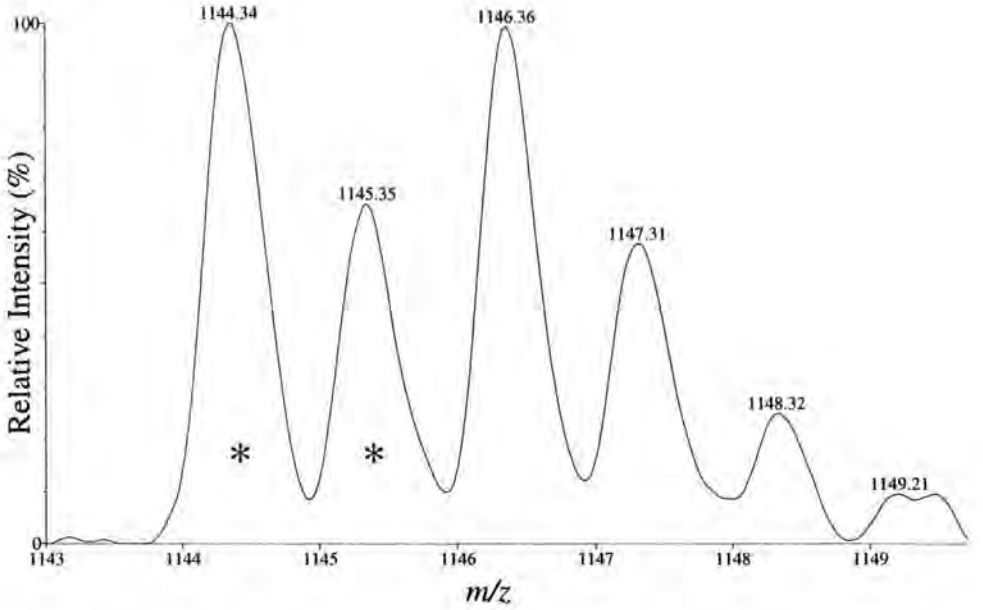

Figure 2.5.1. Expanded reflectron MALDI spectrum of the decamer of *11*.

The first functional group interconversion reaction of the carboxylic acid end-group to be attempted was to produce an acid chloride end-group. Thionyl chloride ($SOCl_2$) is a common reagent for this reaction, but the question arose as to whether or not pendant methyl esters would also be converted to the acid chloride. However, $SOCl_2$ exhibits low reactivity towards methyl esters,[14] so an undesirable side reaction would be avoided. Therefore a sample of *10* was reacted with $SOCl_2$ to give Sample *12*, the stoichiometric formula being given in Figure 2.5.2.

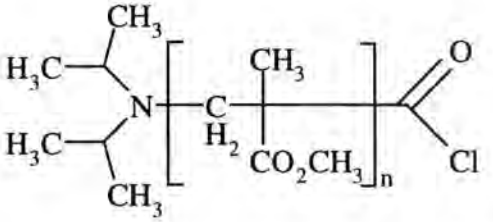

Figure 2.5.2. Stoichiometric formula of *12*.

As the anticipated end-group did not contain any protons, proton NMR was of no value, and no evidence for the carbonyl of the end-group could be found in the carbon NMR spectrum. Elemental analysis also gave a negative result for the presence

of chlorine in the polymer. Precautions against the possible hydrolisation of the acid chloride had been taken, and therefore it was assumed that the reaction had failed. The reaction was repeated under slightly different conditions, providing Sample *13*, but subsequent analysis gave exactly the same results as for *12*. The SEC data for both *12* and *13* are given in Table 2.5.1 above.

No evidence for the successful production of an acid chloride end-group was found in the MALDI spectra for either *12* or *13*. The linear spectrum for *12*, shown in Figure 2.5.3, has two main series, **A** and **B**. A peak mass comparison between values for series **A**, and the theoretical $[\mathit{12}+H]^+$ species, reveals obvious disagreement (see Table 2.5.2). The observed values for **A** actually correspond to the acid-functionalised starting material, while those for **B** have close correlation with the $[\mathit{1}+H]^+$ species. The presence of starting material suggests that the reaction was left for too short a time to achieve completion, at the reaction temperature of 40°C. This temperature might be considered too low to allow any reaction to proceed at all, but the presence of the $[\mathit{1}+H]^+$ species indicates that some sort of reaction has taken place, if not the actual one intended. The formation of an acid chloride species, followed by decomposition to give a species apparently terminated by a proton, may explain these results. With the repeated reaction being carried out at a higher temperature, namely 60°C, peaks due to *10* were not expected in the MALDI spectrum for *13*, and this was indeed the case. With only one major series recorded, a peak mass comparison between the observed values, and those for the theoretical species $[\mathit{13}+H]^+$, again showed strong disagreement (see Table 2.5.2). The peaks correlated with to $[\mathit{1}+H]^+$ molecule ions, so the similar conclusions can be drawn here, as were for *12*.

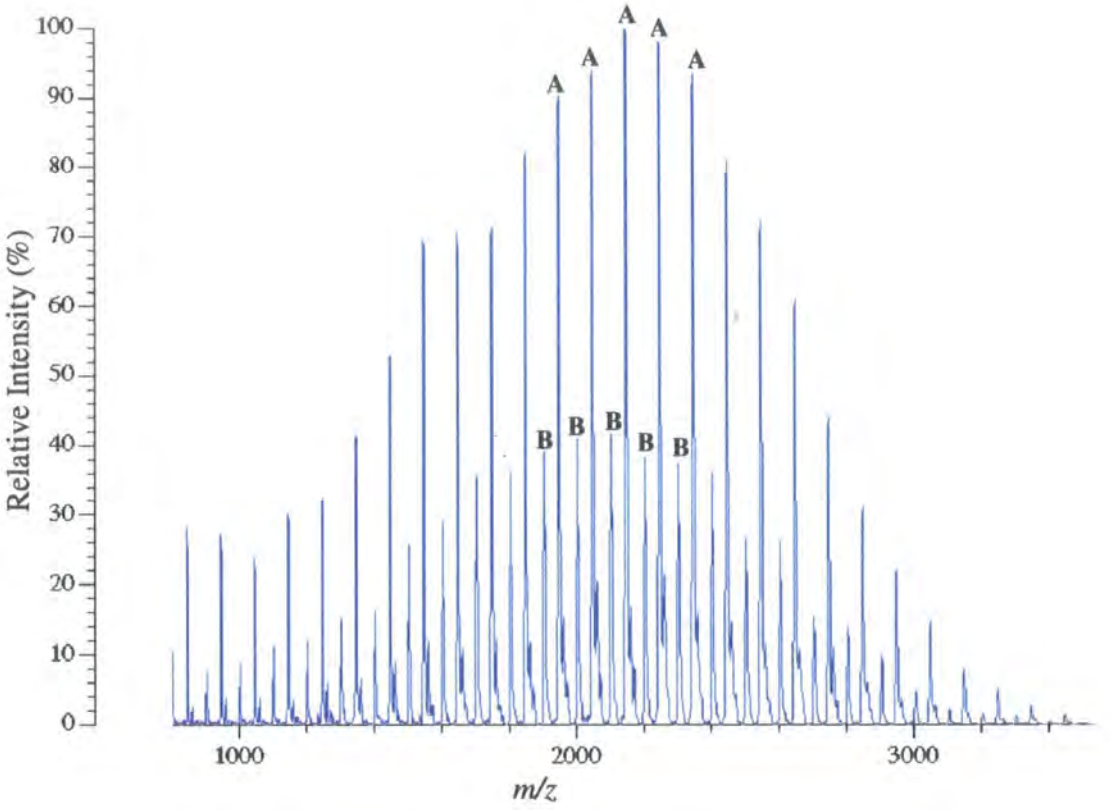

Figure 2.5.3. Linear MALDI spectrum of *12*.

12 (**A** and $[12+H]^+$)			*13* and $[13+H]^+$		
n	Obs.	Calc.	n	Obs.	Calc.
8	947.74	965.61	8	903.91	965.61
9	1047.90	1065.73	9	1003.73	1065.73
10	1147.93	1165.84	10	1103.75	1165.84
11	1248.00	1265.96	11	1203.78	1265.96
12	1348.06	1366.08	12	1304.04	1366.08
13	1448.29	1466.20	13	1403.98	1466.20
14	1547.94	1566.32	14	1504.29	1566.32
15	1648.15	1666.43	15	1604.69	1666.43

Table 2.5.2. Average observed and calculated mass comparisons for *12* and *13*.

Colleagues have recently been utilising the selective reactivity of *N,N'*-carbonyldiimidazole (CDI) in their synthetic strategies. A similar strategy was adopted for the interconversion of the carboxylic acid end-group into other functional groups. CDI will selectively react with the acid end-group to form an acid imidazolide,

while being unreactive towards the pendant main chain ester groups.[15] The acid imidazolide can be then be used as an intermediate to a vast range of functional groups, including esters, aldehydes, ketones, amides and anhydrides. The acid imidazolide intermediate was in itself worthy of investigation by MALDI; hence an amount of *10* was reacted with CDI to give Sample *14*, the stoichiometric formula of which is depicted in Figure 2.5.4.

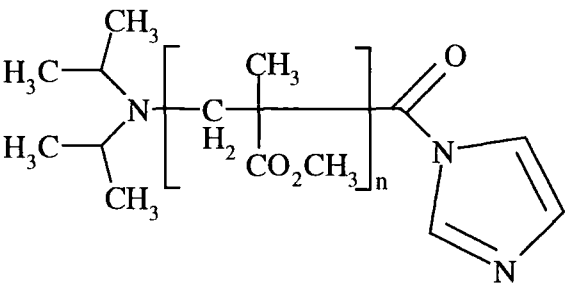

Figure 2.5.4. Stoichiometric formula of *14*.

The molecular weight data for *14* is given in Table 2.5.1 above. The three protons of the imidazole ring should be easily identified in the aromatic region of the proton NMR spectrum. This however, was not what was observed. There should also have been three peaks between δ = 120-140 ppm in the carbon spectrum, due to this ring. Instead, the spectra bore an extremely close resemblance to that of *1*. Further evidence for the polymer being proton-terminated was gained via MALDI, as the masses of the peak series again correlated more closely with the calculated masses for $[1+H]^+$ molecule ions, rather than those for the $[14+H]^+$ species (see Table 2.5.3). Evidently, what had happened to *13* had also happened to *14*. Although it is normally possible to isolate such compounds, it was considered that both the acid chloride and acid imidazolide end-groups might have been decomposing, thus preventing isolation.

14 and $[14+H]^+$			*15* and $[15+H]^+$			*16* and $[16+H]^+$		
n	Obs.	Calc.	n	Obs.	Calc.	n	Obs.	Calc.
14	1501.48	1597.93	14	1503.66	1637.99	14	1505.43	1589.95
15	1601.99	1698.05	15	1603.59	1738.11	15	1605.70	1690.07
16	1701.62	1798.17	16	1703.37	1838.23	16	1706.83	1790.18
17	1801.43	1898.28	17	1803.76	1938.35	17	1806.79	1890.30
18	1901.24	1998.40	18	1903.26	2038.47	18	1906.88	1990.42
19	2001.67	2098.52	19	2003.55	2138.58	19	2007.55	2090.54
20	2101.48	2198.64	20	2103.55	2238.70	20	2108.07	2190.66
21	2201.31	2298.76	21	2203.62	2338.82	21	2208.96	2290.78

Table 2.5.3. Average observed and calculated mass comparisons for *14-16*.

This result did not deter us from this synthetic strategy, as we moved on to experiment with the acid imidazole as an intermediate to an ester end-group. An acid imidazolide will react with primary and secondary alcohols to produce an ester. A sample of *11* was treated with CDI, followed by the addition *in situ* of benzyl alcohol ($PhCH_2OH$) to give *15*. This alcohol was chosen due to the ease with which the resulting ester could be identified. The stoichiometric formula for *15* is shown in Figure 2.5.5.

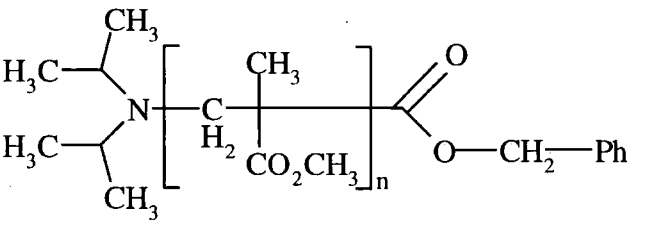

Figure 2.5.5. Stoichiometric formula of *15*.

Unambiguous signals in the aromatic region for both proton and carbon NMR should have been observed, but this was not the case, clearly signifying that the reaction had failed. The results again pointed towards a proton terminated polymer. Perhaps this particular alcohol, even though it is primary, is too bulky to access and react with the acid imidazolide, so leaving this group to decompose as before. Success may be achieved with a simple linear alcohol. The reaction was tried again, this time under

slightly different conditions and with *n*-propyl alcohol (*n*-PrOH), to give Sample *16*, whose stoichiometric formula can be found in Figure 2.5.6.

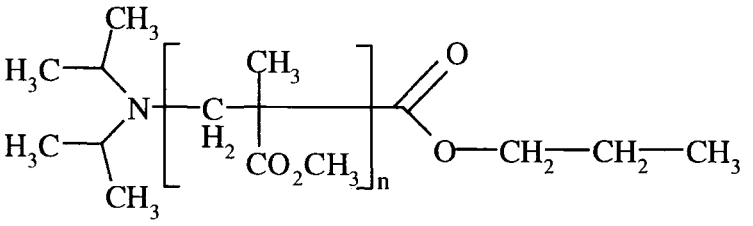

Figure 2.5.6. Stoichiometric formula of *16*.

Although proton NMR peaks corresponding to the methyl and central methylene of the end-group might be indistinguishable from other signals, the peak due to the oxymethylene is expected to occur around $\delta = 4.0$ ppm. These peaks were not detected, and neither were the correlating peaks in the carbon NMR spectrum, expected to be found at roughly $\delta = 10$, 23 and 69 ppm respectively. Yet again, the results said simply a proton was the end-group. MALDI analysis also provided evidence through comparison of observed and calculated masses, given in Table 2.5.3, that both *15* and *16* were proton terminated. The SEC data for both *15* and *16* is given in Table 2.5.1 above.

There had to be a fundamental reason as to why none of the carboxylic acid interconversion reactions were proceeding. Data for all samples indicated a proton terminated polymer, yet decarboxylation would normally not be expected under the relatively mild reaction conditions used. Investigation into the decarboxylation of carboxylic acids provided a highly probable answer. Carboxylic acid compounds that have a carbonyl moiety in a β-position relative to the acid readily undergo decarboxylation upon heating.[16] Previously, the backbone structure of these polymers had not been considered in conjunction with the acid end-groups. When this was done it was apparent that instead of working with just an ordinary carboxylic acid, these reactions had been attempted with a β-keto acid due to the carbonyl of the ultimate repeat unit in the chain. As all the reactions involved heat, it seems that decarboxylation of the acid is the reason why the reactions failed and the anticipated end-groups not observed. The earlier reasoning, that the reactions with $SOCl_2$ and CDI had proceeded and the products had subsequently lost to decomposition, would seem false.

The formation of a 6-membered ring allows the facile decarboxylation of β-keto acids. The mechanism of such a decarboxylation for PMMA with a carboxylic acid end-group is illustrated in Figure 2.5.7. This mechanism is reminiscent of the McLafferty rearrangement, which is often observed with the mass spectrometry of ketones. The polymer configuration is such that the acidic proton hydrogen-bonds with the carbonyl of the ultimate methyl ester, thus forming a 6-membered ring. The movement of electrons around the ring eliminates $CO_2(g)$ leaving an enol product, which subsequently tautomerises back to the methyl ester. The overall result is a proton-terminated polymer and evidence for this, gleaned from NMR and MALDI, has already been given.

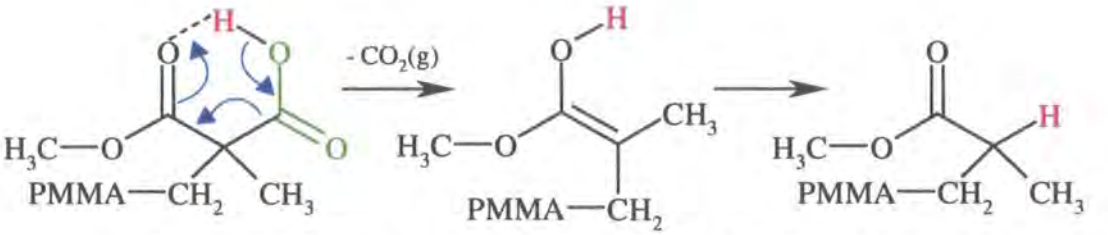

Figure 2.5.7. Mechanism for decarboxylation from *12-16*.

To summarise, $CO_2(g)$ proved an effective capping reagent for methacrylic anions, with functionalisation being ≥ 95% for all samples. MALDI analysis showed that these samples were all of the acid form, rather than the lithium carboxylate salt. The attempts to interconvert the acid functionalisation to an acid chloride or acid imidazolide, and further from the acid imidazolide to a benzyl or *n*-propyl ester, were all shown to be unsuccessful by data from MALDI analysis, as well as that from other techniques. Further investigation revealed that rapid decarboxylation of the acid upon heating, facilitated by the proximity of a keto moiety, provided a reasonable explanation for the results observed. The mechanism for decarboxylation is given and the stoichiometric formula of the polymer product of decarboxylation fits with the recorded data.

2.6 Capping Reactions Involving Silyl Halide Reagents

Silyl halides are another classic reagent group for reactions with polymeric organolithium species.[17] These reactions are usually very efficient and are not complicated by any competing side reactions, so providing a range of functional or protected functional end-groups. Chlorotrimethylsilane ($ClSi(CH_3)_3$) was the first reagent to be tried (Sample *17*), the anticipated stoichiometric formula being given in Figure 2.6.1.

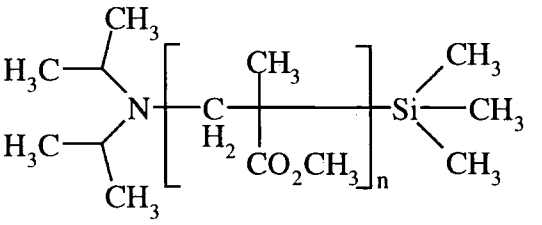

Figure 2.6.1. Stoichiometric formula of *17*.

This end-group should be identified very easily in both proton and carbon NMR, as the signal for the equivalent methyls will be very similar to those for tetramethylsilane (TMS), which is often used as a standard reference compound in NMR, occurring at around $\delta = 0$ ppm in both spectra. This peak was absent in both spectra, *i.e.* the polymer does not have the desired end-group. Given that decolourisation was observed upon addition of the silane, the results contradicted our expectations. Although CH_3OH was not added to the polymerisation, both proton and carbon NMR point towards the polymer being proton terminated and having exactly the same stoichiometric formula as *1*. This stoichiometric formula was further confirmed by MALDI, as the masses observed were associated with $[1+H]^+$ molecule ions and not the $[17+H]^+$ species. The only sensible explanation for these results is that protic impurities were introduced into the polymerisation upon injection of the silane. These impurities may have been contained within the silane itself or the septum may have been damaged at this point, allowing atmospheric impurities into the system. This resulted in the polymer being rapidly terminated by protonation, before the silane could react. Elemental analysis, in order to confirm the presence of silicon within the polymer structure, was not feasible. The molecular weight data for *17* are given in Table 2.6.1.

Sample	$\overline{M}_n$	$\overline{M}_w$	$\overline{M}_w/\overline{M}_n$
17	2320	2530	1.09
18	2960	2990	1.01
19	2020	2150	1.06
20	3500	3590	1.03
21	2710	2860	1.06

Table 2.6.1. SEC molecular weight data for *17-21*.

This reaction was repeated with a longer capping reaction time and with DPHLi as the initiator (Sample *18*), aiming to give the stoichiometric formula in Figure 2.6.2. Before the polymerisation was allowed to warm to room temperature, CH_3OH was added in case the capping reaction had not proceeded. Along with proton NMR, MALDI again confirmed the absence of a capping reaction and the polymer being proton terminated, as $[2+Li]^+$ molecule ions instead of the $[18+Li]^+$ species were recorded. The logical conclusion is that ($ClSi(CH_3)_3$) is not sufficiently reactive enough to cap methacrylate anions at the reaction temperature.

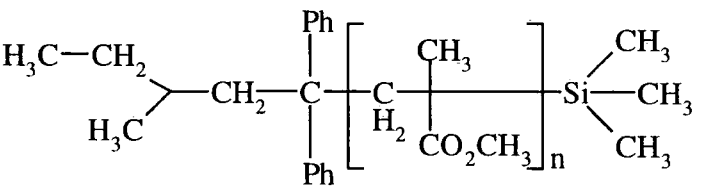

Figure 2.6.2. Stoichiometric formula of *18*.

How might we increase the reactivity of the capping reagent? The Br-Si bond is measurably weaker than the Cl-Si bond, and therefore, using the analogous bromosilane as the capping reagent may provide more fruitful results. A few capping reactions (Samples *19-21*) were attempted with ($BrSi(CH_3)_3$) with each of the initiators and various reaction times and excesses of capping reagent. In each of these experiments, CH_3OH was added prior to the polymerisation being warmed to room temperature. In all cases, proton NMR and MALDI data (with both dithranol and *all-trans*-retinoic acid matrices) implied that the polymer was proton terminated. The SEC data for polymers *19-21* are given in Table 2.6.1.

In conclusion, neither ($ClSi(CH_3)_3$) nor ($BrSi(CH_3)_3$) proved useful as end-capping reagents for methacrylic anions at –78°C, as determined via data from both NMR and MALDI. The analogous iodosilane was not tested as an effective capping reagent, but with a still weaker Hal-Si bond, a successful reaction might be achieved. The electron-donating methyl groups of the silane stabilise the Hal-Si bond, which may account for the unreactivness of the silanes used in these experiments.

2.7 Capping Reactions Involving Alkyl Halide Reagents

The final discussion section deals with the use of alkyl halides as capping reagents. As part of a series of papers, Al-Takrity *et. al.* used alkyl halides to end-cap methacrylate anions directly.[18,19] Sample *22* was prepared utilising allyl iodide (3-iodopropene, $CH_2=CHCH_2I$) as the capping reagent. The stoichiometric formula for *22* is represented in Figure 2.7.1.

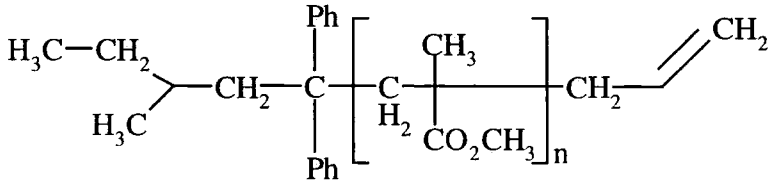

Figure 2.7.1. Stoichiometric formula of *22*.

The proton NMR for *22* is shown in Figure 2.7.2. As well as the peaks corresponding to the polymer backbone, the initiator peaks, especially those of the phenyl rings, are clearly visible, plus some other signals not previously observed. The complicated multiplet at δ = 5.7 ppm can be attributed to the *geminal* proton of the unsaturated end-group. The doublet of doublets occurring at around δ = 5.0 ppm are due to the *cis* and *trans* protons of the carbon double bond, with the peak for the *cis* proton appearing at slightly lower field. The peak due to methylene group of the end-group is most likely to be hidden under signals from the methylenes of the main chain. No signals due to residual capping reagent are seen. The peak at δ = 2.3 ppm may be due to contamination of the sample with toluene.

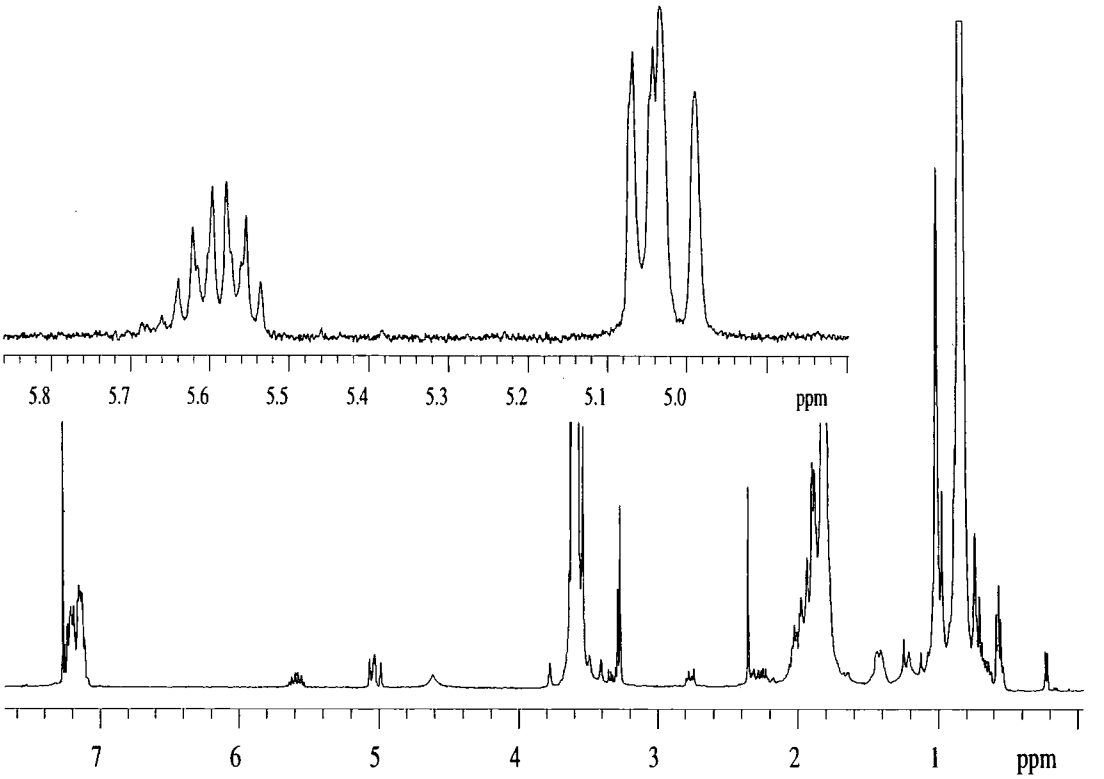

Figure 2.7.2. Proton NMR spectrum of *22* with expanded lower field region.

The carbon NMR for *22* is shown in Figure 2.7.3. In addition to main chain and initiator derived signals, there is a peak at δ = 133 ppm corresponding to the methine of the unsaturated end-group. There is also a peak at δ = 119 ppm due to the allylic methylene group. There appear to be some other signals in this region that cannot be accounted for within the polymer structure, and again are possibly due to a small amount of toluene present. There is a peak partially obscured by signals from the quaternary carbons of the polymer chain, which could be due to the other methylene group. In short, both proton and carbon NMR support the stoichiometric formula given in Figure 2.7.1.

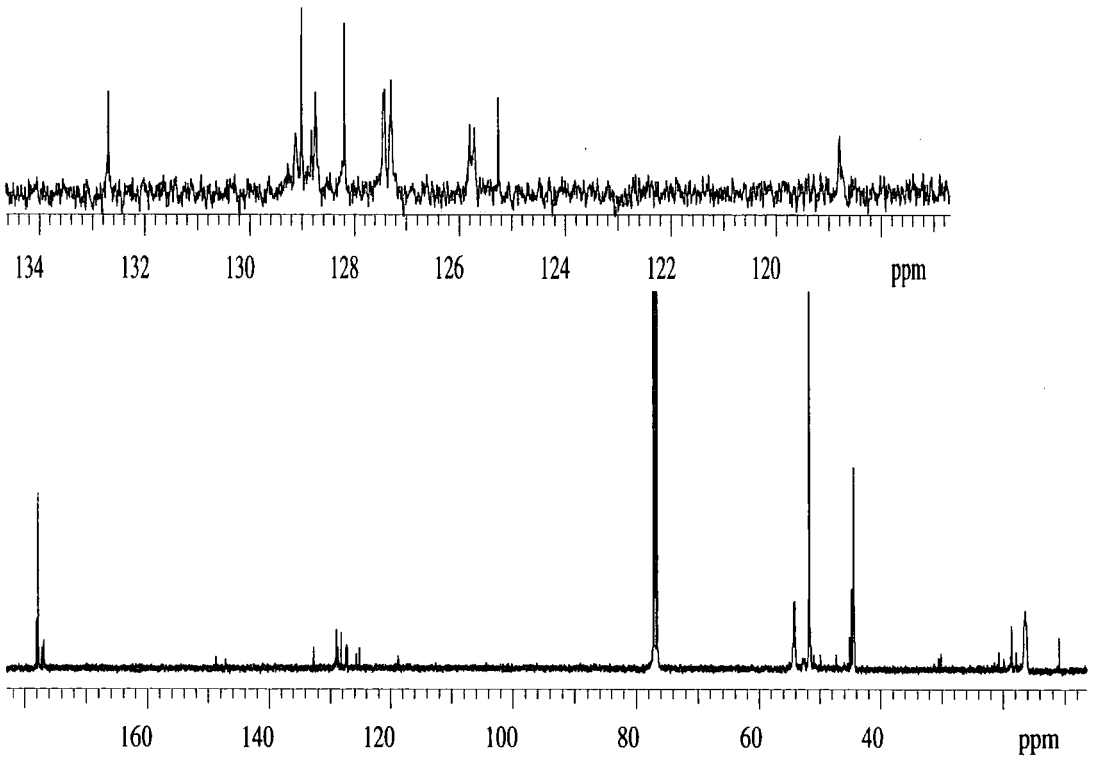

Figure 2.7.3. Carbon NMR spectrum of *22* with expanded lower field region.

Sample *23* was prepared by employing 1-naphthoyl chloride ($C_{10}H_7COCl$) as the capping reagent. The anticipated stoichiometric formula for *23* is represented in Figure 2.7.4.

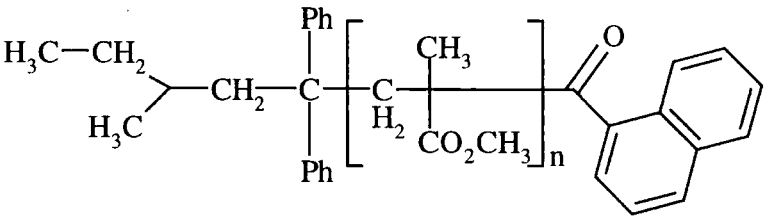

Figure 2.7.4. Stoichiometric formula of *23*.

The proton NMR for *23* is shown in Figure 2.7.5. Aside from the peaks of the polymer backbone and initiator, there is a collection of peaks in the δ = 7.3-8.0 ppm range. These are due to the many methines of the fused ring system, which are all slightly different due to the unsymmetrical nature of the end-group.

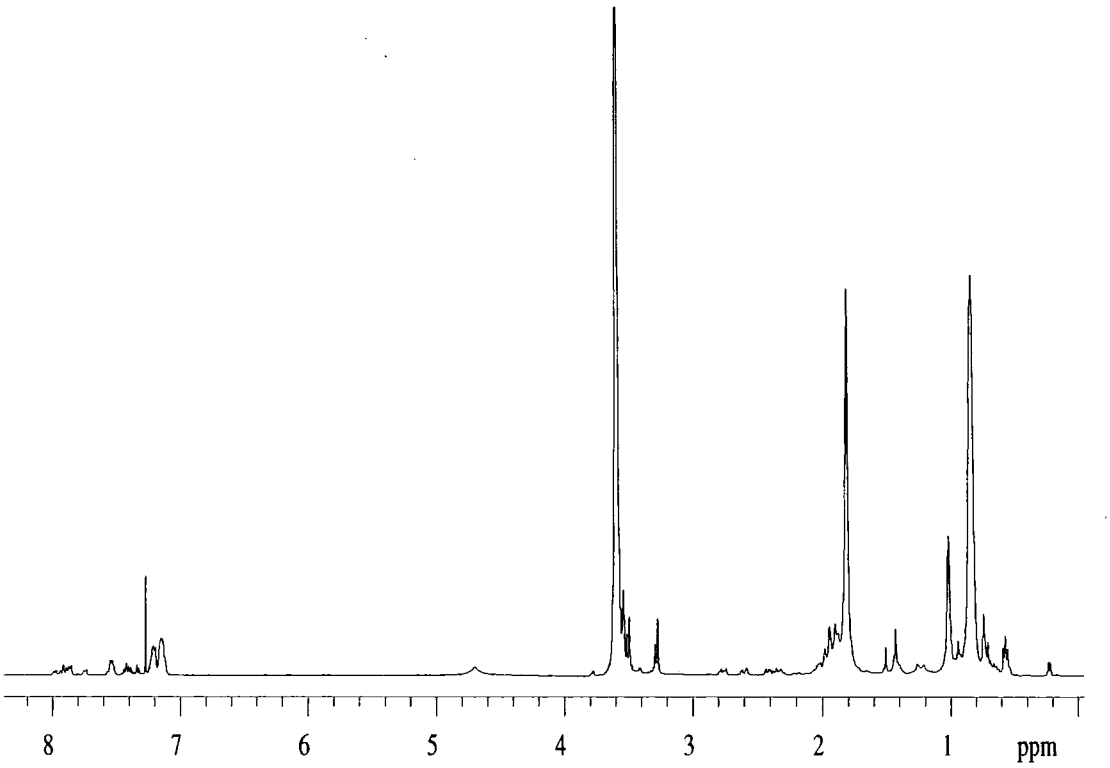

Figure 2.7.5. Proton NMR spectrum of *23*.

The carbon NMR for *23* is shown in Figure 2.7.6. There is a similar collection of peaks to that observed in the proton spectrum, again matching to the fused rings of the end-group. These peaks overlap with those due to the phenyl rings of the initiator and range from δ = 123-137 ppm. The carbonyl of the end-group is expected to appear at δ = 200 ppm or thereabouts, and either of the weak signals in this region could be in accordance with this group. The peak at δ = 60 ppm is probably due to quaternary carbon to which the terminating group is bonded. The peak at δ = 14 ppm most likely is due to the pendant methyl of the final repeat unit. Hence, the stoichiometric formula for *23* given in Figure 2.7.4 is proven correct.

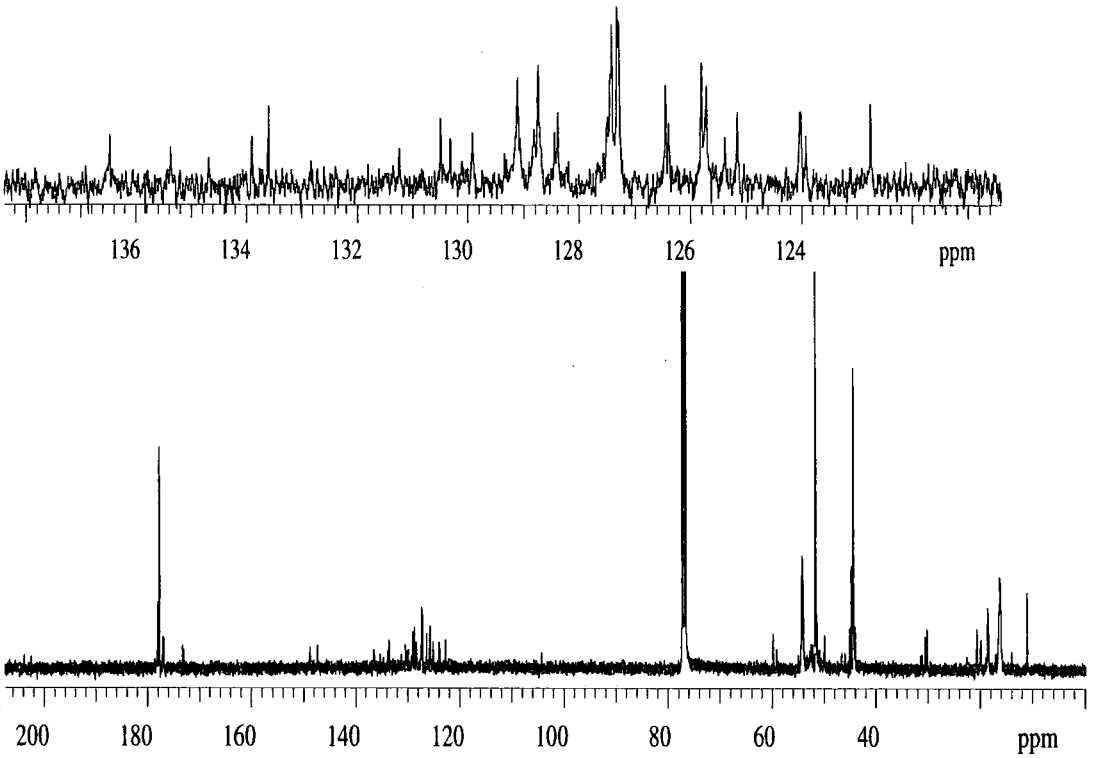

Figure 2.7.6. Carbon NMR spectrum of *23* with expanded lower field region.

The molecular weight data from SEC for both *22* and *23* are given in Table 2.7.1.

Sample	$\overline{M}_n$	$\overline{M}_w$	$\overline{M}_w / \overline{M}_n$
22	3570	3880	1.09
23	2700	2970	1.10

Table 2.7.1. SEC molecular weight data for *22* and *23*.

A low mass region section of the reflectron MALDI spectrum for a sample of *22*, obtained using *all-trans*-retinoic acid as the matrix and to which LiCl was added, is featured in Figure 2.7.7. The peak masses of the major series observed compare very favourably with the theoretical values for the $[22+Li]^+$ species, as shown in Table 2.7.2. Expansion of the peak set for individual oligomers also revealed an extremely close match with the corresponding theoretical isotopic peak distribution for the $[22+Li]^+$ species. Therefore, MALDI data provides further evidence for the successful capping reaction with allyl iodide.

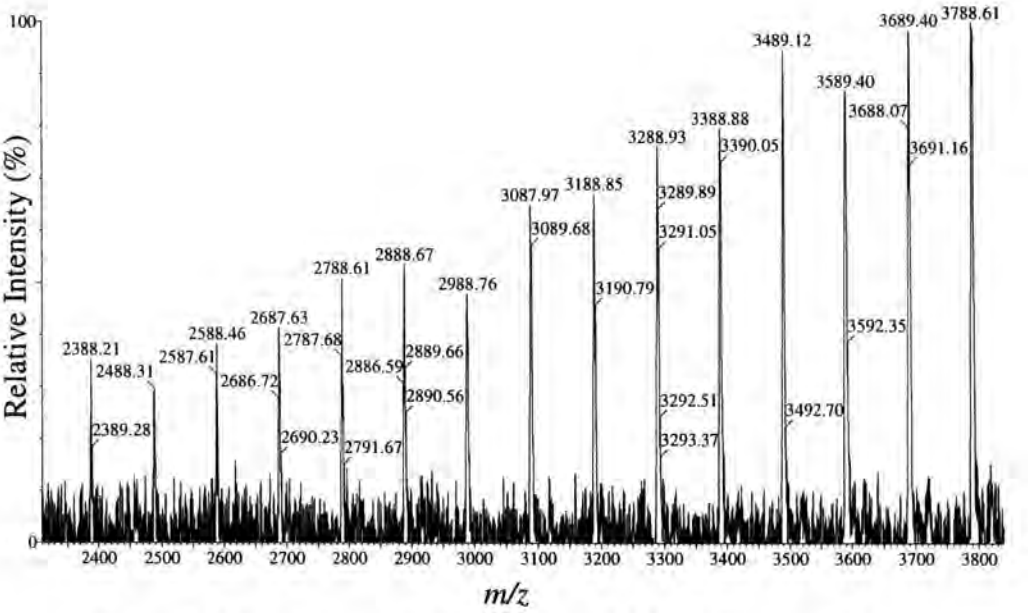

Figure 2.7.7. Expanded reflectron MALDI spectrum of *22*.

22 and $[22+Li]^+$			*23* and $[23+Li]^+$		
n	Obs.	Calc.	n	Obs.	Calc.
23	2588.99	2588.10	21	2502.11	2501.97
24	2689.12	2688.22	22	2602.17	2602.09
25	2789.62	2788.34	23	2702.25	2702.21
26	2888.65	2888.46	24	2802.34	2802.32
27	2989.48	2988.57	25	2902.41	2902.44
28	3088.83	3088.69	26	3002.97	3002.56
29	3189.22	3188.81	27	3103.05	3102.68
30	3289.48	3288.93	28	3203.19	3202.80

Table 2.7.2. Average observed and calculated mass comparisons for *22* and *23*.

A low mass region section of the reflectron MALDI spectrum for a sample of *23*, also obtained using *all-trans*-retinoic acid and added LiCl, is given in Figure 2.7.8. The peak masses of the major series observed are in excellent agreement with the theoretical values for the $[23+Li]^+$ species in Table 2.7.2. In addition, expansion of the peak set for individual oligomers again revealed a very close equivalence with the corresponding theoretical isotopic peak distribution for the $[23+Li]^+$ species. Thus, results obtained by MALDI analysis confirm that the capping reaction with 1-naphthoyl chloride was a success.

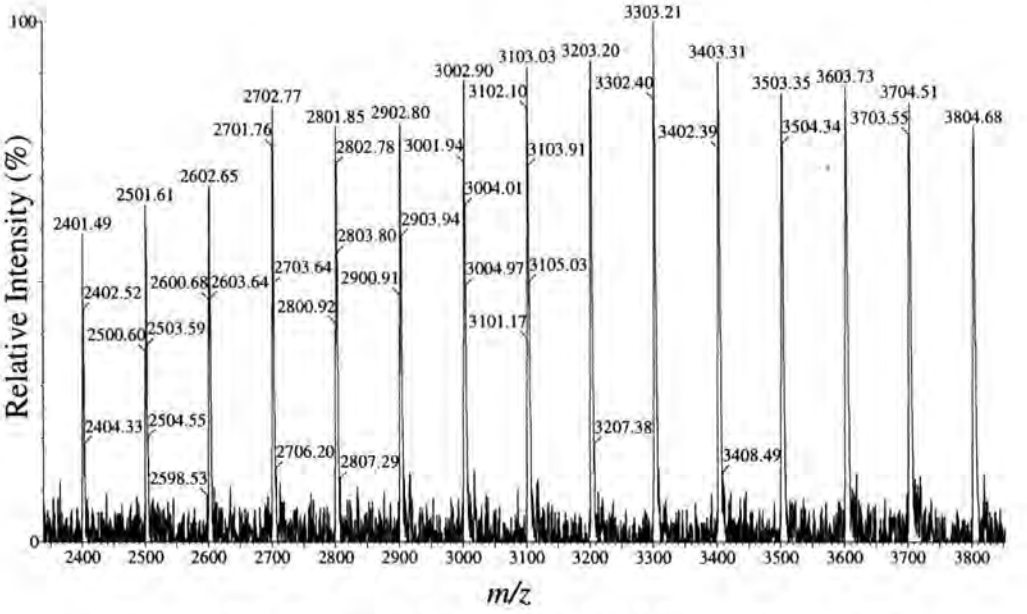

Figure 2.7.8. Expanded reflectron MALDI spectrum of *23*.

To summarise, MALDI data complemented that from other analytical techniques in corroborating the successful capping reactions of active anionic PMMA chains with both allyl iodide and 1-naphthoyl chloride. Moreover, the MALDI analysis of both these samples was shown to be relatively straightforward, *i.e.* without any observed fragmentation or elimination.

2.8 Analytical Experimental

All polymers were submitted for SEC and proton and carbon NMR prior to MALDI analysis. The SEC apparatus was a Viscotek GPC, fitted with a Ralls light scattering and Viscotek refractive index/viscometry detectors. All molecular weights obtained from SEC have units of g mol^{-1} and were calculated using a conventional calibration involving PMMA standards (Polymer Laboratories).

NMR-spectra were recorded using a Varian VXR400S (^1H at 399.95 MHz and ^{13}C at 100.58 MHz), a Varian Mercury (^1H at 399.95 MHz and ^{13}C at 100.58 MHz), a Varian Gemini (^1H at 200 MHz and ^{13}C at 50.2 MHz), a Varian Unity (^1H at 299.91 MHz and ^{13}C at 75.41 MHz) or a Varian Inova (^1H at 500 MHz and ^{13}C at 125 MHz). Chemical shifts are reported in parts per million with respect to the deuterated solvent used. Where references are not specified, chemical shifts have been assigned with the aid of tables and equations given by Williams and Fleming,[20] and by NMR prediction[21]

and database[22] websites. Deuterated solvents, $CDCl_3$ (Aldrich) or CD_2Cl_2 (Apollo/Aldrich), were used as supplied. Samples were run in $CDCl_3$, unless otherwise stated.

Certain samples were submitted for elemental analysis, which was performed using an Exeter Analytical CE-440 elemental analyser and a Dionex DX-500 ion chromatograph. All oxygen elemental percentages were calculated by difference.

The MALDI-TOF-MS analysis of the polymers was performed using both a Kratos Kompact MALDI IV, pictured in Figure 2.8.1, (for a schematic of this instrument, see Figure 1.3.3) and a Micromass TofSpec 2E time-of-flight mass spectrometer, a schematic of which is given in Figure 2.8.2. Both machines utilise a N_2 laser, which emits a beam with a wavelength of 337 nm. Dithranol was used as matrix for all samples unless otherwise stated and THF was used as the common solvent similarly. The dried droplet sample deposition technique was used for all samples. Matrix, analyte and salt solutions were mixed together in a 100:20:1 ratio, unless otherwise stated. All samples analysed with linear detection are done so in the Kompact MALDI IV, with the machine in positive ion/high mass mode. All samples analysed with reflectron detection are done so in the TofSpec 2E, with the machine in positive ion/high mass mode, unless otherwise stated. The Kompact MALDI IV was calibrated with a PMMA standard, while the TofSpec 2E was calibrated with a peptide mixture. MALDI-CID data was collected using a Micromass QTOF, which comprises of the first analyser being a quadrupole, the second being a TOF, and a hexapole collision cell employing argon as the collision gas.

Figure 2.8.1. Photograph of the Kompact MALDI IV mass spectrometer.

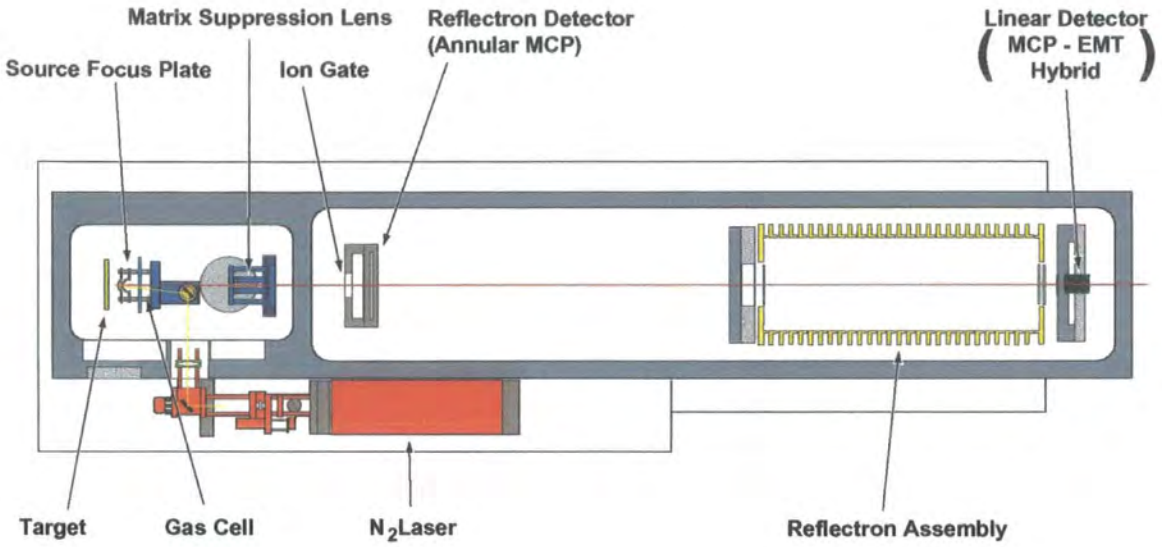

Figure 2.8.2. Schematic of the TofSpec 2E MALDI mass spectrometer.

2.9 Polymer Synthesis

All polymerisations were carried out using '*Christmas tree*' glass vessels (see Figure 2.9.1), of which a small side-bulb contained an amount of LiCl (Aldrich) that was five times greater than the molar amount of initiator. The vessel was evacuated overnight prior to a polymerisation, and then rinsed (apart from the side-bulb containing LiCl) with a living poly(styryl)lithium benzene solution, in order to remove any impurities still present. This living polymer was washed back into its side-bulb with its own solvent, until the washings became clear.

Figure 2.9.1. Photograph of a '*Christmas tree*' polymerisation vessel.

2.9.1 Monomer purification

100 ml of MMA (Hopkin & Williams/Aldrich) monomer was transferred to a 500 ml separating funnel and washed with **3 × 100 ml** aliquots of 10% sodium hydroxide solution (NaOH(aq)), in order to remove the polymerisation inhibitor. The resultant yellow-brown aqueous layers were discarded and the monomer was washed further with **3 × 100 ml** aliquots of distilled water. The monomer was then dried in a stoppered conical flask, over calcium chloride ($CaCl_2$, BDH). The flask was wrapped in foil to prevent any UV initiated polymerisation.

The monomer was decanted into a 500 ml round-bottomed flask (rbf), which was then connected to vacuum distillation apparatus, and the monomer distilled at 28°C, 60 mbar pressure. The first 10 ml and last 5 ml were discarded, the remainder being collected in a 250 ml rbf, to which were added two spatulas of calcium hydride (CaH_2, Aldrich). The flask was wrapped in foil and the contents stirred for an hour. The flask was then attached onto a high-vacuum line and, in order to degas the flask, a freeze (with N_2(liq))/evacuation/thaw process was performed, followed by several hours stirring. This was repeated 3-4 times until no more H_2(g) was evolved. The flask of pure, dry MMA was left on the vacuum line wrapped in foil, but was found to polymerise in 6-8 weeks. Distilling the monomer into a side-arm and storing, wrapped in foil, in the fridge was found to increase its usable lifetime greatly.

2.9.2 Solvent purification

All solvents were purchased from either Fisher or BDH.

Anhydrous tetrahydrofuran (THF) was kept over sodium metal (Aldrich) and under N_2. Approximately **250 ml** was transferred to an oven-dried 500 ml rbf, via applied N_2 pressure, and a magnetic stirrer bar added. A small amount of sodium (BDH) wire was added followed by enough benzophenone (Aldrich) to produce a deep purple colour, indicating the formation of the sodium benzophenone complex, and, more importantly, the dryness of the solvent. The flask was attached to a high-vacuum line and the same freeze/evacuation/thaw process applied to the monomer was performed until the solvent was completely degassed.

250 ml of toluene were dried in a similar manner to THF except for the sodium benzophenone complex being replaced by CaH_2.

50 ml of dichloromethane (DCM) were placed over 3A-grade molecular sieve (Aldrich) in a 100 ml rbf, put under high-vacuum, and stirred for several days until dry. The solvent was then carefully cold distilled into a side-arm. The same procedure was adopted for chloroform ($CHCl_3$) and nitromethane (NO_2CH_3).

2.9.3 Initiators

LDA initiator solution (Aldrich) was used as received. DPHLi initiator was freshly prepared for each polymerisation by the reaction of *s*-butyllithium (*s*-BuLi, Aldrich) and DPE (Aldrich) in a 1:1 ratio. A side-arm with a magnetic stirrer and septum was attached to the vacuum-line, evacuated, and then put under dry N_2. **1-2 ml** of dry THF and the relevant amount of DPE were injected through the septum via a syringe. While this solution was stirred, *s*-BuLi was added dropwise via a syringe, in order to titrate out any impurities. A persistent orange/red colour indicates the onset of formation of pure (dry) initiator and is the end-point of the titration. The relevant amount of *s*-BuLi was then added in order to form the relevant amount of initiator, which is deep-red in colour.

2.9.4 Synthesis of PMMA *(1)* using LDA initiator (aim = 1000 g mol^{-1})

7.48 g (7.47×10^{-2} mol) of dry MMA were cold distilled into an evacuated side-arm fitted with a septum and magnetic stirrer, with the weight being determined by difference. Approximately 80 ml of dry THF were cold distilled into the main bulb of the polymerisation vessel and a freeze/evacuation process was performed. To check that the MMA was still dry, 1 ml of a 1.0 M triethylaluminium solution (Aldrich) was injected through the septum, a green colourisation being evidence of purity. The monomer was then cold distilled from the side-arm into the main bulb and a freeze/evacuation/thaw cycle performed. The next step was to dissolve the LiCl contained in the side-bulb. The main bulb was then submerged in an acetone/CO_2(s) bath, and the contents stirred for 20 minutes, in order to reach the polymerisation temperature of –78°C. While stirring continued, **3.75 ml (7.47×10^{-3} mol)** of LDA initiator solution (2.0 M) were injected into the main bulb via a syringe, and initiation was noted by the appearance of a faint orange colour. The polymerisation was left to proceed for 30 minutes to ensure full monomer conversion, and then terminated by

injecting **1 ml** of N_2-sparged CH_3OH into the main bulb, with the colour changing to a faint straw-yellow. The polymer solution was then allowed to warm up to room temperature.

The polymer was precipitated into approximately **800 ml** of hexane, i.e. 10 times as much non-solvent wrt solvent, previously cooled by CO_2(s), so removing any non-polar impurities. The polymer was vacuum-filtered through a No.3 glass sinter and dried overnight in a vacuum oven at room temperature. It was then dissolved in THF and re-precipitated in distilled water, in order to remove any polar impurities, vacuum-filtered through a No.5 glass sinter and dried in a vacuum oven at 50°C. The polymer was quite waxy, off-white in colour, and the yield was **7.30 g**.

2.9.5 Synthesis of PMMA *(2)* using DPHLi initiator (aim = 2000 g mol^{-1})

The polymerisation procedure was that described above. The quantity of MMA was **4.63 g (4.62×10^{-2} mol)**. The amount of *s*-BuLi (1.4 M) and DPE required equalled **1.80 ml (2.32×10^{-3} mol)** and **0.45 ml (2.32×10^{-3} mol)** respectively, while the total volume of the DPHLi initiator solution was roughly 4 ml. The polymer was a fine, white powder and the yield was **5.38 g**.

2.9.6 Synthesis of PMMA *(3)* with a cyclic ketone end-group derived from backbiting self-termination (aim = 1500 g mol^{-1})

The polymerisation was performed in the normal way. The quantity of MMA was **3.21 g (3.21×10^{-2} mol)**, so the amount of LDA (2.0 M) required equalled **1.07 ml (2.14×10^{-3} mol)**. Upon completion of the polymerisation, the acetone/CO_2(s) bath was removed and the solution allowed to warm slowly to room temperature, while stirring continued. The polymer was precipitated as normal and was a fine, white powder, with a yield of **2.76 g**.

2.9.7 Attempted synthesis of PMMA (*4a*/*4b*/*4c*) capped with combinations of DPE and CO_2(g) (aim = 1000 g mol^{-1})

The polymerisation was performed in the normal way. The quantity of MMA was **14.58 g** (**1.46×10^{-1} mol**), so the amount of LDA (2.0 M) required equalled **7.29 ml** (**1.46×10^{-2} mol**), and **200 ml** of THF solvent was used. Once the polymerisation was complete, roughly a third of the living solution was transferred to a 100 ml side-bulb, and kept at –78°C. Distilled and dried DPE (**3.50 ml, 1.98×10^{-2} mol**) was added to the remainder, this amount being approximately double that required to functionalise the living chains. The mixture was stirred for 1 hour during which time no colour change was observed and the solution was allowed to warm to room temperature. Roughly half of this solution was then transferred into a second 100 ml side-bulb, where it was terminated as usual (*4b*). Both the remaining fractions were opened to an atmosphere of CO_2(g) (BDH), and were stirred for 1 hour. No colour change was observed for the main bulb fraction (*4a*), but the first side-bulb fraction (*4c*) went colourless. Both portions were terminated in the usual manner and fraction *4c* allowed to warm to room temperature, with a Young's tap being opened to allow the expanding gas to escape safely. All three fractions were precipitated separately, as normal. *4a* yielded **4.15 g**, *4b* yielded **1.88 g**, and *4c* yielded **2.14 g**, so the total yield was **8.17 g**.

2.9.8 Attempted synthesis of PMMA (*5*) capped with DPE (aim = 3000 g mol^{-1})

The polymerisation was performed in the normal way. The quantity of MMA was **4.47 g** (**4.46×10^{-2} mol**), so the amount of LDA (2.0 M) required equalled **0.75 ml** (**1.49×10^{-3} mol**). Distilled and dried DPE (**0.50 ml, 2.83×10^{-3} mol**) was added, this amount being approximately double that required to functionalise the living chains. The solution was stirred at –78°C for 6 hours and no colour change was observed. The polymer was warmed to room temperature, terminated and precipitated as normal, and was a fine, white powder, with a yield of **3.97 g**.

2.9.9 Attempted synthesis of PMMA *(6)* capped with DPE (aim = 2000 g mol^{-1})

The polymerisation proceeded as normal except that the vessel was packed in dry ice instead of being in a dry ice/acetone bath. **5.13 g (5.12×10^{-2} mol)** of MMA were used, thus requiring **1.28 ml (2.56×10^{-3} mol)** of LDA (2.0 M). Distilled and dried DPE **(4.53 ml, 2.56×10^{-3} mol)** was added, this being a 10-fold excess of the amount required. The vessel was covered (apart from the septum) in foil and the contents stirred for 4 days, at a temperature no higher than –55°C. A colour change was not observed during this time. The polymer solution was allowed to warm to room temperature very gradually, then terminated and precipitated as normal. The yield was **5.75 g**.

2.9.10 Attempted quaternisation *(7)* of (*i*-Pr)$_2$N-PMMA *(1)* using methyl bromide (CH_3Br)

Into a 100 ml side-arm containing a magnetic stirrer were weighed **1.05g (7.55×10^{-4} mol)** of PMMA *(1)*, which was then put under high-vacuum overnight. Dry NO_2CH_3 **(5.19 ml)** and dry THF **(13.95 ml)** of were cold distilled into separate side-arms, the latter amount being roughly 3 times greater by volume. These were then cold distilled into the side-arm containing the polymer and the polymer was dissolved. Over a 300 times excess amount of CH_3Br **(22.52 g, 2.37×10^{-1} mol)** was gently cold distilled into this side-arm, and the solution was stirred for 2.5 weeks, after which it was a pale brown colour. Precipitation as normal could not be achieved and so allowing all volatile reagents to evaporate isolated the polymer. The polymer was pale brown and the yield was **1.12g**.

2.9.11 Attempted synthesis of PMMA *(8)* capped with 1,3-propanesultone (aim = 2000 g mol^{-1})

The quantity of MMA was **5.46 g (5.45×10^{-2} mol)**, so the amount of LDA initiator required equalled **1.34 ml (2.73×10^{-3} mol)**. Upon completion of the polymerisation, **0.57 ml** of a 58.60 g 100 ml^{-1} THF solution of 1,3-propane sultone was added. This amount was a slight excess on the stoichiometric amount required for the

functionalisation of all the chains. The solution was stirred at –78°C for 2 hours and no colour change was observed. N_2-sparged CH_3OH was added and the polymer precipitated as normal, and was a fine, white powder, with a yield of **4.34 g**.

2.9.12 Synthesis of PMMA *(9)* capped with CO_2(g) + HCl(aq) (aim = 2000 g mol^{-1})

The polymerisation was performed in the normal way. The quantity of MMA was **3.33 g** (**3.33×10^{-2} mol**), so the amount of LDA (2.0 M) required equalled **0.83 ml** (**1.66×10^{-3} mol**). CO_2(g) was introduced to the vessel as previously described and the polymer solution was stirred under this atmosphere for 1.5 hours. The faint orange colour disappeared and the polymer was terminated with **1 ml** of N_2-sparged HCl(aq). The polymer was precipitated as normal, but not reprecipitated into water, and was an off-white powder, with a yield of **3.90 g**.

2.9.13 Synthesis of PMMA *(10)* capped with CO_2(g) + CH_3OH (aim = 2000 g mol^{-1})

The polymerisation was performed in the normal way. The quantity of MMA was **9.30 g** (**9.29×10^{-2} mol**), so the amount of LDA (2.0 M) required equalled **2.33 ml** (**4.65×10^{-3} mol**). CO_2(g) was introduced to the vessel as and the polymer solution was stirred under this atmosphere for 1.5 hours. The faint orange colour disappeared and the polymer was terminated with **1 ml** of N_2-sparged CH_3OH. The polymer was precipitated as normal, but not reprecipitated into water, and was an off-white powder, with a yield of **10.93 g**.

2.9.14 Synthesis of PMMA *(11)* capped with CO_2(g) + glacial acetic acid (aim = 1500 g mol^{-1})

The polymerisation was performed in the normal way. The quantity of MMA was **4.23 g** (**4.23×10^{-2} mol**), so the amount of LDA (2.0 M) required equalled **1.41 ml** (**2.82×10^{-3} mol**). The polymer solution was stirred under the CO_2(g) atmosphere for 1.5 hours. The faint orange colour disappeared and the polymer was terminated with **1 ml**

of N_2-sparged glacial acetic acid. The polymer was precipitated as normal, but not reprecipitated into water, and was an off-white powder, with a yield of **5.95 g**.

2.9.15 Attempted end-group conversion of PMMA-CO_2H *(10)* to COCl *(12)* using $SOCl_2$

Into a 50 ml double-necked rbf, fitted with a magnetic stirrer and a water-cooled condenser, were weighed **1.50 g (6.00×10^{-4} mol)** of dry carboxylated PMMA (*10*), and the whole apparatus placed under an atmosphere of N_2(g). Approximately **20 ml** of dry DCM was added to the flask and the polymer was dissolved. A 10 times excess amount of $SOCl_2$ (**0.44 ml, 6.00×10^{-3} mol,** Aldrich) was added to the flask via syringe and the mixture was refluxed for 4 hours at roughly 40°C, using an oil bath. Once the mixture had cooled to room temperature, the polymer was precipitated into cold hexane and stored under N_2 once dried. The polymer was an off-white powder, with a yield of **1.61 g**.

2.9.16 Attempted end-group conversion of PMMA-CO_2H *(10)* to COCl *(13)* using $SOCl_2$

Into a 50 ml double-necked rbf, fitted with a magnetic stirrer and a water-cooled condenser, were weighed **1.07 g (4.28×10^{-4} mol)** of dry carboxylated PMMA (*10*), and the whole apparatus placed under an atmosphere of N_2(g). Approximately **20 ml** of dry $CHCl_3$ was added to the flask and the polymer was dissolved. A 10 times excess amount of $SOCl_2$ (**0.31 ml, 4.28×10^{-3} mol,** Aldrich) was added to the flask via syringe and the mixture was refluxed for 4 hours at roughly 60°C, using an oil bath. Once the mixture had cooled to room temperature, the polymer was precipitated into cold hexane and stored under N_2 once dried. The polymer was an off-white powder, with a yield of **1.03 g**.

2.9.17 Attempted end-group conversion of PMMA-CO_2H *(10)* to acid imidazolide *(14)* using CDI

Into a 100 ml double-necked rbf, fitted with a magnetic stirrer and a water-cooled condenser, were weighed **1.38 g (5.52×10^{-4} mol)** of dry carboxylated PMMA (*10*), and the whole apparatus placed under an atmosphere of N_2(g). Approximately **30 ml** of dry toluene was added to the flask and the polymer was dissolved. CDI (**0.09 g, 5.52×10^{-3} mol,** Aldrich) was added and the solution was stirred for 4 hours at roughly 60°C, using an oil bath. Once the mixture had cooled to room temperature, the polymer was precipitated into cold hexane and stored under N_2 once dried. The polymer was an off-white powder, with a yield of **1.21 g**.

2.9.18 Attempted end-group conversion of PMMA-CO_2H *(11)* to CO_2Bz *(15)* via an acid imidazolide intermediate

Into a 100 ml double-necked rbf, fitted with a magnetic stirrer and a water-cooled condenser, was weighed **0.75 g (4.60×10^{-4} mol)** of dry carboxylated PMMA (*11*), and the whole apparatus placed under an atmosphere of N_2(g). Approximately **30 ml** of dry toluene was added to the flask and the polymer was dissolved. Roughly a 1.75 times excess of CDI (**0.13 g, 8.05×10^{-4} mol,** Aldrich) was added and the solution was stirred for 1.5 hours at roughly 35°C, using an oil bath. $PhCH_2OH$ (**0.25 ml, 2.42×10^{-3} mol,** Aldrich), previously dried over 3A-grade molecular sieve and roughly a 3 times excess wrt the original acid concentration, was added via syringe. Approximately **2 mg** of potassium hydroxide powder (KOH, Fisher) was also added and the solution was stirred at 60°C overnight. Once the mixture had cooled to room temperature, the polymer was precipitated into cold hexane and stored under dry N_2(g) once dried. The polymer was an off-white powder, with a yield of **0.32 g**.

2.9.19 Attempted end-group conversion of PMMA-CO_2H *(11)* to CO_2n-Pr *(16)* via an acid imidazolide intermediate

Into a 100 ml double-necked rbf, fitted with a magnetic stirrer and a water-cooled condenser, was weighed **0.98 g (6.13×10^{-4} mol)** of dry carboxylated PMMA (*11*), and the whole apparatus placed under an atmosphere of N_2(g). Approximately **30**

ml of dry THF was added to the flask and the polymer was dissolved. Roughly a 1.5 times excess of CDI (**0.15 g, 9.20×10^{-4} mol,** Aldrich) was added and the solution was stirred for 1.5 hours, being maintained at roughly 35°C using an oil bath. Previously dried over 3A-grade molecular sieve and roughly a 3 times excess wrt the original acid concentration, **0.14.ml (1.84×10^{-3} mol)** of *n*-PrOH (Aldrich) was added via syringe. Approximately **2 mg** of KOH powder was also added and the solution was stirred at 60°C overnight. Once the mixture had cooled to room temperature, the polymer was precipitated into cold hexane and stored under dry N_2(g) once dried. The polymer was an off-white powder, with a yield of **0.58 g**.

2.9.20 Attempted synthesis of PMMA *(17)* capped with $ClSi(CH_3)_3$ (aim = 2000 g mol^{-1})

The polymerisation was performed in the normal way. The quantity of MMA was **2.90 g (2.90×10^{-2} mol)**, so the amount of LDA (2.0 M) required equalled **0.73 ml (1.45×10^{-3} mol)**. When the polymerisation was judged to be complete, **1.84 ml (1.45×10^{-2} mol)** (Aldrich), roughly a 10 times excess amount, were injected into the reaction vessel. The pale orange colour was immediately lost and after 10 minutes, the solution was allowed to warm slowly to room temperature. The polymer was precipitated and dried as normal, was a white powder, and had a yield of **3.02 g**.

2.9.21 Attempted synthesis of PMMA *(18)* capped with $ClSi(CH_3)_3$ (aim = 2000 g mol^{-1})

The polymerisation was performed in the normal way. The quantity of MMA was **0.96 g (9.59×10^{-3} mol)**, so the amount of *s*-BuLi (1.5 M) required for the DPHLi initiator equalled **0.33 ml (4.80×10^{-4} mol)** and that for DPE equalled **0.09 ml (4.80×10^{-4} mol)**. When the polymerisation was judged to be complete, **0.30 ml (2.40×10^{-3} mol)** of $ClSi(CH_3)_3$, roughly a 5 times excess amount, were injected into the reaction vessel. There was no visible colour change and the solution was stirred at the reaction temperature (–78°C) for a further 16 hours. **1 ml** of N_2-sparged CH_3OH was then added and the solution allowed to warm slowly to room temperature. The polymer was precipitated and dried as normal, was a white powder, and had a yield of **1.03 g**.

2.9.22 Attempted synthesis of PMMA *(19)* capped with $BrSi(CH_3)_3$ (aim = 1250 g mol^{-1})

The polymerisation was performed in the normal way. The quantity of MMA was **2.87 g** (2.87×10^{-2} **mol**), so the amount of LDA (2.0 M) required equalled **1.15 ml** (2.30×10^{-3} **mol**). Upon completion of the polymerisation reaction, **0.45 ml** (3.45×10^{-3} **mol**) of $BrSi(CH_3)_3$ (Aldrich), previously dried over CaH_2 and roughly 1.5 times excess amount, were injected into the reaction vessel. There was no visible colour change and the solution was stirred at the reaction temperature (–78°C) for a further 16 hours. **1 ml** of N_2-sparged CH_3OH was then added and the solution allowed to warm slowly to room temperature. The polymer was precipitated and dried as normal, was a white powder, and had a yield of **3.06 g**.

2.9.23 Attempted synthesis of PMMA *(20)* capped with $BrSi(CH_3)_3$ (aim = 2000 g mol^{-1})

The polymerisation was performed in the normal way. The quantity of MMA was **1.14 g** (1.14×10^{-2} **mol**), so the amount of *s*-BuLi (1.5 M) required for the DPHLi initiator equalled **0.38 ml** (5.70×10^{-4} **mol**) and that for DPE equalled **0.10 ml** (5.70×10^{-4} **mol**). When the polymerisation was judged to be complete, **0.38 ml** (2.85×10^{-3} **mol**) of $BrSi(CH_3)_3$, roughly a 5 times excess amount, were injected into the reaction vessel. There was no visible colour change and the solution was stirred at the reaction temperature (–78°C) for a further 16 hours. **1 ml** of N_2-sparged CH_3OH was then added and the solution allowed to warm slowly to room temperature. The polymer was precipitated and dried as normal, was a white powder, and had a yield of **1.36 g**.

2.9.24 Attempted synthesis of PMMA *(21)* capped with $BrSi(CH_3)_3$ (aim = 1250 g mol^{-1})

The polymerisation was performed in the normal way, except that the vessel was packed in dry ice instead of being in a dry ice/acetone bath. The quantity of MMA was **2.61 g** (2.61×10^{-2} **mol**), so the amount of LDA (2.0 M) required equalled **1.04 ml** (2.09×10^{-3} **mol**). When the polymerisation was judged to be complete, **0.41 ml**

(3.13×10^{-3} mol) of $BrSi(CH_3)_3$, roughly a 1.5 times excess amount, was injected into the reaction vessel. There was no visible colour change and the solution was stirred at the reaction temperature (–78°C) for a further 4 days. **1 ml** of N_2-sparged CH_3OH was then added and the solution allowed to warm slowly to room temperature. The polymer was precipitated and dried as normal, was a yellow powder, and had a yield of **2.58 g**.

2.9.25 Synthesis of PMMA *(22)* capped with CH_2=$CHCH_2I$ (aim = 2000 g mol^{-1})

The polymerisation was performed in the normal way. The quantity of MMA was **1.07 g (1.07×10^{-2} mol)**, so the amount of *s*-BuLi (1.5 M) required for the DPHLi initiator equalled **0.36 ml (5.40×10^{-4} mol)** and that for DPE equalled **0.095 ml (5.40×10^{-4} mol)**. Into a 50 ml rbf were placed approximately **5 ml** of allyl iodide, which were stirred and dried over 3A-grade molecular sieve for 2 days, while under high-vacuum. The allyl iodide was then carefully vacuum transferred to a side-arm and let down to an atmosphere of dry N_2(g). When the polymerisation was judged to be complete, **0.24 ml (2.70×10^{-3} mol)** of dry allyl iodide, roughly a 5 times excess amount, were injected into the reaction vessel. There was no visible colour change and the solution was stirred at the reaction temperature (–78°C) for a further 16 hours. **1 ml** of N_2-sparged CH_3OH was then added and the solution allowed to warm slowly to room temperature. The polymer was precipitated and dried as normal, was a yellow-white powder, and had a yield of **1.12 g**.

2.9.26 Synthesis of PMMA *(23)* capped with $C_{10}H_7COCl$ (aim = 2000 g mol^{-1})

The polymerisation was performed in the normal way. The quantity of MMA was **1.24 g (1.24×10^{-2} mol)**, so the amount of *s*-BuLi (1.5 M) required for the DPHLi initiator equalled **0.41 ml (6.20×10^{-4} mol)** and that for DPE equalled **0.11 ml (6.20×10^{-4} mol)**. **1.38 g (7.24×10^{-3} mol)** of $C_{10}H_7COCl$ were weighed into one bulb of a double-bulb side-arm, which contained a No. 3 glass sinter between the two bulbs. 3A-grade molecular sieve, stirrer and **5 ml** of dry THF were added, to give a solution of **0.276 g ml^{-1}**. The solution was put under high vacuum, dried for 2 days, and then let down to a N_2(g) atmosphere. The side-arm was then angled to allow the solution to be

filtered through the glass sinter, with the filtrate being collected in the second bulb. Upon completion of the polymerisation, **2.14 ml (2.85×10^{-3} mol)** of $C_{10}H_7COCl$ solution, roughly a 5 times excess amount, were injected into the reaction vessel. There was no visible colour change and the solution was stirred at the reaction temperature (–78°C) for a further 16 hours. **1 ml** of N_2-sparged CH_3OH was then added and the solution allowed to warm slowly to room temperature. The polymer was precipitated and dried as normal, was a white powder, and had a yield of **1.39 g**.

2.10 References

1. Antoun, S.; Teyssié, P.; Jérôme, R. *J. Polym. Sci. Pol. Chem.* **1997**, *35*, 3637-3644
2. Antoun, S.; Teyssié, P.; Jérôme, R. *Macromolecules* **1997**, *30*, 1556-1561
3. Varshney, S. K.; Hautekeer, J. P.; Fayt, R.; Jérôme, R.; Teyssié, P. *Macromolecules* **1990**, *23*, 2618-2622.
4. Schilling, F. C.; Bovey, F. A.; Bruch, M. D.; Kozlowski, S. A. *Macromolecules* **1985**, *18*, 1418-1422
5. Randall, J. C. *Polymer Sequence Determination: Carbon-13 NMR Method*; Academic Press: New York, N. Y., 1977, pp 111-114.
6. Peat, I. R.; Reynolds, W. F. *Tetrahedron Lett.* **1972**, *14*, 1359-1362
7. Gidden, J.; Jackson, A. T.; Scrivens, J. H.; Bowers, M. T. *Int. J. Mass Spectrom.* **1999**, *188*, 121-130
8. Jackson, A. T.; Bunn, A.; Hutchings, L. R.; Kiff, F. T.; Richards, R. W.; Williams, J.; Green, M. R.; Bateman, R. H. *Polymer* **2000**, *41*, 7437-7450
9. Jackson, A. T.; Yates, H. T.; Scrivens, J. H.; Green, M. R.; Bateman, R. H. *J. Am. Soc. Mass Spectrom.* **1997**, *8*, 1206-1213
10. Bowden, R. D. *The chemistry of ionised, protonated and cationated amines in the gas phase*; *The Chemistry of Functional Groups*; Patai, S.; Wiley: New York, N. Y., 1982, pp 236-241.
11. Bozanko, A.; Carswell, W. D.; Hutchings, L. R.; Richards, R. W. *Polymer* **2000**, *41*, 8175-8182
12. Schädler, V.; Spickermann, J.; Räder, H. J.; Wiesner, U. *Macromolecules* **1996**, *29*, 4865-4870

13. Hsieh, H. L.; Quirk, R. P. *Functionalised polymers and macromonomers*; Marcel Dekker: New York, N. Y., 1996, pp 275-276.

14. Greene, T. W.; Wuts, P. G. M. *Protective Groups in Organic Synthesis*; 2nd ed.; John Wiley and Sons: New York, N.Y., 1991, pp 436.

15. Staab, H. A. *Angew. Chem. Internat. Edit.* **1962**, *1*, 351-367

16. Doonan, S. *Biological formation and reactions of the -COOH and -COOR groups*; *The Chemistry of Functional Groups*; Patai, S.; Wiley: New York, N. Y., 1969, pp 1001-1005.

17. Hsieh, H. L.; Quirk, R. P. *Functionalised polymers and macromonomers*; Marcel Dekker: New York, N. Y., 1996, pp 279.

18. Altakrity, E. T. B.; Jenkins, A. D.; Walton, D. R. M. *Makromol. Chem.* **1990**, *191*, 3069-3072

19. Altakrity, E. T. B.; Jenkins, A. D.; Walton, D. R. M. *Makromol. Chem.* **1990**, *191*, 3073-3076

20. Williams, D. H.; Fleming, I. *Spectroscopic Methods in Organic Chemistry*; 4th ed.; Mcgraw-Hill: Maidenhead, U.K., 1987.

21. http://www.upstream.ch/cgi-bin/topnmr.pl.

22. http://www.aist.go.jp/RIODB/SDBS/menu-e.html.

Chapter 3

Characterisation of Non-Classically Synthesised PMMA

3.1 Introduction

The PMMA samples discussed in the previous chapter were synthesised via what can be termed as *'classical'* anionic methods. That is, using organolithium initiators, stringently purified reagents, and a polymerisation temperature of –78°C. Under these conditions, difficulties in successfully performing capping reactions to give end-functionalised PMMA were noted. Therefore, two alternative, *'non-classical'* routes to the desired low molecular weight, low polydispersity, end-functionalised materials were investigated. The first method was a variation of standard anionic polymerisation that involved the use of lithium silanolates, while the second was a controlled free-radical technique known as Reversible Addition-Fragmentation Chain Transfer (RAFT). The results of polymers synthesised using these two routes are reported and discussed.

3.2 PMMA Synthesised via Lithium Silanolate Ligated *s*-BuLi

The Jérôme/Teyssié group recently reported the polymerisation of MMA using *s*-BuLi ligated by a lithium silanolate as the initiator.[1] This system not only prevents the unwanted attack on the ester carbonyl by the initiator, which has been previously observed with this initiator, but also allows the polymerisation to proceed at a temperature of 0°C. The strategy for using such a system was that the capping reactions we had previously attempted at –78°C might prove more successful, when attempted at this higher temperature.

The lithium silanolate ligand is formed by the reaction of *s*-BuLi with cyclic diorganosiloxanes (D_x), *i.e.* hexamethyltrisiloxane ($(((CH_3)_2SiO)_3$, D_3). The reaction does not form the *s*-BuD_3Li species, but instead forms the *s*-BuD_1Li species, *i.e.* *s*-Bu$(CH_3)_2$SiOLi, because of rapid redistribution reactions.[2] Any excess D_3 does not polymerise in hydrocarbon media. Due to the tendency of lithium silanolate compounds to aggregate, the actual initiator/ligand system is believed to be a mixed associated species of the form {*x*s-BuLi, $(y - x)$*s*-BuD_1Li}. Therefore, the initial ratio of [*s*-BuLi]$_0$/[D_3]$_0$ (r) dictates the actual [*s*-BuD_1Li]/[*s*-BuLi] ratio (R) of the initiating system. When $r \leq 2.9$, and therefore $R \geq 21$, complete conversion of monomer was observed and the molecular weight distribution was considered to be both monomodal

and narrow. This result suggested the presence of only one type of active initiating species, *i.e.* {*s*-BuLi, $(y - 1)$*s*-BuD_1Li}, which would be converted into {*s*-$Bu(CH_2C(CH_3)CO_2CH_3)_nLi$, $(y - 1)$*s*-BuD_1Li} propagating chains. As a result of the theoretical value of $\overline{M}_n$ for this particular sample being 70% of the experimental value gathered via SEC, it was assumed that approximately 70% of the {*s*-BuLi, $(y - 1)$ *s*-BuD_1Li} species are actually available for initiation.

However, the value of y was not numerically defined. Therefore, preliminary investigations of samples terminated by a proton were carried out in order to gain a clearer understanding of the system, so exerting control of the polymers produced by it. Sample *24* was produced with $r = 2.8$, thus $R > 21$. A target molecular weight of 1200 g mol^{-1} was set based upon $[s\text{-BuLi}]_0$. With an initiator efficiency of approximately 70%, the actual value of $\overline{M}_n$ for *24* was expected to be closer to 2000 g mol^{-1}. However, the experimental molecular weight data obtained via SEC, shown in Table 3.2.1, gives a much greater value for $\overline{M}_n$. The sample did have a narrow polydispersity; hence some control of polymerisation had been exercised. In order to remove the possibility that this discrepancy was caused by impurities within the initiating system, the purification procedure for the D_3 reagent was altered so that a D_3/toluene solution was initially made then dried. Sample *25* was also produced with $r = 2.8$, and with a target molecular weight of 1500 g mol^{-1}. The SEC data again showed a much greater value for $\overline{M}_n$ than was anticipated (see Table 3.2.1), though the magnitude was slightly less than that for *24*. The polydispersity of *25* was also very narrow. It was suspected that the discrepancies observed with regard to the calculated and experimental molecular weights of *24* and *25* were not due to impurities, but instead related to the absolute amounts of $[s\text{-BuLi}]_0$ and $[D_3]_0$.

Sample	$\overline{M}_n$	$\overline{M}_w$	$\overline{M}_w/\overline{M}_n$
24	48100	50800	1.06
25	38200	41000	1.07
26	25900	29300	1.13

Table 3.2.1. SEC molecular weight data for *24-26*.

At this time, the Jérôme/Teyssié group reported the results of a ^7Li NMR study of the initiating system.[3] The study revealed that the mixed associated species were

actually in the form of hexamers, {*xs*-BuLi, (6 – *x*)*s*-BuD_1Li}, with *x* having values of 1-4. When $R \geq 21$, the {*s*-BuLi, 5*s*-BuD_1Li} mixed species is the only one to prevail, as a result of an excess of {6*s*-BuD_1Li} species, and can be regarded as the single initiator of MMA. Sample *26* was produced, again with $r = 2.8$ and a target molecular weight of 1500 g mol^{-1}, but with $[s\text{-BuLi}]_0$ six times greater than that required by the target molecular weight. This was to allow for the formation of five ligands per initiator molecule. However, the SEC data again showed a greater value than that anticipated (see Table 3.2.1). Normally, adding six times more initiator than necessary to an anionic polymerisation would result in a polymer molecular weight six times smaller. Therefore, regardless of the fact that the experimental values of $\overline{M}_n$ for *25* and *26* are vastly different from their common target value, the value for *26* may be expected to be six times smaller than that for *25*. In fact, the value is roughly two-thirds that for *25*. Although very narrow polydispersity polymers can be produced using this initiating system, it is apparent that the molecular weight of such polymers cannot be controlled to a high degree.

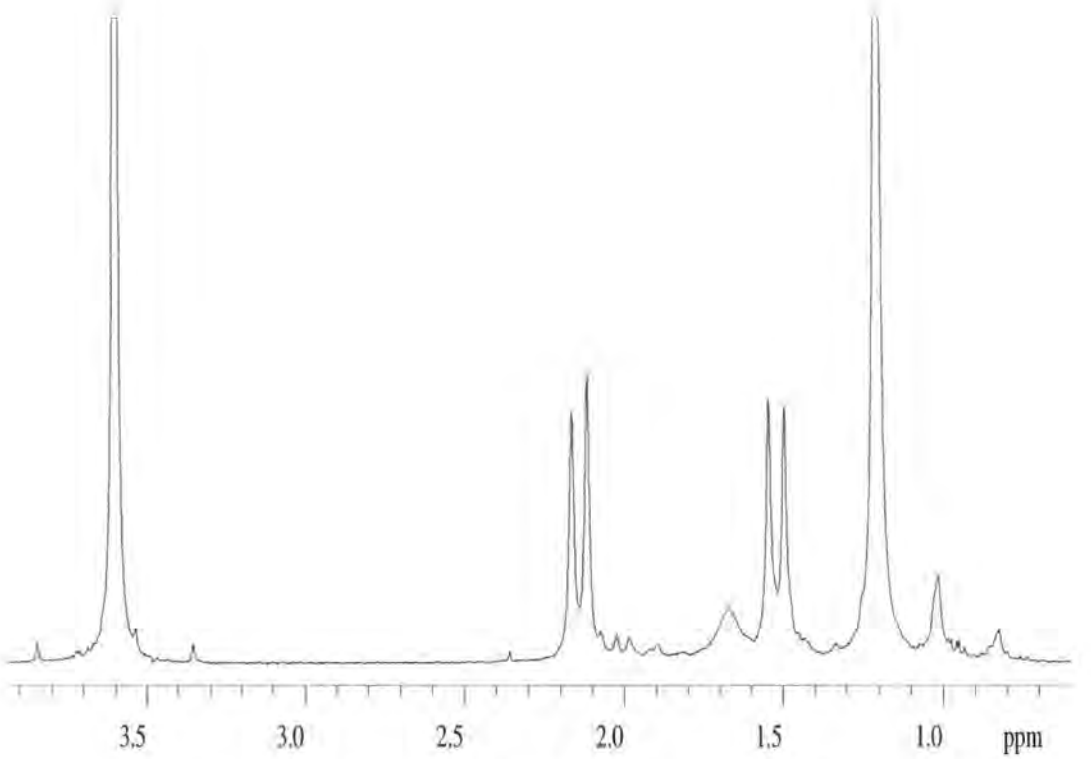

Figure 3.2.1. Proton NMR spectrum of *26*.

The proton NMR spectrum of *26* is featured in Figure 3.2.1 as an example. The signals due the methoxy groups (δ = 3.6 ppm), methylene groups (between δ = 1.4-2.2 ppm) and methyl groups (between δ = 0.6-1.4 ppm) of the repeat unit can easily be

assigned. The methylene signals differ from those observed previously due to the high isotacticity of the sample. Even at this relatively low molecular weight, the signals due to the butyl and proton end-groups are too weak to be readily distinguished from the background noise. The peak expected at $\delta = 2.5$ ppm due to the terminating proton is not observed. There is the added complication of probable overlap with repeat unit signals with regard to the butyl-group peaks. MALDI analysis was not performed on *24-26* as the molecular weights were to high to provide any useful information regarding end-group structure. As well-defined samples cannot be easily synthesised with this system, it was not further explored experimentally.

It is clear that this system is not comprehensibly reported in the literature mentioned above. A further study of both papers revealed only greater uncertainty about the system, rather than greater clarity. It appeared initially that as long as $r \leq 2.9$, this would automatically lead to $R \geq 21$, and a controlled polymerisation would ensue; hence R was largely overlooked. This appears true in terms of polydispersity, but not so with regard to molecular weight, so how is R related to r? The reported values of R were determined by a haloalkane double-titration method.[4] The reported values of r against R are plotted in Figure 3.2.2. The data (squares) has been fitted to a second order exponential model (line), with the exception of one data point (triangle), which was considered anomalous. It is clear that r and R are consistently related, though this does not explain how R is related to molecular weight.

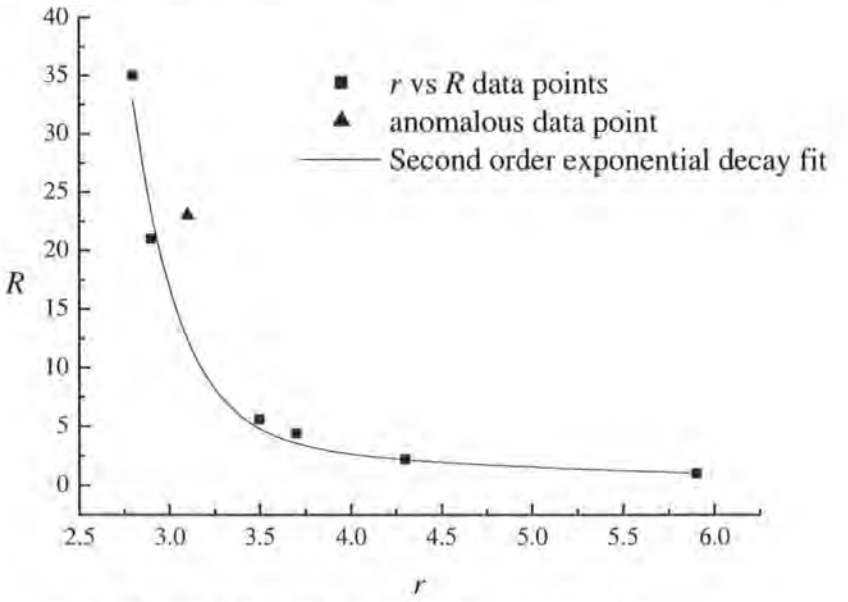

Figure 3.2.2. Plot of r vs R with fitted curve.

A value for the theoretical $\overline{M}_n$ (26000 g mol^{-1}) is only given for one sample were r = 2.9 and R = 21, and where it is speculated, via comparison with the SEC value (37000 g mol^{-1}), that only 70% of the mixed species are available for initiation. From this theoretical molecular weight value and the initial concentrations of *s*-BuLi and MMA ([*s*-BuLi]$_0$ and [MMA]$_0$) that [*s*-BuLi]$_0$ is twenty-one times greater than that normally needed to produce such a polymer. Is it coincidence that this excess has the same value as R? It may mean that [*s*-BuLi]$_0$ must be twenty-one times greater than necessary, in addition to $r = 2.9$, to produce a polymer that has a molecular weight approximately 43% higher than intended. This hypothesis is summarised below in Equation 3.2.1.

$$[s\text{-BuLi}]_0/[s\text{-BuLi}]_{required} = [s\text{-BuD}_1\text{Li}]/[s\text{-BuLi}] = R \qquad \textbf{Eqn 3.2.1}$$

This hypothesis was tested with concentration and SEC values of $\overline{M}_n$ for *24-26*, where $r = 2.8$, hence R = 35, in all cases. The generated values for measured molecular weights were 60600, 75190 and 12540 g mol^{-1} for *24-26* respectively. A comparison of these values and those provided by SEC show clear disagreement; thus this hypothesis does not accurately describe the system.

The literature mentions that the {*s*-BuLi, 5*s*-BuD$_1$Li} initiating species co-exists with the {6*s*-BuD$_1$Li} species. This may explain why the theoretical mass for the example given above is 70% of that observed. As this relationship appears to be isolated, the equilibrium between the hexameric organolithium may be controlled by other factors than the initial ratio r. Data are also given in the literature for two samples where r (2.8), R (35) and [MMA]$_0$ are identical, but [*s*-BuLi]$_0$ is halved for the second sample. The first sample has a value of $\overline{M}_n$ = 79000 g mol^{-1}, while the second sample has a value of $\overline{M}_n$ = 100000 g mol^{-1}, only a 27% increase instead of the 100% increase normally observed. It was shown above that r and R are consistently related yet this result suggests that the amount of initiating species is independent of these ratios. Again, the equilibrium, and therefore the initiator concentration, appears to be controlled by other factors than the initial ratio r.

A further problem with this system was discovered when samples *24-26* were analysed by a triple detector SEC array. Let us recall that when $r \leq 2.9$, and therefore $R \geq 21$, a monomodal distribution should be observed. This was shown by a series of

SEC traces for a set of samples with *r*-values ranging from 5.9-2.8.[1] The samples were analysed by SEC using a refractive index (RI) detector only. The triple detector SEC trace for *24* is shown in Figure 3.2.3. In descending order, the traces are due to light scattering (LS, green), differential pressure (DP, blue) and RI (red) detectors. The value of *r* for *24-26* was 2.8 and the RI trace appears to show only one peak as expected. However, a closer inspection of the RI trace reveals an additional peak at a higher molecular weight, around 300000 g mol^{-1}. This peak is more prominent in both the LS and DP traces, and could easily be overlooked when considering only the RI trace. By comparing the peak areas of the RI trace, this higher molecular weight species constitutes approximately 5.7% of the sample. This result would appear to indicate that even with $r = 2.8$, multiple active species are present within the system. Consequently, it may be extremely difficult, if not impossible, to control polymer molecular weight with this system.

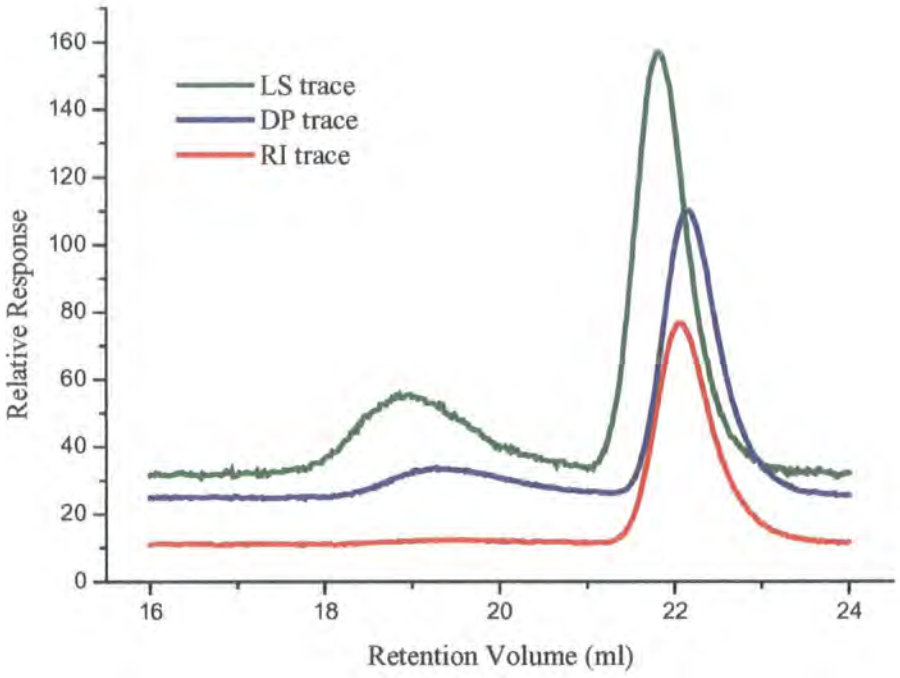

Figure 3.2.3. Triple detector SEC trace for *24*.

In conclusion, polymerisations of MMA were carried out at 0°C using a novel initiating system that involved *s*-BuLi ligated by a lithium silanolate. The molecular weights of these samples were much higher than anticipated. The reported literature of the system was investigated further to try to ascertain the factors that control the formation of the initiator. Even with certain factor kept constant the amount of initiator formed appears to be fairly random, therefore it would not seem possible to produce

polymers of controlled molecular weight with this system. The inventor's claims that monomodal distributions are produced under certain conditions were refuted by SEC data.

3.3 PMMA Synthesised via RAFT

The RAFT polymerisation technique was recently invented by Rizzardo *et. al.* at CSIRO Molecular Science, Australia.[5,6] Along with atom transfer radical polymerisation (ATRP),[7] RAFT has rapidly become a widely used route to specifically tailored materials. Like ATRP, RAFT is a controlled free-radical technique (also termed pseudo-living), meaning that it possesses some of the characteristics of living polymerisations, which were outlined in Chapter 1. These characteristics include polymers of narrow polydispersity (usually <1.2; sometimes <1.1) and the ability to form block copolymers by further monomer addition.

The technique is very versatile and robust, and is centred on the use of dithioesters[6,8] (ZCS_2R) and certain dithiocarbamates[9] (R'_2NS_2R) as chain transfer agents. Once a polymerisation has been initiated using a standard free-radical initiator, the propagating radicals react with the RAFT agents (RA) such that the R-group is released as a radical, which initiates further chains. These RA confer living character on the polymerisation by rapidly transferring the ZCS_2-moiety between active and dormant chains. The net result is a polymer comprising of an R-group at one end and a ZCS_2-moiety at the other, plus a small amount of initiator derived chains. The total number of moles of both RA and initiator determines the total number of polymer molecules, so the final polymer molecular weight may be predicted. The mechanism of polymerisation is summarised in Figure 3.3.1, and has been given credence by electron spin resonance (ESR)[10] and kinetic[11] studies. An effective RA is required to have a high transfer constant (C_{tr}), in the order of 2 or greater. In other words, both rates of addition and fragmentation must be faster than the rate of propagation. The nature of Z, R'_2N and R-groups is very important to performing a RAFT polymerisation successfully. The Z or R'_2N-moieties should activate (or at least not deactivate) the C=S double bond toward radical addition, thus ensuring a high C_{tr}. Typical examples of a Z-moiety are aryl and alkyl groups. The R-group should be a good free-radical leaving group, and be an effective free-radical polymerisation initiator.

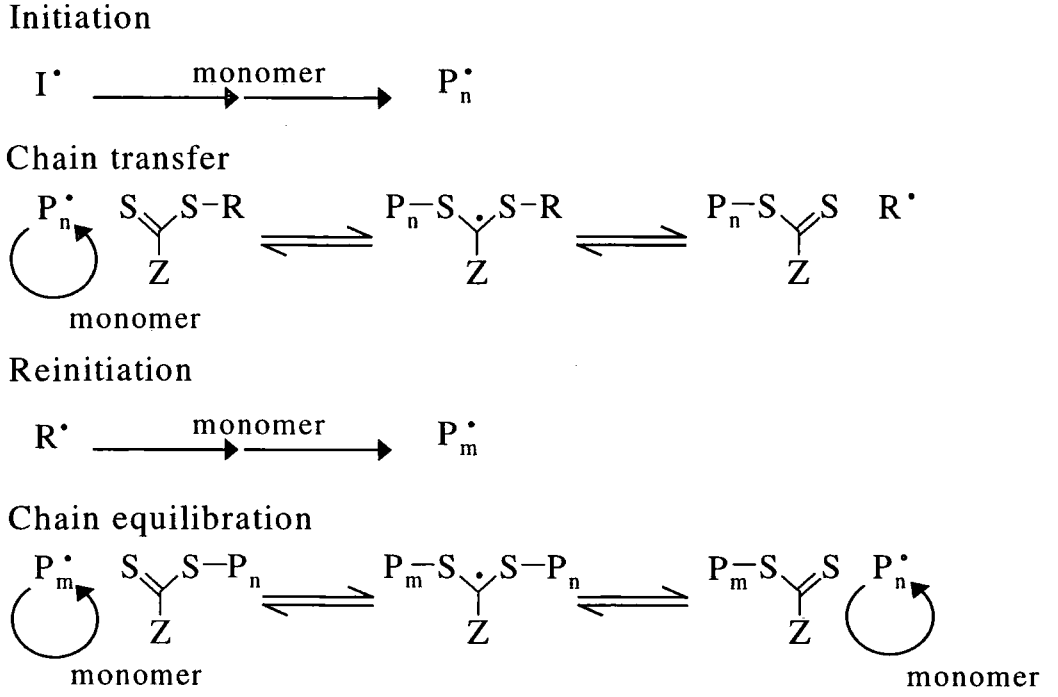

Figure 3.3.1. General mechanism of the RAFT polymerisation technique.

A wider variety of dithioester reagents than dithiocarbamate reagents are known to be effective RA. The synthesis of these compounds is relatively difficult, requiring several synthetic and purification steps, so attention turned to commercially available compounds. At the time, the only commercially available dithioester compound was *S*-(thiobenzoyl)thioglycolic acid ($PhCS_2CH_2CO_2H$, Aldrich), henceforth denoted as RA′. The first attempt at producing PMMA via RAFT employed RA′ and 2,2′-azobis(2-cyanopropane) (AIBN) free-radical initiator in a 2:1 ratio, giving a RA: initiating radical ratio of 1:1. The result was Sample *27* and the fact that the product was pink in colour, due to the incorporation of the dithiobenzyl chromophore as an end-group, indicated a successful polymerisation. However, as a substantial increase in viscosity was noticed during the polymerisation, a high molecular weight polymer was anticipated. This was confirmed via data from SEC, given in Table 3.3.1, which showed that *27* had a much higher molecular weight than that targeted and had a relatively broad polydispersity. The SEC trace also showed a second peak corresponding to very high molecular weight polymer ($\overline{M}_n \approx 1.6\times10^6$ g mol^{-1}), which constituted approximately 1.3% of the sample. Therefore, the synthesis of *27* was not well controlled.

To exercise greater control of the polymerisation, in terms of both polymer molecular weight and polydispersity, the RA:initiator ratio was increased. Sample *28*

was synthesised with a RA′:AIBN ratio of 40:1. Similar observations were made regarding colour and viscosity as for *27*. The SEC data, again given in Table 3.3.1, showed that *28* was monomodal, but the molecular weight much higher than that targeted. Even though the polydispersity was slightly lower than that for *27*, these results again show a severe lack of control of the polymerisation. Further attempts at producing low molecular weight polymers were made by using the same RA′:AIBN ratio, but with much shorter reaction times. This was done to try to achieve low conversions, though this might increase the polydispersity.[6,12] Samples *29-31* were the result and similar observations were made regarding colour and viscosity as before. The SEC data (see Table 3.3.1) again gave high molecular weights and were monomodal for all samples. Neither proton or carbon NMR spectra were recorded for these samples as no valuable information regarding end-group structure would be gained. The conclusion drawn from these findings is that RA′ is not very effective with regard to the controlled polymerisation of MMA.

Sample	$\overline{M}_n$	$\overline{M}_w$	$\overline{M}_w/\overline{M}_n$
27	35400	76600	2.16
28	436900	838300	1.92
29	180900	352300	1.95
30	342900	546500	1.59
31	216400	389700	1.80
32	4920	5630	1.14

Table 3.3.1. SEC molecular weight data for *27-33*.

The research now focussed on a non-commercially available RA, but one already proven to be effective in RAFT polymerisations of MMA. The dithioester chosen was 2-phenylprop-2-yl dithiobenzoate ($PhCS_2C(CH_3)_2Ph$; also know as cumyl dithiobenzoate), henceforth denoted as RA″. The synthesis of RA″ is summarised in Figure 3.3.2 below:[13]

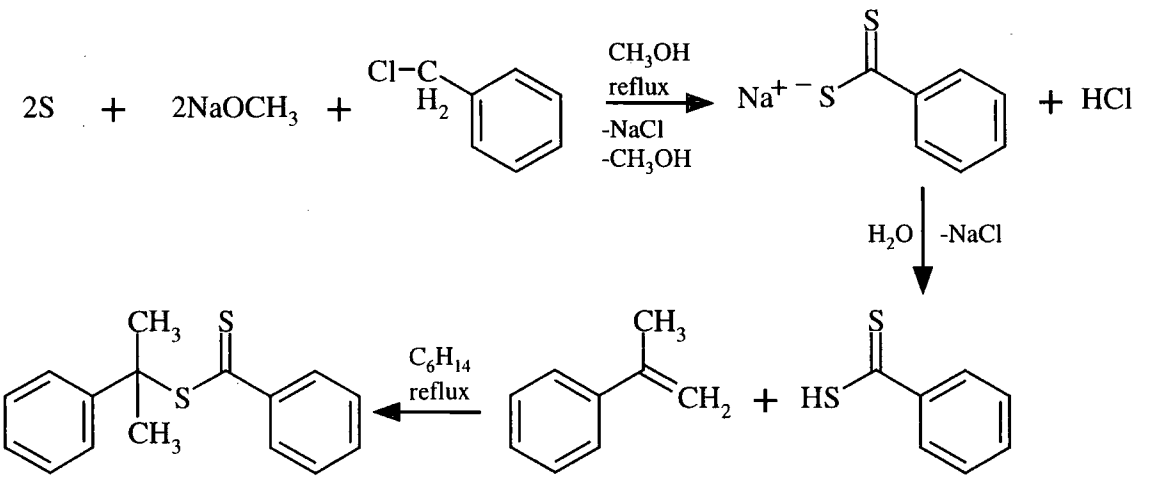

Figure 3.3.2. Synthetic route to RA″.

The expanded aromatic region of the proton NMR of RA″ is featured in Figure 3.3.3. The peaks are too numerous for only one singly substituted aromatic ring. The doublet at δ = 7.8 ppm can easily be assigned to the H_d-protons, as they are the furthest down field, due to the close proximity of the thiocarbonyl group, and are coupled to the H_e-protons only. The integrations of both peaks between δ = 7.4-7.6 ppm are equivalent to two protons. The doublet must correspond to the H_a-protons of the other ring, as these are also coupled to the H_b-protons only. The triplet can be assigned to the H_e-protons, as this peak occurs at relatively low field and these protons are coupled to both the H_f and H_d-protons. The other signals occurring between δ = 7.1-7.4 ppm cannot be assigned easily as they appear to overlap, and there is also a signal due to the solvent. The peak due to the H_c-proton is likely to be the furthest up field at around δ = 7.2 ppm, while signals due the H_f and H_b-protons are more likely to be around δ = 7.3 ppm. The integration of these peaks was equal to more than four protons, which is attributed to the presence of the solvent peak. A single peak at δ = 2.0 ppm was due to the two equivalent methyl groups. Some other peaks due to remaining impurities were observed, but this was not considered too important given the reported robustness of the RAFT system.

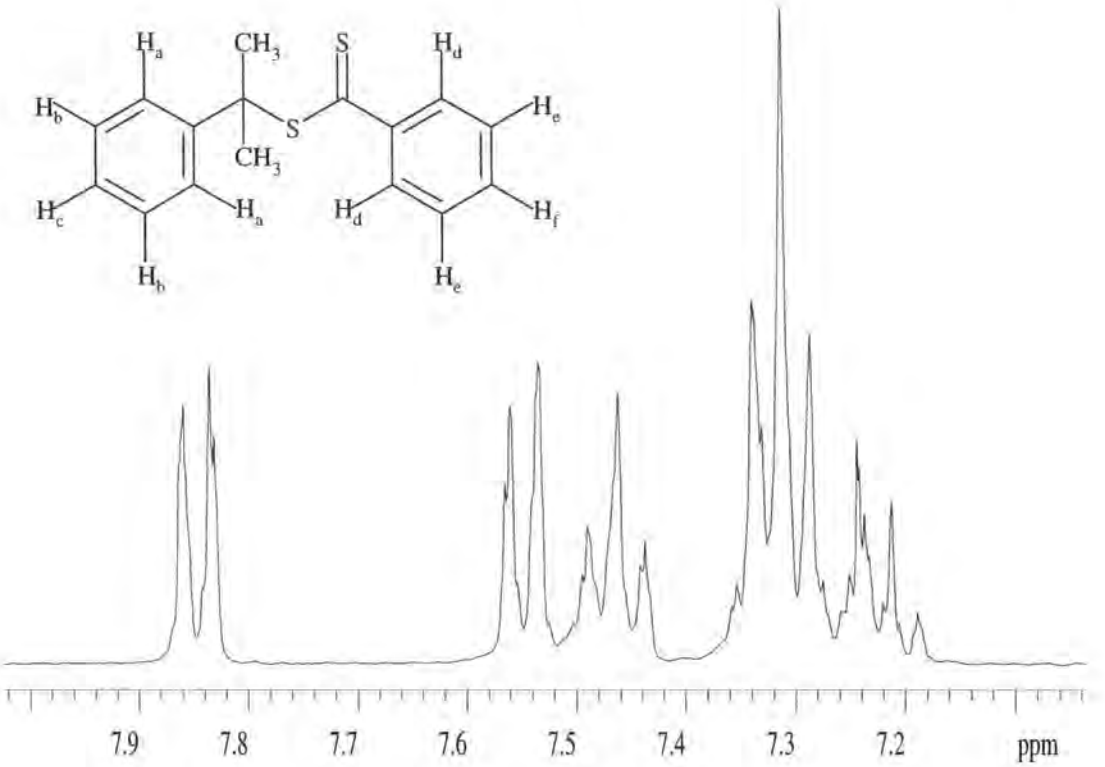

Figure 3.3.3. Aromatic region of the proton NMR spectrum of RA″.

Sample *32* was produced with a RA″:AIBN ratio of 10:1. As before, the polymer was pink, but an increase in viscosity was not observed during the polymerisation. This was taken as a good indication that a more controlled polymerisation had been performed. The SEC trace showed only one peak and the data (see Table 3.3.1 above) indicated *32* to be both low molecular weight and have a relatively narrow polydispersity. Thus the desired RAFT polymerisation of MMA employing RA″ has been successful. The molecular weight is roughly double that expected and conversion was not 100%, which suggests that RA″ has a low C_{tr}. This observation has been noted before when RA″ is used in high concentrations in order to form low molecular polymers and is attributed to slower fragmentation and changes in radical specificity.[12]

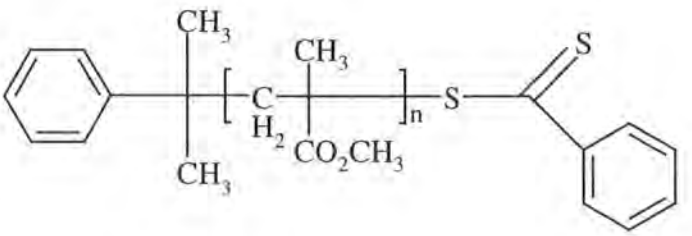

Figure 3.3.4. Stoichiometric formula of *32*.

The stoichiometric formula of *32* is pictured in Figure 3.3.4 above. The proton NMR of *32* is shown in Figure 3.3.5, which was performed in CD_2Cl_2 in order to avoid signal overlap in the aromatic region ($\delta = 5.3$ ppm). The peaks due to mainchain groups are easily recognised. In the midst of the peaks corresponding to the methylene groups is a sharp, single peak at $\delta = 1.2$ ppm, which corresponds to the equivalent methyl groups of the initiator end-group. The other peaks of interest occur in the aromatic region, which has been expanded for greater clarity. Similar to the proton spectrum of RA″, the peak pattern is too complicated to correspond to only one singly substituted aromatic ring, indicating that both aromatic groups of RA″ have been incorporated into the polymer. Using the same convention that was given for the aromatic protons of RA″, the peak at $\delta = 7.9$ ppm corresponds to the H_d-protons. Peak integrations show that the peaks between $\delta = 7.1$-7.2 ppm and $\delta = 7.5$-7.6 ppm correspond to a single proton each. Therefore, the former can be assigned to the H_c-proton and the latter to the H_f-proton. The peak around $\delta = 7.4$ ppm is most likely to correspond to the H_e-protons, while the other two signals appear to overlap at around $\delta = 7.3$ ppm; hence these peaks cannot be assigned with any great certainty from a standard NMR spectrum.

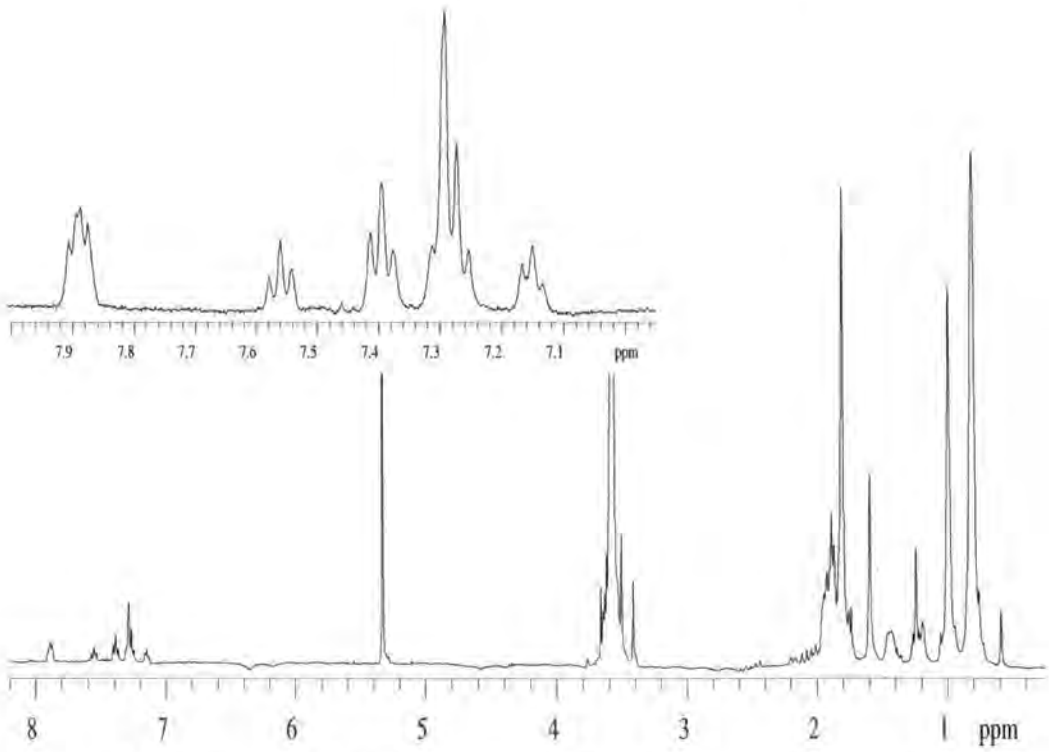

Figure 3.3.5. Proton NMR spectrum of *32* with expanded aromatic region.

Two-dimensional (2D) NMR provided further information regarding end-group structure of *32*. The expanded aromatic region of the ^{1}H-^{1}H COSY spectrum is shown in Figure 3.3.6. The peak due to the H_d-protons is coupled to the peak around $\delta = 7.4$ ppm, confirming that this is due to the H_e-protons. This peak is in turn coupled to the peak between $\delta = 7.5$-7.6 ppm, which fits with the H_f-proton assignment given to it. This means the other signals must correspond to the $H_{a\text{-}c}$-protons, with the overlapping peaks corresponding to the H_a and H_b-protons. The ^{1}H-^{1}H COSY spectrum confirmed this assignment.

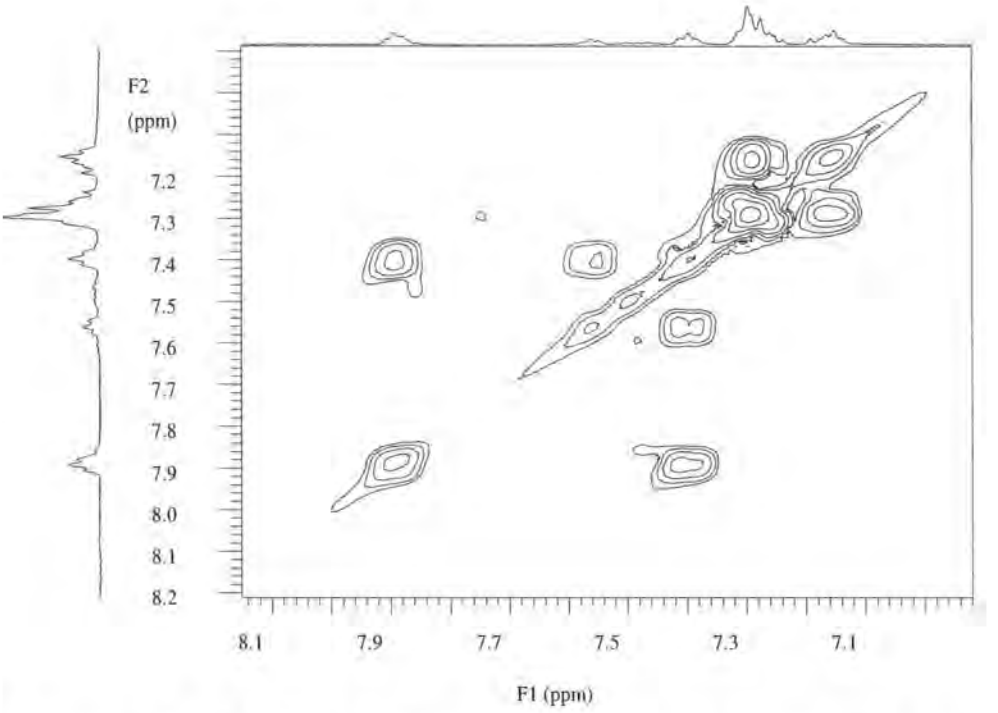

Figure 3.3.6. ^{1}H-^{1}H COSY spectrum for the aromatic region of *32*.

The carbon NMR spectrum of *32* is pictured in Figure 3.3.7. In addition to the peaks corresponding to the polymer backbone assigned previously, there are peaks between $\delta = 120$-140 ppm corresponding the phenyl rings of both end-groups. There is also a peak at $\delta = 28$ ppm that is likely to correspond to the equivalent methyl groups of the initiator end-group, while the peak at $\delta = 226$ ppm is likely to be due to the thiocarbonyl group. Other signals are due to groups of the ultimate and penultimate repeat units at either chain-end.

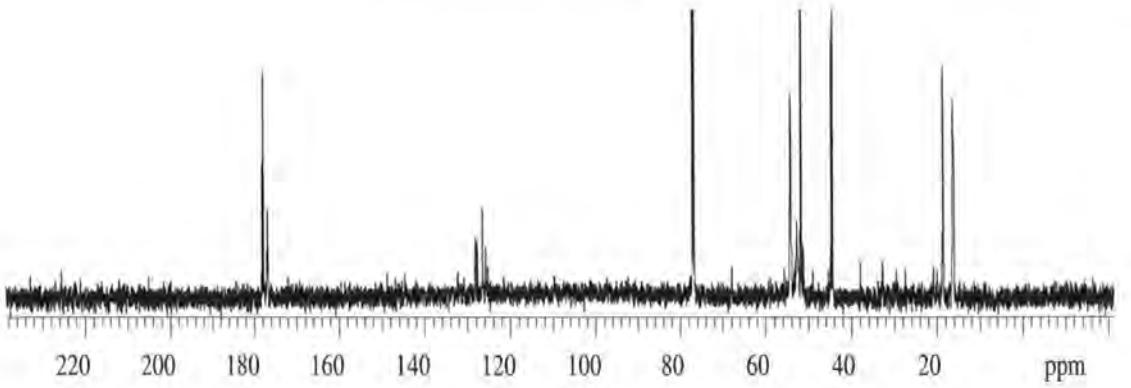

Figure 3.3.7. Carbon NMR spectrum of *32*.

Further confirmation of these peak assignments was derived from the 2D ^{1}H-^{13}C HETCOR spectrum. The regions of particular interest have been expanded and are shown in Figure 3.3.8. The left-hand spectrum shows the aromatic region. Six separate signals are observed, corresponding to the six different C-H groups ($H_{a\text{-}f}$-protons) present in the end-groups. It is clear that the peak around $\delta = 7.3$ ppm is due to two overlapping proton signals. The right-hand spectrum shows the alkyl region, with the strongest signals corresponding to the methyl groups of the backbone. What is most important about this region is that a signal is observed that corresponds to both the peak at $\delta = 1.2$ ppm in the proton spectrum and $\delta = 28$ ppm in the carbon spectrum. Both these peaks have previously been assigned to the methyl groups of the initiator end-group independently; hence the original assignments have been confirmed.

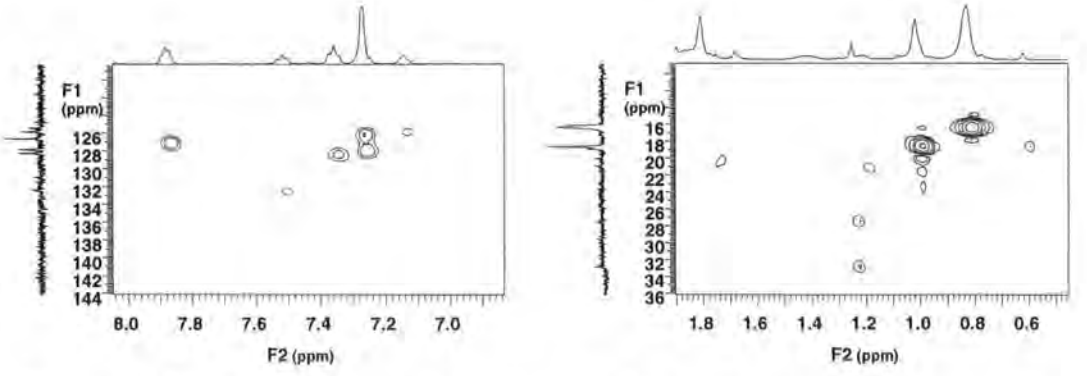

Figure 3.3.8. Regions of note from the 2D ^{1}H-^{13}C HETCOR spectrum of *32*.

Usually PMMA is white or colourless, but *32* was coloured pink due to the incorporation of the dithiobenzyl chromophore as an end-group. Therefore, *32* can be characterised further by UV/Vis spectroscopy and the recorded spectrum is given in

Figure 3.3.9. The fact that such a strong absorbance spectrum is observed again confirms the presence of the dithiobenzyl end-group. The maximum absorbance (λ_{max}) was observed at 303 nm. Thus, the structure given in Figure 3.3.4 was confirmed by proton and carbon NMR and UV/Vis spectroscopies.

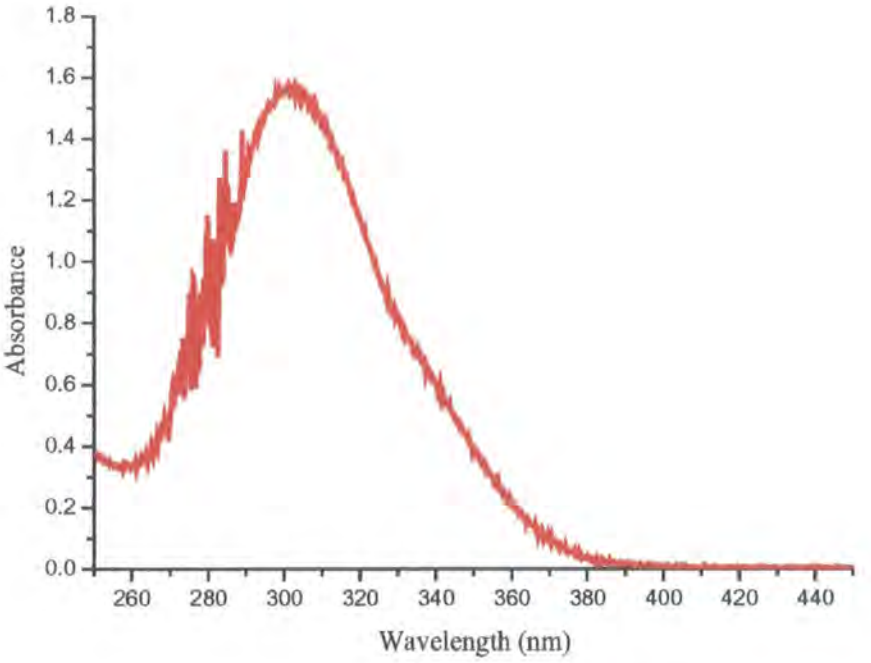

Figure 3.3.9. UV/Vis spectrum of *32*.

The reflectron MALDI spectrum of *32* is shown in Figure 3.3.10. The spectrum was obtained with the addition of a lithium salt. The spectrum clearly shows only one series of peaks, indicating there is only one polymeric species present in the sample. However, the peak mass values showed strong disagreement when compared with the theoretical mass values for the $(32+Li)^+$ species, given in Table 3.3.2. The observed values appear to be 54 or 154 amu lower than expected. A spectrum was also obtained for sodium cationised samples and similar discrepancies between observed and calculated mass values were noted. There are high degrees of confidence that lithium and sodium cationised species are being observed, and not species cationised by different ions, due to a difference of 16 amu between the respective series.

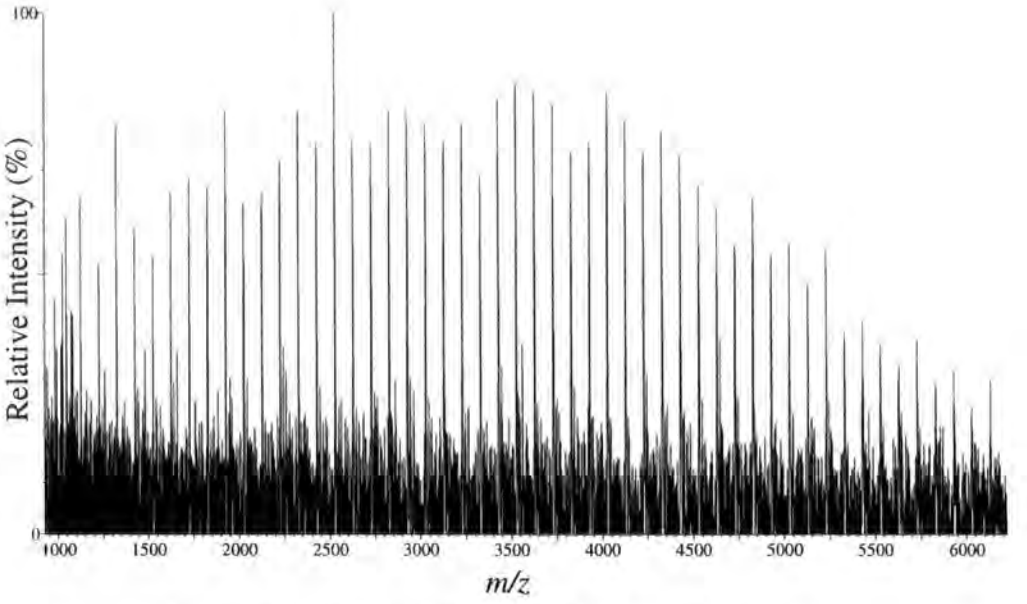

Figure 3.3.10. Reflectron MALDI spectrum of *32*.

32 and $[32+Li]^+$			*32* and $[32+Na]^+$		
n	Obs.	Calc.	n	Obs.	Calc.
10	1226.80	1280.56	10	1242.63	1296.61
11	1326.76	1380.68	11	1342.06	1396.73
12	1426.93	1480.80	12	1442.72	1496.84
13	1526.67	1580.91	13	1542.66	1596.96
14	1627.00	1681.03	14	1642.56	1697.08
15	1726.91	1781.15	15	1742.71	1797.20
16	1827.12	1881.27	16	1842.73	1897.32
17	1927.34	1981.39	17	1943.14	1997.44

Table 3.3.2. Average observed and calculated mass comparisons for *32*.

As the end-group structure of *32* has been well established via other analytical methods, the mass value discrepancies must be attributed to the MALDI analysis. It has already been noted that elimination is the most likely mechanism for any observed mass losses during MALDI analysis. This particular mass loss has not been observed with other PMMA samples (*i.e.* those discussed in Chapter 2) and is therefore probably derived from the end-groups. The masses of the initiator and terminator end-groups are 119 and 153 respectively, so it is reasonable to assume that the dithiobenzyl group is involved in the elimination. Not only does this group have almost the exact same mass

value as the observed loss, but it also contains an ester moiety that is more prone to elimination than the initiator end-group. Hence, intramolecular proton abstraction, resulting in the elimination of dithiobenzoic acid having a mass of 154 amu, and leaving the polymer with an unsaturated end-group (*32*†) would explain the observed mass loss. A common mechanism that would achieve this result is that for ester pyrolysis, and this is illustrated with respect to *32* in Figure 3.3.11. Due to the ultimate repeat unit forming the new end-group, the n oligomer of the original polymer forms the n-1 oligomer of the elimination product. A comparison of the observed masses and the calculated elimination product masses, both cationised with lithium and which show very good agreement, is given in Table 3.3.3.

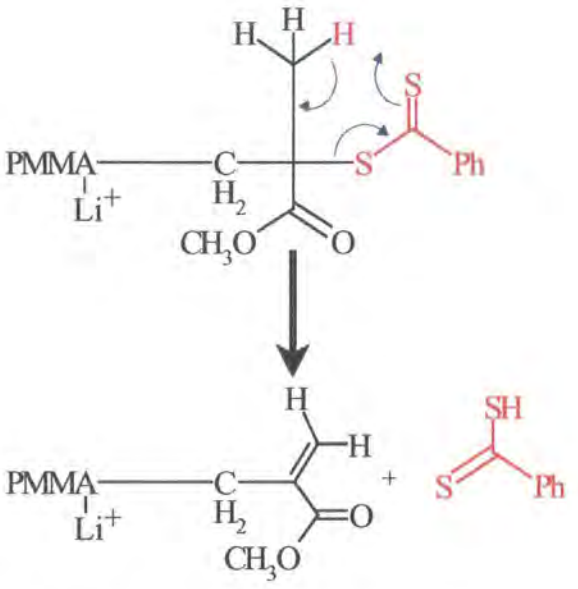

Figure 3.3.11. Proposed elimination mechanism from *32* to *32*†.

32 and $[32^{\dagger}+Li]^{+}$		
n	Obs.	Calc.
10	1226.80	1226.42
11	1326.76	1326.54
12	1426.93	1426.66
13	1526.67	1526.78
14	1627.00	1626.89
15	1726.91	1727.01
16	1827.12	1827.13
17	1927.34	1927.25

Table 3.3.3. Average observed and calculated mass comparisons for *32*†.

A comparison of the theoretical and observed isotope distributions provided a further indication that an unsaturated end-group is produced during MALDI analysis. For example, the isotope distributions for the n = 11 peak of *32*† are compared in Figure 3.3.12. The small peak at 1324.76 amu corresponding to *32*† being cationised by ^{6}Li, the next peak at 1325.79 amu corresponding to a mixture of the species containing one ^{13}C being cationised by ^{6}Li and the 100% ^{12}C species being cationised by ^{7}Li, and so on for higher masses. Hence, there is very close agreement between the two spectra, though of course this does not confirm the mechanism.

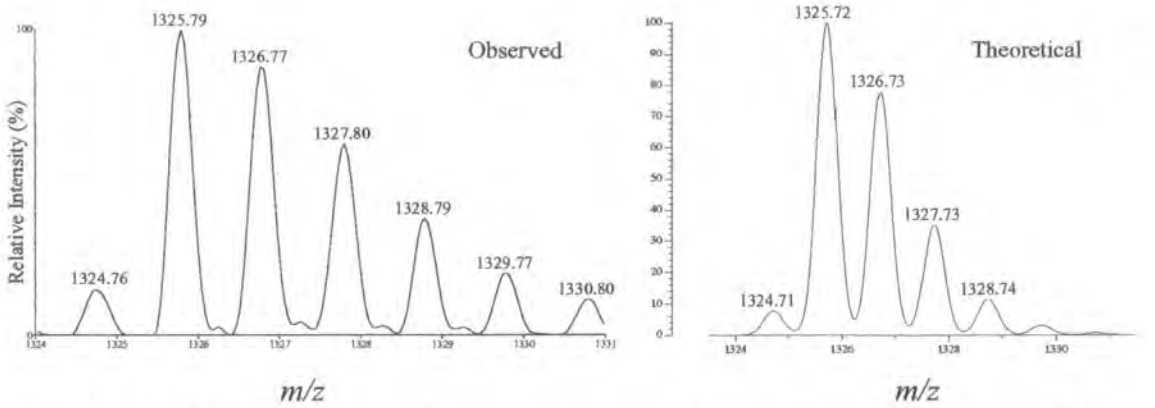

Figure 3.3.12. Observed and theoretical isotope distributions for *32*† (n = 11).

In order to confirm the nature of the end-groups individually, MALDI-CID analysis was performed on *32*. The fragmentation spectrum for the n = 11 peak at 1325.79 amu is featured in Figure 3.3.13. The spectrum gave us several peak series, **A-G**, most notably due to mainchain bond scissions from the initiator chain-end, series **B** (red), and from the terminator chain-end, series **A** (green). The stoichiometric formula of *32*† is also given in Figure 3.3.13, and shows the scission points from which the peak series **A** and **B** are derived. The other series observed (series **C-G**) are due to mid-chain rearrangement processes, the mechanisms for which are given elsewhere.[14] Series **A**, **D** and **E** fit with *32*† having the structure containing an unsaturated end-group. These results provided further evidence of the likelihood of the elimination mechanism proposed.

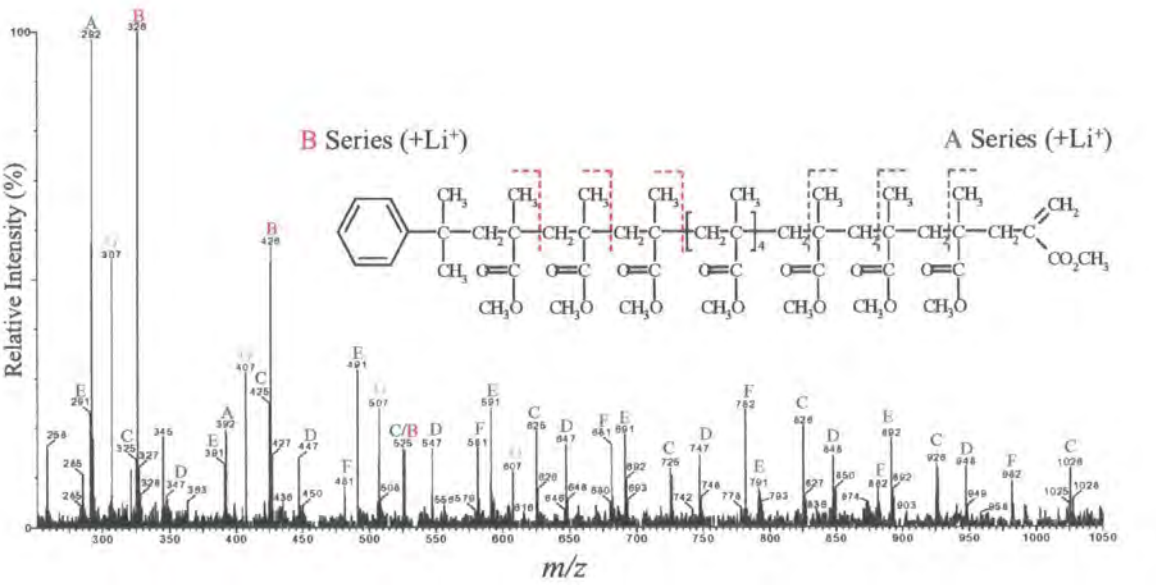

Figure 3.3.13. MALDI-CID spectrum of *32*† (n = 11).

A similar observation has already been reported for a sample of poly(*N*-isopropylacrylamide) (PNIPAM), which was synthesised using benzyl dithiobenzoate as the RA.[15] An unsaturated end-group results from the elimination, though no elimination mechanism for its formation is provided by the authors. Instead, it is suggested that either transfer to monomer, or through termination by disproportionation forms the unsaturated end-groups. However, these processes are part of the synthetic procedure, so there should be evidence for unsaturated end-groups from other analytical methods, such as NMR, but this was not discussed. The NMR spectra of *32* showed no evidence for unsaturated end-groups, so elimination within the mass spectrometer would appear the more probable explanation for these observed end-groups.

The matrix used during sample preparation for the PNIPAM samples was 2,5-dihydroxybenzoic acid (DHB) and a sodium salt was added, with peak series being observed for sodium, potassium and proton cationised elimination species. However, three analogous series for the intact polymer were observed, which indicates that the degree of elimination may be related to the nature of the polymer repeat unit or matrix. Additionally, no elimination is observed for a similar sample analysed with a different mass spectrometer or for PNIPAM samples synthesised with RA″, which all have the same terminator end-group. Based upon both these results and those gathered for *32*, there would appear to be no pattern as to what conditions are necessary that would lead to the elimination. The dithiobenzyl end-group absorbed strongly in the UV/Vis region at 303 nm and most MALDI mass spectrometers use N_2-lasers having a wavelength of 337 nm. These wavelengths are relatively close, so it is possible that the dithiobenzyl end-group absorbs the laser radiation directly, enough to facilitate the end-group elimination. In order to test this hypothesis, *32* was analysed without the addition of a matrix, but no spectra were obtained. The conditions required for the elimination are obviously complex, probably involving polymer structure, matrix type, solvent, concentration, laser power and sample deposition method, all to varying degrees.

To summarise, several PMMA samples were synthesised via RAFT using $PhCS_2CH_2CO_2H$ (RA′). SEC data revealed that these polymerisations were poorly controlled, so it can be concluded that RA′ should not be used in conjunction with MMA. $PhCS_2C(CH_3)_2Ph$ (RA″) was synthesised and used to produce a well-controlled PMMA sample (*32*), which was well characterised by NMR and UV/Vis spectroscopies. MALDI analysis of *32* revealed discrepancies between the observed

and theoretical mass values, thought to be the result of an *in situ* elimination process. A mechanism for the elimination was proposed, and is supported by the comparison of peak isotope distributions and peaks series from MALDI-CID studies. The exact nature of the elimination and the condition required for it to occur are as yet unknown.

3.4 Experimental

The details of the analytical equipment and protocols were given in Section 2.8 of Chapter 2. UV/Vis data was collected using an ATI Unicam UV2 spectrometer. THF solutions at a concentration of 1.0×10^{-4} M and 1 cm path-length quartz cells were used.

The purification procedures for MMA monomer (Aldrich) and solvents are detailed in Sections 2.9.1 and 2.9.2 of Chapter 2 respectively. Benzene and diethyl ether solvents were used as received. All solvents were purchased from either Fisher or BDH. AIBN (Acros) was purified via recrystallisation from hot CH_3OH.

3.4.1 Preparation of PMMA (*24*) using a lithium silanolate ligated *s*-BuLi initiator

Into a 100 ml side-arm was placed **0.26 g (1.19×10^{-3} mol)** of D_3 (Aldrich), along with two spatulas of CaH_2 (Aldrich). A freeze-degas-thaw cycle was performed and the D_3 dried by stirring overnight. The dry D_3 was vacuum-distilled into a dry, degassed 250 ml side-arm (the main reaction vessel), which was furnished with a stirrer bar and septum. The main vessel was let down to an atmosphere of N_2(g). Approximately 100 ml of toluene was vacuum-distilled from over CaH_2 into a dry side-arm fitted with a septum, which was subsequently let down to an atmosphere of N_2(g). 5 ml of toluene was transferred to the main vessel via a syringe. This was followed by **2.56 ml (3.33×10^{-3} mol)** of *s*-BuLi (1.3 M, Aldrich) and a pale yellow colouration was observed. The solution was placed into a cold-water bath and left for 20 hours at 20°C.

The remaining amount of toluene was transferred into the main vessel using a cannula. The solution was cooled to 0°C by means of an ice bath to which a little NaCl had been added. Next, **4.27 ml (4.00 g, 4.00×10^{-2} mol)** of MMA was introduced via a syringe. The polymerisation was allowed to proceed for 1 hour and was then terminated

by adding 1 ml of N_2-sparged CH_3OH. The polymer was precipitated into hexane, previously cooled by dry ice, vacuum-filtered through a No.3 glass sinter and dried overnight in a vacuum oven at room temperature. The polymer was a fine, white powder and the yield was **4.01 g**.

3.4.2 Preparation of PMMA (*25*) using a lithium silanolate ligated *s*-BuLi initiator (aim = 1500 g mol^{-1})

In a 50 ml side-arm, 5 ml of D_3/toluene solution was made to a concentration of **0.27 g ml^{-1}**. CaH_2 was added, the side-arm was evacuated and the solution dried by stirring overnight. The dry solution was vacuum-distilled into a dry 10 ml side-arm fitted with a septum, which was subsequently let down to a N_2(g) atmosphere. The initiator solution was prepared as described above, using **0.40 ml (0.11 g, 4.76×10^{-4} mol)** of D_3/toluene solution, **0.96 ml (1.33×10^{-3} mol)** of *s*-BuLi (1.4 M) and 5 ml of toluene.

After 20 hours at 20°C, roughly 95 ml of toluene was introduced to the main vessel via a cannula. The solution was cooled to 0°C and **2.14 ml (2.00 g, 2.00×10^{-2} mol)** of MMA was then introduced via a syringe. The polymerisation was allowed to proceed for 1 hour and was then terminated by adding 1 ml of N_2-sparged CH_3OH. The polymer was precipitated and dried as normal, and was a fine, white powder and the yield was **1.44 g**.

3.4.3 Preparation of PMMA (*26*) using a lithium silanolate ligated *s*-BuLi initiator (aim = 1500 g mol^{-1})

The initiator solution was prepared as described above, using **3.41 ml (0.92 g, 4.16×10^{-3} mol)** of D_3/toluene solution (0.27 g ml^{-1}), **8.31 ml (1.16×10^{-2} mol)** of *s*-BuLi (1.4 M) and 5 ml of toluene. After 20 hours at 20°C, roughly 95 ml of toluene was introduced to the main vessel via a cannula. The solution was cooled to 0°C and **3.11 ml (2.91 g, 2.91×10^{-2} mol)** of MMA was then introduced via a syringe. The polymerisation was allowed to proceed for 15 minutes and was then terminated by adding 1 ml of N_2-sparged CH_3OH. The polymer was precipitated and dried as normal, and was a fine, white powder and the yield was **2.37 g**.

3.4.4 Preparation of PMMA (*27*) via RAFT using $PhCS_2CH_2CO_2H$ (RA′) (aim = 2000 g mol^{-1})

Into a 10 ml side-arm were placed **0.0640 g** (**3.90×10^{-4} mol**) of AIBN, **0.30 g** (**1.41×10^{-3} mol**) of RA′, **4.37 g** (**4.37×10^{-2} mol**) of MMA and **2 ml** of benzene. A stirrer bar was added and the vessel was subjected to several freeze-evacuate-thaw cycles, until thoroughly degassed. The solution was stirred until all solids had dissolved. The vessel was placed into an oil bath at 60°C and the polymerisation was left to proceed for 16 hours, during which time there was a notable increase in viscosity. The vessel was removed from the oil bath and allowed to cool to room temperature. The polymer solution was made less viscous by adding toluene, and the polymer was precipitated and dried as normal. The polymer was a fine, pale-pink powder and the yield was **3.63 g**.

3.4.5 Preparation of PMMA (*28*) via RAFT using RA′ (aim = 2000 g mol^{-1})

The polymer was prepared as described above, using **0.0062 g** (**3.75×10^{-5} mol**) of AIBN, **0.31 g** (**1.46×10^{-3} mol**) of RA′, **3.04 g** (**3.04×10^{-2} mol**) of MMA and **2 ml** of benzene. After 15 hours in an oil bath at 60°C, during which time there was a notable increase in viscosity, the vessel was removed and allowed to cool to room temperature. The polymer solution was made less viscous by adding toluene, and the polymer was precipitated and dried as normal. The polymer was a pale-pink, flaky solid and the yield was **2.11 g**.

3.4.6 Preparation of PMMA (*29*) via RAFT using RA′ (aim = 2000 g mol^{-1})

The polymer was prepared as described above, using **0.0062 g** (**3.75×10^{-5} mol**) of AIBN, **0.31 g** (**1.46×10^{-3} mol**) of RA′, **2.97 g** (**2.97×10^{-2} mol**) of MMA and **2 ml** of benzene. After 2 hours in an oil bath at 60°C, during which time there was a notable increase in viscosity, the vessel was removed and allowed to cool to room temperature. The polymer solution was made less viscous by adding toluene, and the polymer was precipitated and dried as normal. The polymer was a fine, pink powder and the yield was **0.89 g**.

3.4.7 Preparation of PMMA (*30*) via RAFT using RA′ (aim = 2000 g mol^{-1})

The polymer was prepared as described above, using **0.0062 g (3.75×10^{-5} mol)** of AIBN, **0.31 g (1.46×10^{-3} mol)** of RA′, **3.04 g (3.04×10^{-2} mol)** of MMA and **2 ml** of benzene. After 1 hour in an oil bath at 60°C, during which time there was a notable increase in viscosity, the vessel was removed and allowed to cool to room temperature. The polymer solution was made less viscous by adding toluene, and the polymer was precipitated and dried as normal. The polymer was a fine, dark-pink powder and the yield was **0.56 g**.

3.4.8 Preparation of PMMA (*31*) via RAFT using RA′ (aim = 2000 g mol^{-1})

The polymer was prepared as described above, using **0.0062 g (3.75×10^{-5} mol)** of AIBN, **0.31 g (1.46×10^{-3} mol)** of RA′, **2.97 g (2.97×10^{-2} mol)** of MMA and **2 ml** of benzene. After 1 hour in an oil bath at 60°C, during which time there was a notable increase in viscosity, the vessel was removed and allowed to cool to room temperature. The polymer solution was made less viscous by adding toluene, and the polymer was precipitated and dried as normal. The polymer was a fine, dark-pink powder and the yield was **0.59 g**.

3.4.9 Preparation of $PhCS_2C(CH_3)_2Ph$ (RA″)

A double-necked 250 ml rbf was fitted with a water–cooled condenser and stirrer bar, and the apparatus placed under an atmosphere of dry N_2(g). The rbf was placed into an ice bath and dry CH_3OH **(125 ml)** was added via the second neck, followed in small amounts by **4.60 g (2.00×10^{-1} mol)** of sodium metal (BDH), forming a $NaOCH_3$ solution. The solution was stirred until all the metal had dissolved, and then **4.60 g (2.00×10^{-1} mol)** of sulphur (Aldrich) was added. To this mixture, **12.66 g (1.00×10^{-1} mol)** of benzyl chloride (C_7H_7Cl, Aldrich) was added dropwise over 30 minutes. The mixture was then refluxed for 15 hours using an oil bath.

The resulting red-brown solution was cooled with an ice-bath and NaCl was removed by filtering through a No.3 glass sinter, followed by rinsing with dry CH_3OH. The CH_3OH was removed via rotary evaporation to leave the red-brown sodium dithiobenzoate salt. The salt was dissolved in approximately **50 ml** distilled water,

transferred to a separating funnel, and washed with **6 × 50 ml** aliquots of diethyl ether, in order to remove any unreacted organic reagents. A **100 ml** layer of fresh ether was placed on top of the aqueous layer and **50 ml** HCl(aq) (2.0 M) was added dropwise slowly. Dithiobenzoic acid was formed as dark, purple-red oil, which dissolved into the ether layer. The layers were separated and the aqueous layer was washed with **4 × 50 ml** aliquots of fresh ether. The ether aliquots were combined and dried by stirring over $CaCl_2$ for 1 hour. The $CaCl_2$ was removed via filtration of the solution through a No.3 glass sinter and the ether removed via rotary evaporation, to leave **6.25 g** of dithiobenzoic acid.

All the dithiobenzoic acid was transferred to a double-necked 250 ml rbf fitted with reflux apparatus, and then flushed with dry $N_2(g)$. Via the second neck, **5.80 ml (5.28 g, 4.47×10^{-2} mol)** of α-methylstyrene (a slight excess) was added and stirred neat for 1 hour at 70°C. Dry hexane **(50 ml)** was added and the solution was refluxed overnight, resulting in a dark-purple solution. Being passed through a silica-gel column, using hexane as the eluent, purified the solution. The colourless fractions were set aside and the dark purple fraction collection by increasing the eluent polarity with ether (~3%). Passing through a neutral alumina column purified this fraction further. The solvent was removed via rotary evaporation to leave the product (RA″) as dark-purple oil. The yield was **2.52 g**.

3.4.10 Preparation of PMMA (*32*) via RAFT using RA″ (aim = 2000 g mol^{-1})

The polymer was prepared as described above, using **0.0083 g (5.05×10^{-5} mol)** of AIBN, **0.11 g (4.04×10^{-4} mol)** of RA″, **1.01 g (1.01×10^{-2} mol)** of MMA and **2 ml** of benzene. After 15 hours in an oil bath at 60°C, during which time no notable increase in viscosity was observed, the vessel was removed and allowed to cool to room temperature. The polymer solution was made more dilute by adding toluene, and the polymer was precipitated and dried as normal. The polymer was a fine, pink powder and the yield was **0.26 g**.

3.5 References

1. Zundel, T.; Teyssié, P.; Jérôme, R. *Macromolecules* **1998**, *31*, 2433-2439.
2. Frye, C. L. S., R. M.; Fearon, F. W. G.; Klosowski, J. M.; DeYoung, T. *J. Org. Chem.* **1970**, *35*, 1308-1314.
3. Zundel, T.; Zune, C.; Teyssié, P.; Jérôme, R. *Macromolecules* **1998**, *31*, 4089-4092.
4. Gilman, H.; Cartledge, F. K. *J. Organometal. Chem.* **1964**, *2*, 447-454.
5. Le, T. P. T.; Moad, G.; Rizzardo, E.; Thang, S. H. *Chem. Abstr.* **1998**, *128*.
6. Chiefari, J.; Chong, Y. K.; Ercole, F.; Krstina, J.; Jeffery, J.; Le, T. P. T.; Mayadunne, R. T. A.; Meijs, G. F.; Moad, C. L.; Moad, G.; Rizzardo, E.; Thang, S. H. *Macromolecules* **1998**, *31*, 5559-5562.
7. Wang, J.-S.; Matyjaszewski, K. *Macromolecules* **1995**, *28*, 7901-7910.
8. Chong, B. Y. K.; Le, T. P. T.; Moad, G.; Rizzardo, E.; Thang, S. H. *Macromolecules* **1999**, *32*, 2071-2074.
9. Mayadunne, R. T. A.; Rizzardo, E.; Chiefari, J.; Chong, Y. K.; Moad, G.; Thang, S. H. *Macromolecules* **1999**, *32*, 6977-6980.
10. Hawthorne, D. G.; Moad, G.; Rizzardo, E.; Thang, S. H. *Macromolecules* **1999**, *32*, 5457-5459.
11. Goto, A.; Sato, K.; Tsujii, Y.; Fukuda, T.; Moad, G.; Rizzardo, E.; Thang, S. H. *Macromolecules* **2001**, *34*, 402-408.
12. Moad, G.; Chiefari, J.; Chong, Y. K.; Krstina, J.; Mayadunne, R. T. A.; Postma, A.; Rizzardo, E.; Thang, S. H. *Polym. Int.* **2000**, *49*, 993-1001.
13. Davis, T. P., Personal communication.
14. Jackson, A. T.; Yates, H. T.; Scrivens, J. H.; Green, M. R.; Bateman, R. H. *J. Am. Soc. Mass Spectrom.* **1997**, *8*, 1206-1213.
15. Ganachaud, F.; Monteiro, M. J.; Gilbert, R. G.; Dourges, M. A.; Thang, S. H.; Rizzardo, E. *Macromolecules* **2000**, *33*, 6738-6745.

Chapter 4

Synthesis and Characterisation of Methacrylate Block Copolymers

4.1 Introduction

The synthesis of block copolymers of MMA with other methacrylate monomers and their subsequent characterisation via MALDI-TOF-MS is reported. The aim was to show that copolymer architecture could be identified directly from the MALDI spectra. The block copolymers were synthesised anionically via the sequential monomer addition method, employing the LDA initiating system that has already been shown to be highly efficient for methacrylate monomers.[1,2] The comonomers were *t*-butyl methacrylate (*t*-BMA) and hexyl methacrylate (HMA) and their homopolymers were also studied. MALDI-TOF-MS investigations have been performed previously on polymers of the primary monomer isomer (PBMA), but not on those of the tertiary isomer (P*t*-BMA).[3-6] Similarly with MMA/BMA copolymers, MALDI analysis to date has only involved samples containing the primary monomer isomer.[6-10] MALDI studies of PHMA samples have been limited to homopolymers only.[4] Eisenberg *et. al.* have reported a series of studies of the composition of various copolymers by MALDI-TOF-MS.[11-13] They utilised the peak areas of individual oligomers to create distribution profiles for each comonomer and verification of the random coupling hypothesis for block copolymer synthesis.

4.2 P*t*-BMA Homopolymer

A sample of P*t*-BMA (*33*) was synthesised and characterised initially to aid the subsequent characterisation of the PMMA–P*t*-BMA copolymers, but became an interesting study exercise in its own right. Sample *33* was initiated with LDA and terminated with a proton. The SEC data for *33* is given in Table 4.2.1 and the stoichiometric formula is pictured in Figure 4.2.1.

Sample	$\overline{M}_n$	$\overline{M}_w$	$\overline{M}_w/\overline{M}_n$
33	4790	4930	1.03

Table 4.2.1. SEC molecular weight data for *33*.

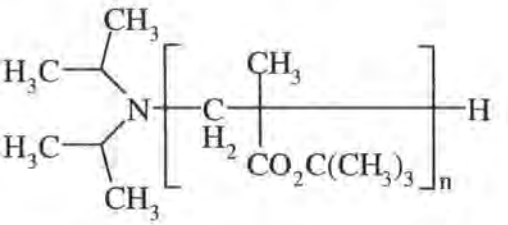

Figure 4.2.1. Stoichiometric formula of *33*.

The proton NMR spectrum of *33* is shown in Figure 4.2.2. Similar to the observations made regarding PMMA samples, the peak at δ = 2.6 ppm corresponds to the terminating methine proton and the peak at δ = 2.8 ppm is due to the methine protons of the isopropyl groups of the initiator end-group. Furthermore, the peaks occurring between δ = 0.8-1.3 ppm corresponds to the pendant methyl groups of the repeat unit and the peaks occurring between δ = 1.6-2.3 ppm correspond to the methylene groups of the same. In contrast to the PMMA spectra, the signal at δ = 3.6 ppm that was due to the pendant methoxy groups is absent and there is an additional, very intense, single peak at δ = 1.4 ppm, which corresponds to the nine equivalent *t*-butyl protons.

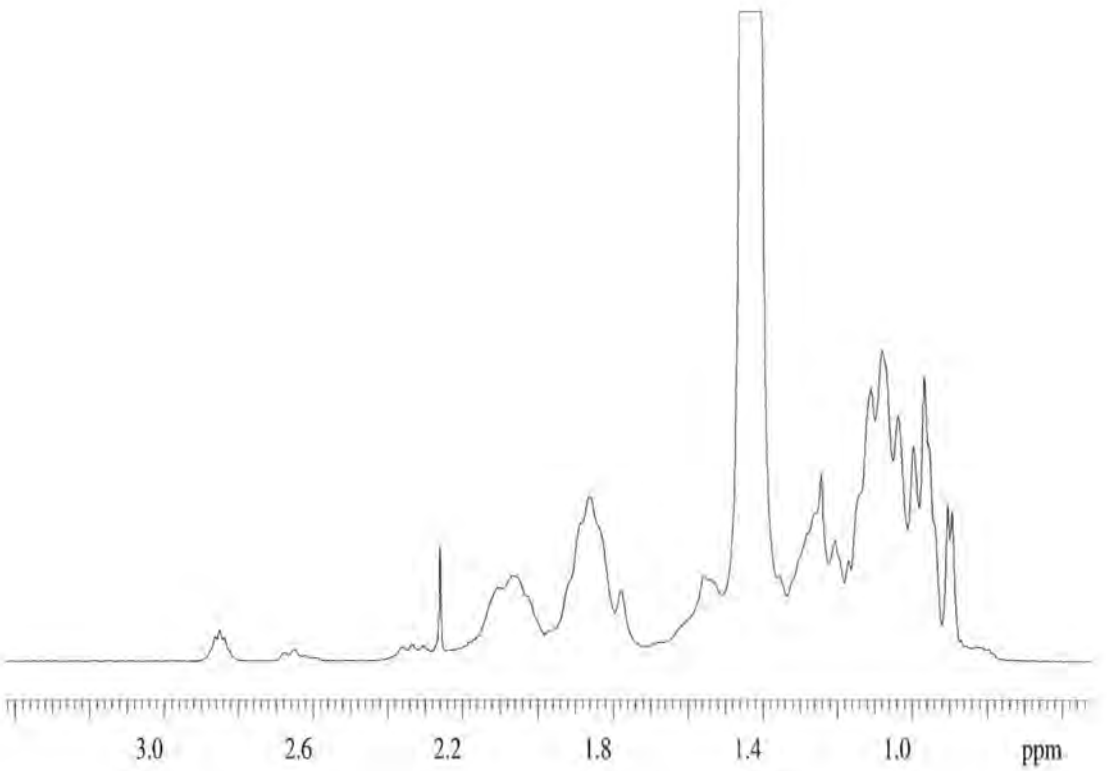

Figure 4.2.2. Proton NMR spectrum of *33*.

The carbon NMR spectrum of *33* (Figure 2.2.3) shows six major signals due to carbons in the polymer repeat units. Similar to the observations made regarding PMMA samples, the peaks around δ = 177 ppm are due to the carbonyl of the pendant ester groups and the peaks occurring between δ = 17-20 ppm correspond to the pendant methyl group of the repeat unit. Additionally, the two signals due to the backbone carbons occur between δ = 53-55 ppm, corresponding to the methylene groups, and between δ = 46-47 ppm, corresponding to the quaternary carbons. In contrast to the PMMA spectra, the peaks occurring between δ = 80-82 ppm correspond to the quaternary carbons of the *t*-butyl ester groups and the peak at δ = 28 ppm corresponds to the three equivalent methyl groups of the same. The peak at δ = 30 ppm corresponds to these methyl groups of the ultimate repeat unit, while the peak at δ = 35 ppm corresponds to the tertiary carbon associated with the terminating methine proton. The tertiary carbon of the isopropyl group of the initiator corresponds to the peak at δ = 48 ppm. The remaining signal expected for the methyl groups of the initiator can be found at δ = 22 ppm. Both proton and carbon spectra indicate *33* as having the stoichiometric formula given in Figure 4.2.1.

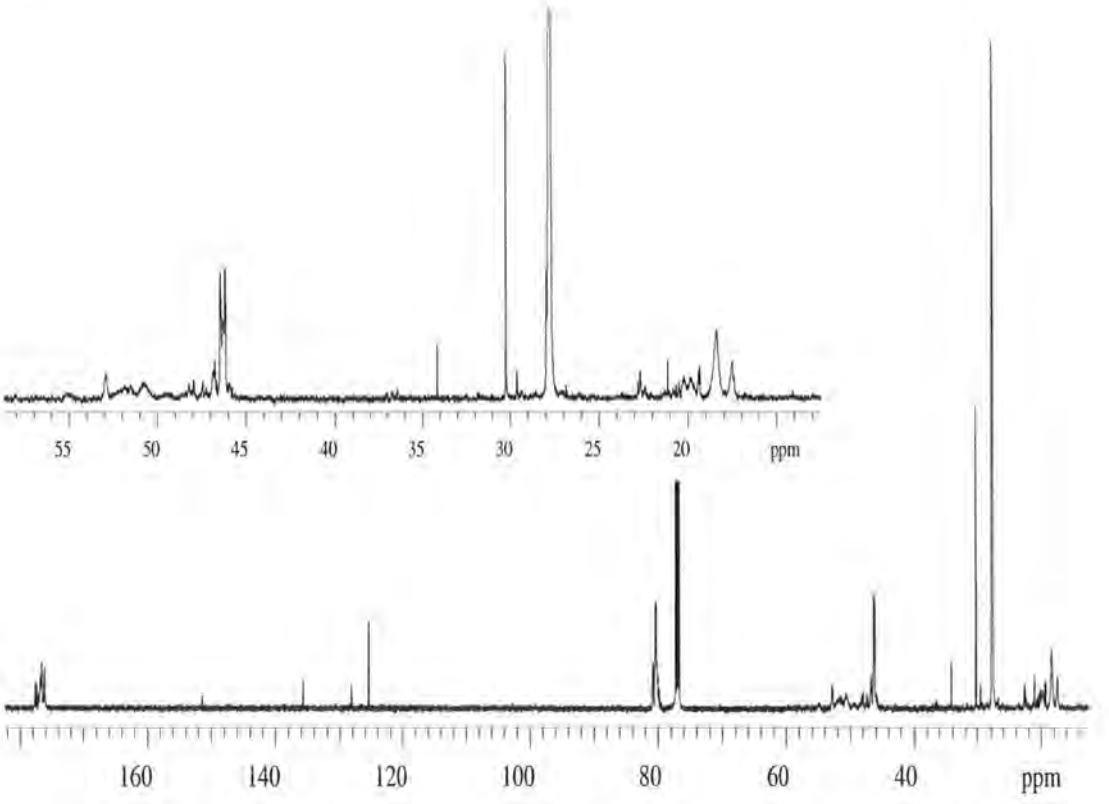

Figure 4.2.3. Carbon NMR spectrum of *33* with expanded higher field region.

The MALDI-TOF analysis of *33* was not so straightforward. Initial attempts to collect data using the same protocol that was used for PMMA sample failed to yield any useful spectra. Alterations to the protocol, including increasing the matrix:sample:salt ratio, cationising salt (none/LiCl/NaI), solvent (THF/$CHCl_3$/acetone), matrix (dithranol/ *all-trans*-retinoic acid) and laser power, made little difference to the data collected. However, the best example of these spectra is shown in Figure 4.2.4, acquired in reflectron mode, with a matrix:sample:salt ratio of 100:20:1, and with LiCl as the added salt and $CHCl_3$ as the solvent.

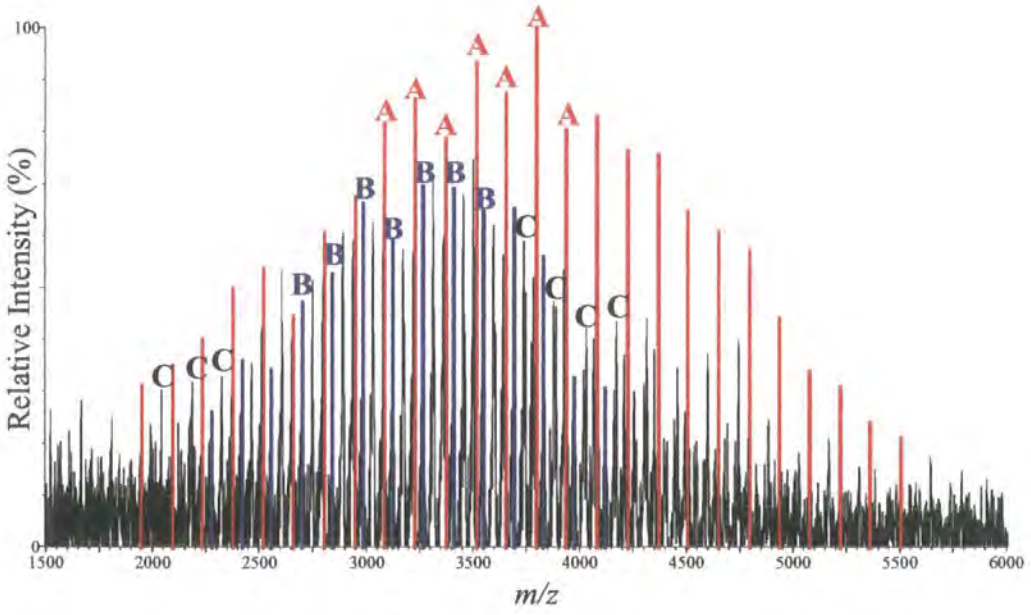

Figure 4.2.4. Reflectron MALDI spectrum of *33*.

The spectrum has relatively poor resolution, as many more laser shots than normal needed to be summed, in order to increase the signal:noise ratio sufficiently to observe the spectrum. The spectrum appears to consist of three series of ion species, all of which have a peak mass difference of roughly 142 amu, confirming the repeat unit as butyl methacrylate. The observed masses of the most intense series (**A**, red) correlate favourably with $[33+H]^+$ molecule ions, illustrated by the average mass comparison for a range of peaks in Table 4.2.2. Even though LiCl was added to the sample, the series due to the $[33+Li]^+$ species was not observed.

The average mass difference between successive peaks of series **A** and series **B** (blue), on going towards higher masses, is 38 amu, which means that this series is possibly due to $[33+K]^+$ molecule ions, further illustrated in Table 4.2.2. Cationisation by trace potassium originating from the solvents or glassware is commonly observed.

The difference on going towards lower masses would be approximately 104 amu, which does not correlate with any reasonable fragmentation or elimination. One possible elimination pathway that has been observed previously with PBMA is loss of butanol (74 amu) via combination of the ultimate butoxy group and the terminating methine proton, which results in the formation of a ketene end-group,[3] but this route does not agree with series **B**. The backbiting self-termination reaction commonly observed with the anionic polymerisation of PMMA is not expected to occur for P*t*-BMA because of the bulky nature of the pendant ester groups, but this would also result in the elimination of butanol and the consequential mass loss of 74 amu.

The average mass difference between successive peaks of series **A** and series **C** (black), on going towards higher masses, is 89 amu, but the likelihood that this series is due to $[33+Zr]^+$ molecule ions is extremely slight. The difference on going towards lower masses would be approximately 53 amu, which does not correlate with ketene formation/butanol elimination, but which could conceivably correspond to a single elimination of isobutene (56 amu), probably via a four-membered ring rearrangement, induced by the high laser power. Additionally, neither series **B** or **C** correspond to multiply charged species.

A and $[33+H]^+$			**B** and $[33+K]^+$		
n	Obs.	Calc.	n	Obs.	Calc.
20	2945.31	2946.19	20	2985.17	2984.28
21	3087.99	3088.39	21	3127.33	3126.48
22	3231.04	3230.59	22	3269.07	3268.68
23	3373.17	3372.79	23	3409.69	3410.88
24	3514.98	3514.99	24	3552.44	3553.08
25	3657.23	3657.19	25	3695.44	3695.28
26	3799.81	3799.39	26	3835.44	3837.48
27	3942.25	3941.59	27	3980.42	3979.68

Table 4.2.2. Average observed and calculated mass comparisons for *33*.

The poor resolution of the spectrum prevents the assignment of the peak series with any great degree of certainty, but why is the resolution so poor for this sample? Poor resolution was the result of having to sum such a large number of laser shots due to the low signal:noise ratio, and an examination the reasons behind this provided a

possible explanation for the observed results. The cationisation of synthetic polymers is believed to be due to two ionisation mechanisms:[14] a) the liberation of preformed metal ion-molecule complexes or salts, and b) in-plume proton/metal ion-molecule reactions. It is possible that the bulky *t*-butyl groups, which cover the entire length of these molecules, are interfering with the formation of either the preformed ions during sample preparation, *i.e.* during sample crystallisation, or the in-plume reactions, by preventing the cations from reaching their preferred binding sites. This would also include the prevention of protons binding to the nitrogen of the initiator end-group. This steric hindrance would lower the molecule ion yield, so lowering the signal:noise ratio.

To summarise, a sample of P*t*-BMA (*33*) was synthesised anionically, using LDA as the initiator and terminating with CH_3OH. In contrast to PMMA samples analysed previously, it was only possible to obtain poorly resolved spectra of *33*, despite making several alterations to aspects of sample preparation, which included the laser power, the type of matrix, solvent and metal salt, and the matrix:sample:salt ratio. These observations have been rationalised in terms of a low molecule ion yield resulting from possible interference in ion-molecule binding processes by the bulky pendant ester groups.

4.3 PMMA–P*t*-BMA Block Copolymers

The PMMA–P*t*-BMA block copolymers were all initiated with LDA and terminated with a proton. The molar percentages of each monomer within a given copolymer sample were set to provide a range of copolymer architectures to investigate. Sample *34* was targeted to have a 75 mole % PMMA block, Sample *35* was targeted to have 50 mole % of both monomers, and Sample *36* was targeted to have a 25 mole % PMMA block. The molecular weight data provided via SEC for *34-36* is given in Table 4.3.1 and the stoichiometric formula is pictured in Figure 4.3.1.

Sample	$\overline{M}_n$	$\overline{M}_w$	$\overline{M}_w/\overline{M}_n$
34	2620	2740	1.05
35	2460	2680	1.09
36	4000	4230	1.06

Table 4.3.1. SEC molecular weight data for *34-36*.

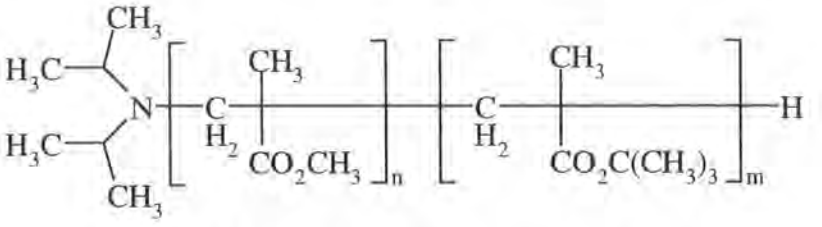

Figure 4.3.1. Stoichiometric formula of *34-36*.

The proton NMR spectrum of *34* is shown in Figure 4.3.2. Similar to the homopolymers observed previously, the peaks $\delta = 2.8$ ppm and $\delta = 2.4$ ppm correspond to the methine protons of the initiating and terminating end-groups respectively. Furthermore, the peaks occurring between $\delta = 0.8$-1.3 ppm correspond to the pendant methyl groups of both repeat units and the peaks occurring between $\delta = 1.6$-2.3 ppm correspond to the methylene groups of the same. Most significantly, there is a signal at $\delta = 3.6$ ppm, due to the pendant methoxy groups of the PMMA block, and a signal at $\delta = 1.4$ ppm, corresponding to the nine equivalent *t*-butyl protons of the P*t*-BMA block; hence the presence of both monomers within the sample is confirmed. A comparison of the peak integrals for these signals gives an indication of the average composition of the copolymer. These integrals should be identical because, based upon the target composition, there are three times as many *t*-butyl protons to methoxy protons, but also three times as many MMA units to *t*-BMA units. The actual methoxy:*t*-butyl integral ratio is 1:0.43, which indicates that the sample contains less *t*-BMA than expected, roughly 11 mole % only, and there are several explanations for this observation. The time allowed for *t*-BMA propagation may have been insufficient or, because P*t*-BMA is soluble in hexane, those oligomers with a higher content of *t*-BMA may have been lost upon precipitation of the copolymer. It may even be due to a combination of both these factors that this ratio is lower than anticipated. Hard evidence that the copolymer possesses a block nature is difficult to attain due to the similar structures of the comonomers. The environmental change for groups adjacent to the crossover point is so subtle that their signals cannot be distinguished from those from mid-block groups easily. The relatively simple nature of the spectrum gives credence to the copolymer having block architecture.

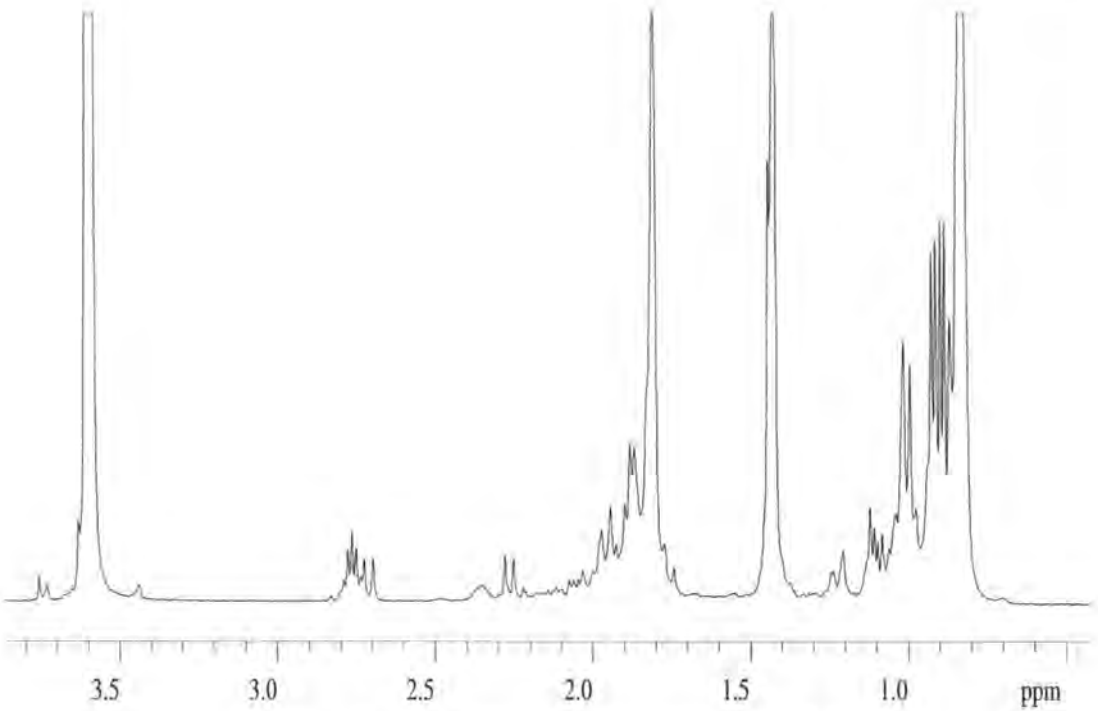

Figure 4.3.2. Proton NMR spectrum of *34*.

The carbon NMR spectrum of *34* (Figure 4.3.3) shows seven major signals due to carbons of both repeat units. Common to both repeat units are the peaks around $\delta = 177$ ppm corresponding to the carbonyl groups, the peaks occurring between $\delta = 16\text{-}20$ ppm corresponding to the pendant methyl groups, the signals occurring between $\delta = 53\text{-}55$ ppm corresponding to the methylene groups, and those between $\delta = 44\text{-}47$ ppm corresponding to the backbone quaternary carbons. Additionally, the peak at $\delta = 52$ ppm corresponds to the methoxy groups of the PMMA block, while the peaks occurring between $\delta = 80\text{-}82$ ppm and at $\delta = 28$ ppm correspond to the quaternary carbons and methyl groups of the *t*-butyl groups of the P*t*-BMA block. Peaks corresponding to the end-groups of the copolymer were observed at $\delta = 22$, 35 and 48 ppm. Once more, the relatively simple nature of the spectrum gives credence to the copolymer having block architecture.

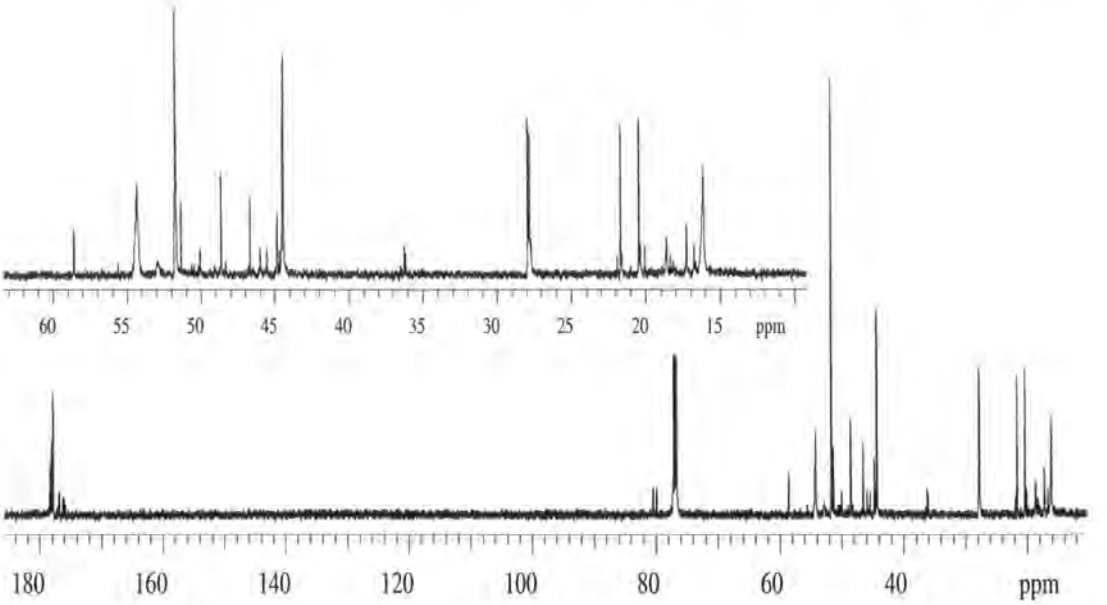

Figure 4.3.3. Carbon NMR spectrum of *34* with expanded higher field region.

The proton and carbon NMR spectra of *35* are shown in Figure 4.3.4. The same signals that were identified and assigned for *34* are found in each spectrum accordingly. The only notable differences are the intensities and integral values for certain peaks. In the proton spectrum for example, the methoxy:*t*-butyl (peaks occurring at δ = 3.6 and 1.4 ppm respectively) integral ratio is 1:2.92, which is in very close agreement with the expected ratio of 1:3, based upon the target copolymer composition. Therefore, the monomer ratio within the sample is approximately 50 mole % for each. With regard to the carbon spectrum, the fact that the intensity of the peak at δ = 28 ppm, due to the methyl groups of the *t*-butyl groups, is now greater than that of the peak at δ = 52 ppm, due to the methoxy groups, reflects the increase in *t*-BMA contained within the sample.

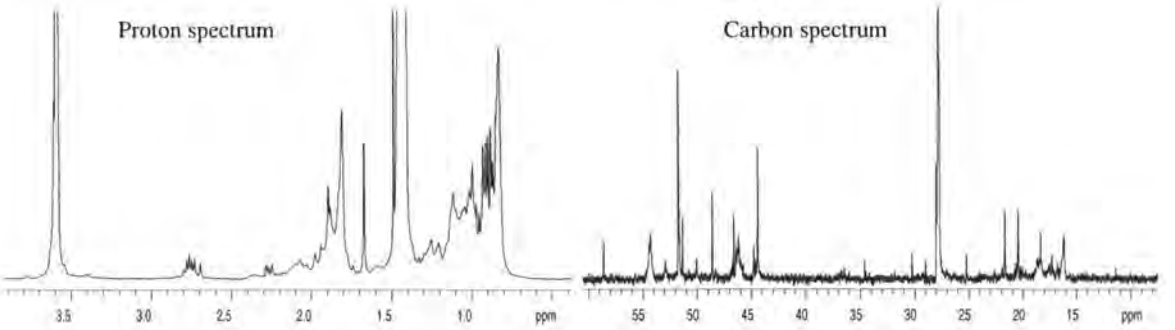

Figure 4.3.4. Proton and carbon NMR spectra of *35*.

Similar observations may be made regarding the proton and carbon NMR spectra of *36* (Figure 4.3.5). The methoxy:*t*-butyl integral ratio is 1:8.38, which is in

close agreement with the expected ratio of 1:9, based upon the target copolymer composition. Therefore, the monomer ratio within the sample is approximately 30 mole % MMA and 70 mole % *t*-BMA. With regard to the carbon spectrum, the fact that the intensity of the peak due to the methyl groups of the *t*-butyl groups is now much greater than that of the peak due to the methoxy groups, reflects the further increase in *t*-BMA contained within the sample. Both proton and carbon spectra indicate *34-36* as having the stoichiometric formula given in Figure 4.3.1.

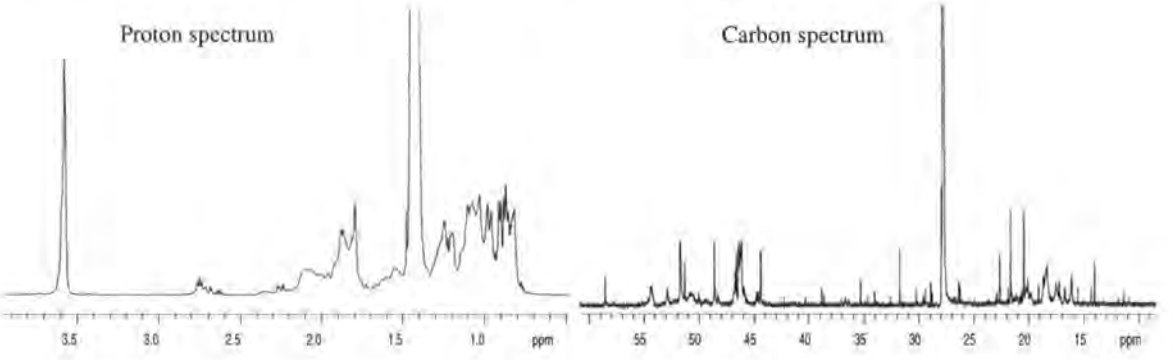

Figure 4.3.5. Proton and carbon NMR spectra of *36*.

The MALDI spectrum of *34* is shown in Figure 4.3.6 and it is obviously much more complicated than that observed previously for homopolymers. No salt was added to the sample, the intention being to generate protonated species only, so making the interpretation easier. There appear to be five series of peaks within the spectrum, **A**-**E**, and for clarity they have different colours. The different series are categorised by how many *t*-BMA repeat units are contained in each oligomer, therefore the peak separation within each series will equal the mass of MMA (100 amu). Series **A** (red) corresponds to molecule ions that do not contain any *t*-BMA units, *i.e.* the $[34(m = 0)+H]^+$ species, which is effectively the same as the $[1+H]^+$ species discussed earlier in Chapter 2. The comparison of observed and calculated average masses, shown in Table 4.3.2, give credence to this assignment. Average mass comparisons (Table 4.3.2) for series **B** (blue) and **C** (green) provide strong evidence that these correspond to $[34(m = 1)+H]^+$ and $[34(m = 2)+H]^+$ molecule ions respectively. Additionally, series **D** (magenta) and **E** (cyan) are due to $[34(m = 3)+H]^+$ and $[34(m = 4)+H]^+$ molecule ions respectively, and no signals were observed for species containing five or more *t*-BMA units. Further proof that these assignments are correct is that the interseries peak separation between consecutive series, *i.e.* **A**-**B** *etc.*, for oligomers with equivalent values of n, is approximately 142 amu. It is interesting to note that the extra peaks 1-2 amu lower than

those expected, observed previously for samples initiated by LDA, are observed again in peaks of the series **A-E**. The fact that there are peaks observed due to PMMA homopolymer (series **A**) may point towards the sample being a block copolymer, with the first block being PMMA. If the sample were a random copolymer then peaks due to homopolymers of either comonomer would not be expected, unless the mole percentage of one comonomer is low. Additionally, each peak series possesses something akin to a Poisson distribution that is normally expected for an anionic polymerisation.

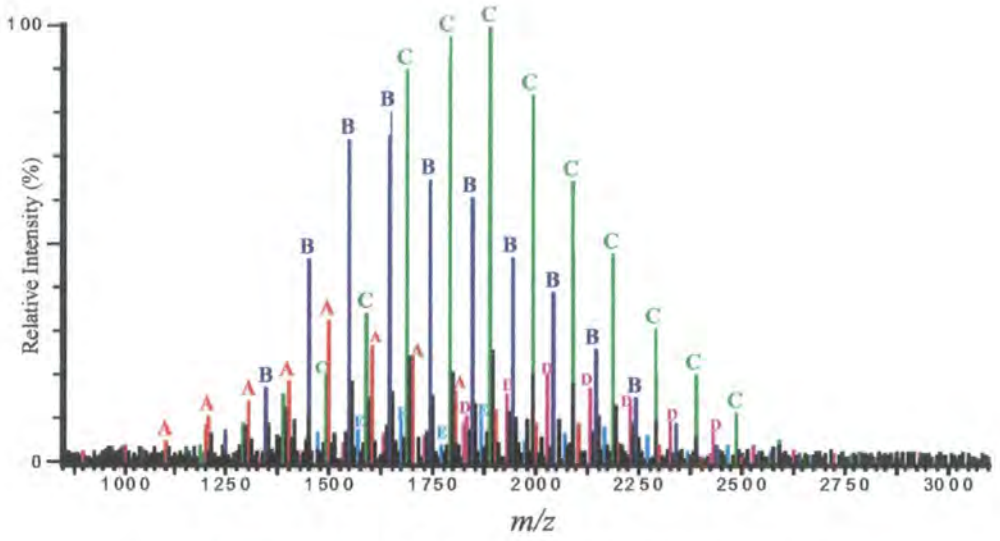

Figure 4.3.6. Reflectron MALDI spectrum of *34*.

A and [*34*(m = 0)+H]$^+$			**B** and [*34*(m = 1)+H]$^+$			**C** and [*34*(m = 2)+H]$^+$		
n	Obs.	Calc.	n	Obs.	Calc.	n	Obs.	Calc.
11	1203.75	1203.50	11	1345.83	1345.70	11	1487.87	1487.90
12	1303.73	1303.62	12	1445.86	1445.82	12	1587.90	1588.02
13	1403.80	1403.74	13	1545.86	1545.94	13	1687.94	1688.14
14	1503.82	1503.86	14	1645.89	1646.06	14	1787.98	1788.26
15	1603.88	1603.97	15	1745.93	1746.17	15	1888.01	1888.37
16	1703.88	1704.09	16	1845.93	1846.29	16	1988.02	1988.49
17	1803.94	1804.21	17	1946.00	1946.41	17	2088.09	2088.61
18	1903.95	1904.33	18	2046.12	2046.53	18	2188.11	2188.73

Table 4.3.2. Average observed and calculated mass comparisons for *34*.

Similarly to Eisenberg *et. al.*, by taking the comonomer composition and percentage area for each oligomer, profile distributions may be plotted for each comonomer within the sample. This was done for *34*, with the resultant plots shown in Figure 4.3.7, and they help visualise the composition of the copolymer. They also show that *34* follows the random coupling hypothesis, *i.e.* the molecular weights of the individual parts are not correlated, which is contrary to the situation expected for a random copolymer. Visualisation of the copolymer composition may be aided further by producing a three-dimensional (3D) plot of both comonomer profile distributions, as illustrated for *34* in Figure 4.3.8. The different series have been given the same colours as the corresponding series **A-E** in the original spectrum.

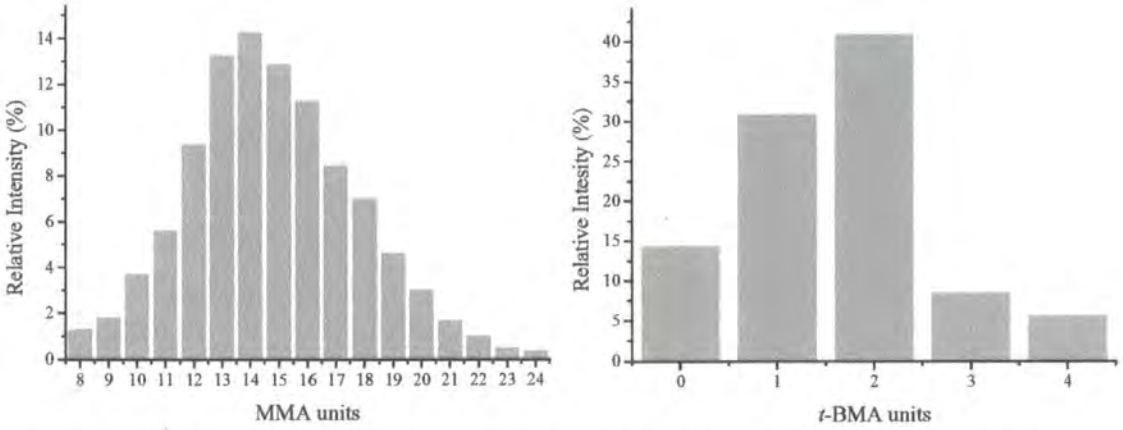

Figure 4.3.7. Distributions profiles of MMA and *t*-BMA composition for *34*.

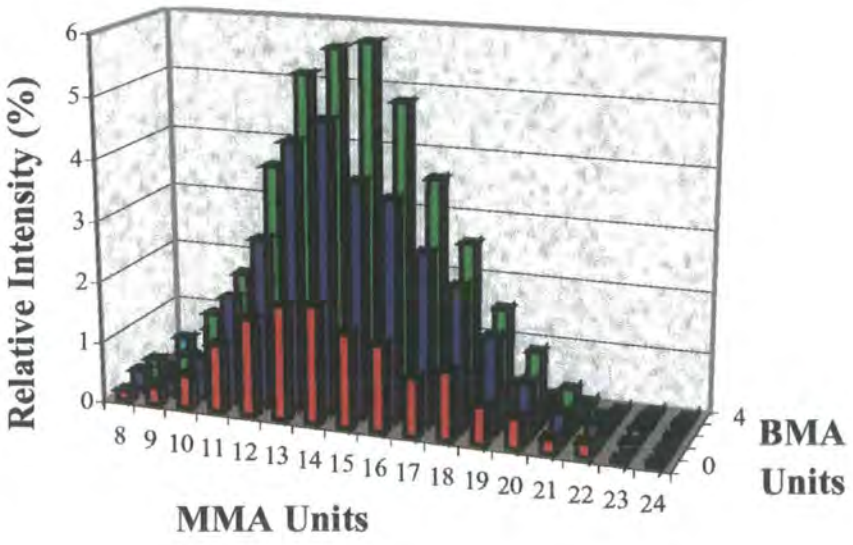

Figure 4.3.8. 3D-plot of MMA and *t*-BMA composition distributions for *34*.

MALDI-CID analysis was also performed on *34*, with the intention of further demonstrating the block nature of the sample from the fragment ion spectrum. Figure 4.3.9 shows the fragmentation spectra for the lithium cationised n = 14/m = 1 oligomer of series **B** (1651.1) and n = 14/m = 2 oligomer of series **C** (1793.2). The spectrum was expected to give us several peak series, **A-G**, due to mainchain bond scissions from either chain-end (**A** and **B** series), as well as mid-chain rearrangement processes (**C-G** series), the mechanisms for which are given elsewhere.[5] However, only the **A** series is recognisable, giving peaks at 236, 336 and 436 amu for the series **B** spectrum, and peaks at 278 and 378 amu for the series **C** spectrum. Fortunately, it is this end of the molecule that contains the *t*-BMA units, so the observation of the **A** series provides evidence that these units are located at the end of the molecule. Sporadic peaks due to the other series are observed at very low intensities, but more noteworthy are the peaks at 180, 280 and 380 amu for the series **B** spectrum, and peaks at 222 and 322 amu for the series **C** spectrum. These peaks would correspond to a single loss of butene from each fragment ion, again most likely a four-membered ring rearrangement, and this result gives further weight to the similar assignment made for series **C** of *34*.

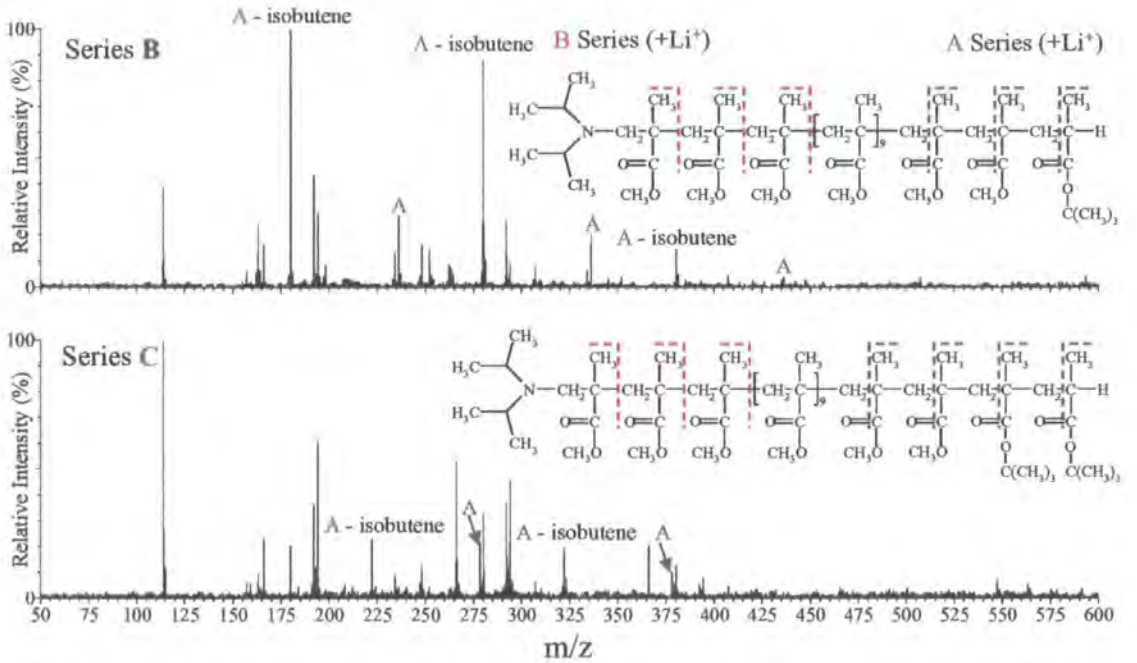

Figure 4.3.9. MALDI-CID spectra of oligomers from series B and C of *34*.

The MALDI spectra of *35* was expected to be much more complicated, owing to the equimolar content of each comonomer within the sample. However, no spectrum

could be obtained using the standard sample preparation procedure. Making similar alterations to this procedure as described above for *33* made little or no improvement to the results obtained. The same situation was observed for *36*. Similar to the case of *33*, interference from the bulky *t*-butyl ester groups of *35* may be lowering the molecule ion yield, thus lowering the signal:noise ratio. Additionally, the highly complex nature of the sample means that even if the ion yields were the same as that for a homopolymer, a considerably lower signal:noise ratio would be expected, for individual peaks. It is possible that the combination of these two factors results in unrecognisable spectra. Therefore, with increasing the *t*-BMA content of the copolymer still further, *i.e. 36*, the same situation may be expected, even though the complexity of the sample would decrease. However, this theory, while fine for metal ion cationisation involving both ends of the molecule, does not explain why peaks corresponding to protonated species are not observed. With the initial block being PMMA, there are no bulky groups to interfere with a proton binding to the nitrogen of the initiator residue, hence the lack of spectra cannot be explained satisfactorily at this time.

In conclusion, three PMMA–P*t*-BMA copolymers (*34-36*) were synthesised anionically, using LDA initiator and terminating with CH_3OH. The samples contained increasing amounts of *t*-BMA. The MALDI spectra of *34*, which contained the least amount of *t*-BMA, were obtained with relative ease, and showed that molecules could contain between 0-4 *t*-BMA units (m = 0-4) and are most likely to contain 2 *t*-BMA units. Graphical representations of the sample composition were obtained for the comonomer composition and percentage peak area for each oligomer. Spectra could not be obtained under various conditions for *35* and *36*, and this observation was rationalised in part in terms of a low molecule ion yield resulting from possible interference in ion-molecule binding processes by the bulky pendant ester groups, combined with an inherently lower signal:noise ratio, due to increased sample complexity.

4.4 PHMA Homopolymer

Similarly to Sample *33*, a sample of PHMA (Sample *37*) was synthesised and characterised initially to aid the subsequent characterisation of the PMMA–PHMA copolymers. Sample *37* was initiated with LDA and terminated with a proton. The

SEC data for *37* is given in Table 4.4.1 and the stoichiometric formula is pictured in Figure 4.4.1.

Sample	$\overline{M}_n$	$\overline{M}_w$	$\overline{M}_w / \overline{M}_n$
37	3090	3230	1.05

Table 4.4.1. SEC molecular weight data for *37*.

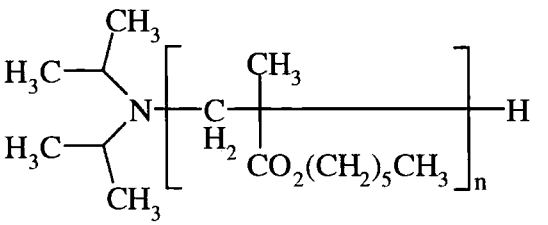

Figure 4.4.1. Stoichiometric formula of *37*.

The proton NMR spectrum of *37* is shown in Figure 4.4.2. Similar to the observations made regarding samples of PMMA and P*t*-BMA, the peaks δ = 2.8 ppm and δ = 2.5 ppm correspond to the methine protons of the initiating and terminating end-groups respectively. Furthermore, the peaks occurring between δ = 0.8-1.2 ppm correspond to the pendant methyl groups, and these probably overlap with the signal due to the methyl of the hexyl chains, while the peaks occurring between δ = 1.7-2.4 ppm correspond to the methylene groups of the backbone. In contrast to the PMMA and P*t*-BMA spectra, the signal at δ = 3.9 ppm is due to the α-methylene group of the hexyl chains with respect to the carboxylate group. It is possible that the peak at δ = 3.6 ppm is due to this group contained within the ultimate repeat unit. The peak at δ = 1.6 ppm is due to the β-methylene group and the peak at δ = 1.3 ppm is due to the three remaining methylene groups, which are all expected to have very similar proton shifts.

The carbon NMR spectrum of *37* (Figure 4.4.3) shows ten major signals due to carbons in the polymer repeat units. Similar to the observations made regarding samples of PMMA and P*t*-BMA, the peaks around δ = 177 ppm are due to the carbonyl groups and the peaks occurring between δ = 16-20 ppm correspond to the pendant methyl groups. Signals occurring at δ = 55 ppm and between δ = 44-46 ppm, correspond to the methylene groups and the quaternary carbons of the backbone. Additionally, there are peaks occurring at δ = 65 and 14 ppm, which correspond to the

α-methylene and methyl groups of the hexyl chains respectively. The peaks that were observed at δ = 32, 28, 26 and 23 ppm correspond to the δ, β, γ, and ε- methylene and methyl groups of the hexyl chains respectively. Peaks pertaining to the end-groups, and initial and ultimate monomer units, were also observed. Both proton and carbon spectra indicate *37* as having the stoichiometric formula given in Figure 4.4.1.

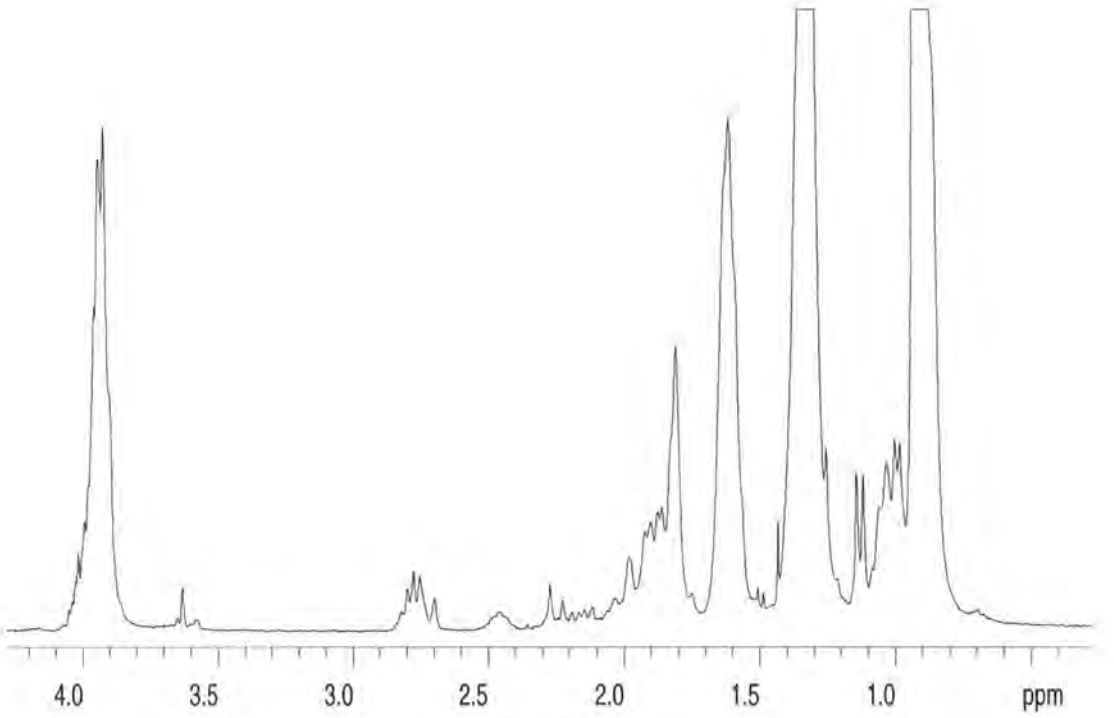

Figure 4.4.2. Proton NMR spectrum of *37*.

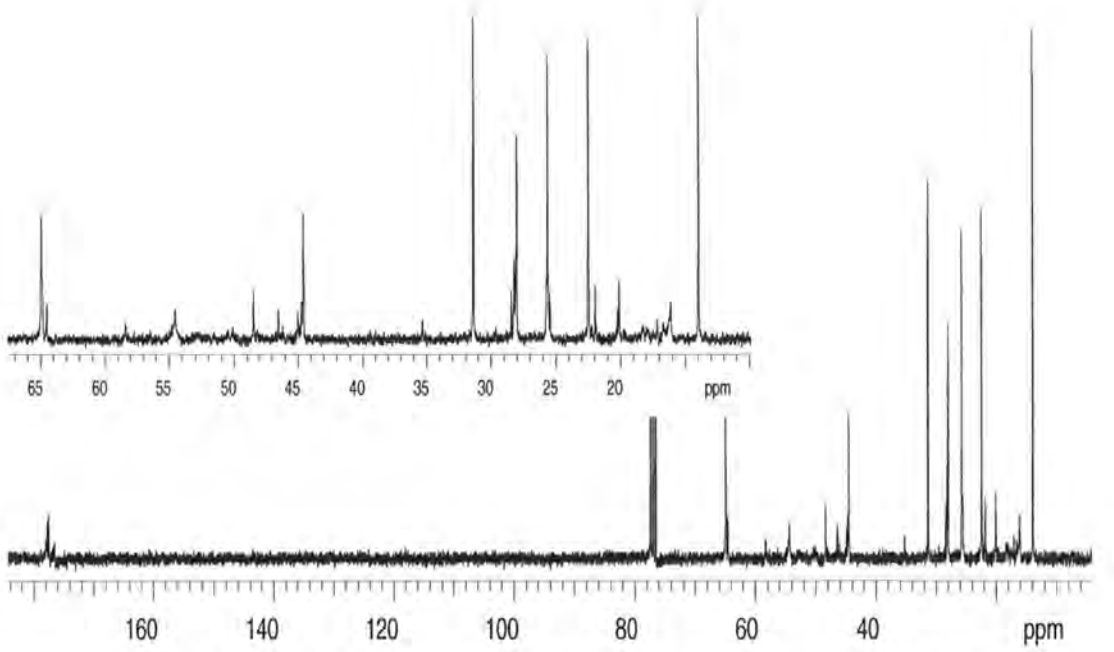

Figure 4.4.3. Carbon NMR spectrum of *37* with expanded higher field region.

The MALDI spectrum of *37*, collected using *all-trans*-retinoic acid as the matrix and with added LiCl, is shown in Figure 4.4.4, and it contains three major peak series, **A**-**C**. Each series has a peak mass difference of 170 amu, confirming the repeat unit as hexyl methacrylate. Low intensity peaks 6 amu lower than each series **A**-**C** are also observed, corresponding to the protonated analogues, and it is interesting to note once again that there are extra peaks, 1-2 amu lower than those expected, within these series. Series **A** corresponds to the $[37+Li]^+$ species, while series **B** is due to the single loss of hexanol from the same molecule ions, as the mass difference between an **A** peak and the next lower **B** peak is 102 amu. The elimination pathway is assumed to be analogous to that observed previously with PBMA, via combination of the ultimate hexoxy group and the terminating methine proton, which results in the formation of a ketene end-group.[3] Further weight is lent to these assignments by the comparison of calculated and observed average peak masses, given in Table 4.4.2. The same mass difference between **A** and **B** would also be observed if the backbiting self-termination reaction that occurs during the anionic synthesis of PMMA were also to occur during the synthesis of PHMA. This is considered unlikely, as the steric bulk of the hexyl chains would hinder this reaction.

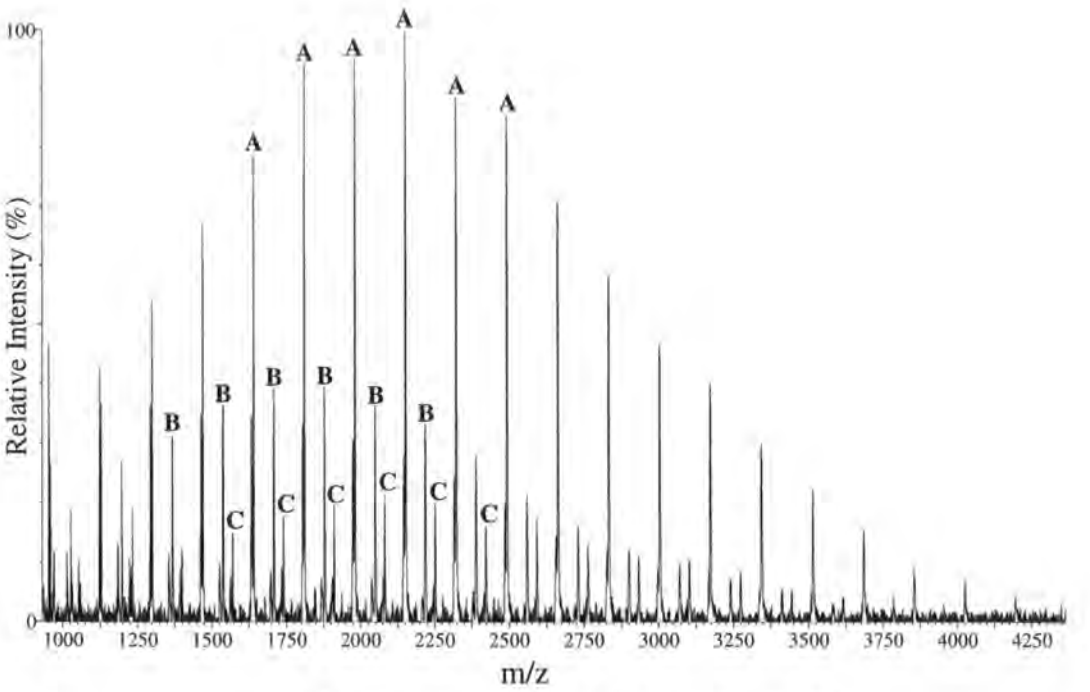

Figure 4.4.4. Reflectron MALDI spectrum of *37*.

A and $[37+Li]^+$			**B** and $[(37-C_6H_{14}O)+Li]^+$		
n	Obs.	Calc.	n	Obs.	Calc.
7	1299.80	1299.91	7	1197.80	1197.73
8	1470.21	1470.16	8	1367.69	1367.98
9	1640.62	1640.41	9	1537.98	1538.23
10	1810.81	1810.67	10	1708.00	1708.49
11	1981.02	1980.92	11	1878.10	1878.74
12	2151.19	2151.18	12	2048.37	2049.00
13	2321.29	2321.43	13	2218.51	2219.25
14	2491.73	2491.68	14	2388.90	2389.51

Table 4.4.2. Average observed and calculated mass comparisons for *37*.

However, the explanation as to the origin of series **C** is not so straightforward. The mass difference between an **A** and **B** peak and the next lower **C** peak is 70 and 138 amu respectively, while the mass difference between an **A** and **B** peak and the next higher **C** peak is 100 and 32 amu respectively. Cationisation via sulphur or a low abundant isotope of ruthenium is extremely unlikely, ruling out the mass increases of 100 and 32 amu as possible explanations for series **C**. Furthermore, it is unlikely that a mass loss of 138 amu is being observed, as this is quite a substantial loss and would probably involve cleavage of the polymer backbone. This only leaves a mass loss of 70 amu from series **A** molecule ions being the origin of series **C**. Pentene has a mass of 70 amu and the elimination of an alkene from an ester group via the McLafferty or four-membered ring rearrangements is perfectly feasible. The question that arises is why, when normally an n-ester eliminates an n-alkene, does it appear that an n-ester eliminates an n−1-alkene? Additionally, why would this particular elimination only occur once per oligomer, given that there are many ester groups, unless either of the end-groups is involved in the mechanism? There are a multitude of other molecules which have a mass of 70 amu, but pentene would seem the one most likely eliminated, given the structure of the polymer. Hence, the observation of series **C** cannot be accounted for with a great degree of confidence.

To summarise, a sample of PHMA (*37*) was synthesised anionically, using LDA as the initiator and terminating with CH_3OH. A MALDI spectrum was recorded with relative ease and showed three distinct peak series. Two of these series have been

assigned to typical molecule ion species, but the origins of the third series remain somewhat elusive.

4.5 PMMA–PHMA Block Copolymers

As before, the PMMA–PHMA block copolymers were all initiated with LDA and terminated with a proton. Again, the molar percentages of each monomer within a given copolymer sample were set to provide a range of copolymer architectures to investigate. Sample *38* was targeted to have a 75 mole % PMMA block, Sample *39* was targeted to have 50 mole % of both monomers, and Sample *40* was targeted to have a 25 mole % PMMA block. The molecular weight data provided via SEC for *38-40* is given in Table 4.5.1 and the stoichiometric formula for *38-40* is pictured in Figure 4.5.1.

Sample	$\overline{M}_n$	$\overline{M}_w$	$\overline{M}_w/\overline{M}_n$
38	3610	3770	1.04
39	3980	4140	1.04
40	4780	5260	1.05

Table 4.5.1. SEC molecular weight data for *38-40*.

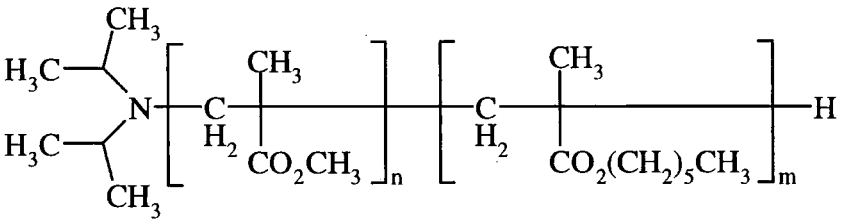

Figure 4.5.1. Stoichiometric formula of *38-40*.

The proton NMR spectrum of *38* is shown in Figure 4.5.2. Similar to the homopolymers observed previously, the peaks δ = 2.8 ppm and δ = 2.5 ppm correspond to the methine protons of the initiating and terminating end-groups respectively. Peaks occurring between δ = 0.7-1.2 ppm correspond to the pendant methyl groups of both repeat units and the peaks occurring between δ = 1.7-2.3 ppm correspond to the methylene groups of the same. The peak at δ = 1.6 ppm is due to the β-methylene groups of the hexyl chains of the PHMA block and the peak at δ = 1.3 ppm is due to the

three remaining methylene groups of the same. Most significantly, there is a signal at $\delta = 3.6$ ppm, due to the methoxy groups of the PMMA block, and a signal at $\delta = 3.9$ ppm, corresponding to the α-methylene groups of the PHMA block; hence the presence of both monomers within the sample is confirmed. It is possible that what appears to be a triplet at $\delta = 3.7$ ppm corresponds to the α-methylene group closest to the crossover point. Analogously to *34-36*, a comparison of the peak integrals for these signals gives an indication of the average composition of the copolymer. The α-methylene:methoxy integral ratio should be 1:4.5 based upon the target composition, as there are 1.5 times as many methoxy protons to α-methylene protons, and also three times as many MMA units to HMA units. Including the presumed crossover peak at $\delta = 3.7$ ppm, the actual α-methylene:methoxy integral ratio is 1:4.06, which is close to the expected ratio, though it indicates that the sample contains slightly less HMA than expected. Therefore, the monomer ratios are roughly 80 mole % MMA and 20 mole % HMA. Once more, the time allowed for HMA propagation may have been insufficient, resulting in less HMA being incorporated into the sample. Again, the relatively simple nature of the spectrum gives credence to the copolymer having block architecture.

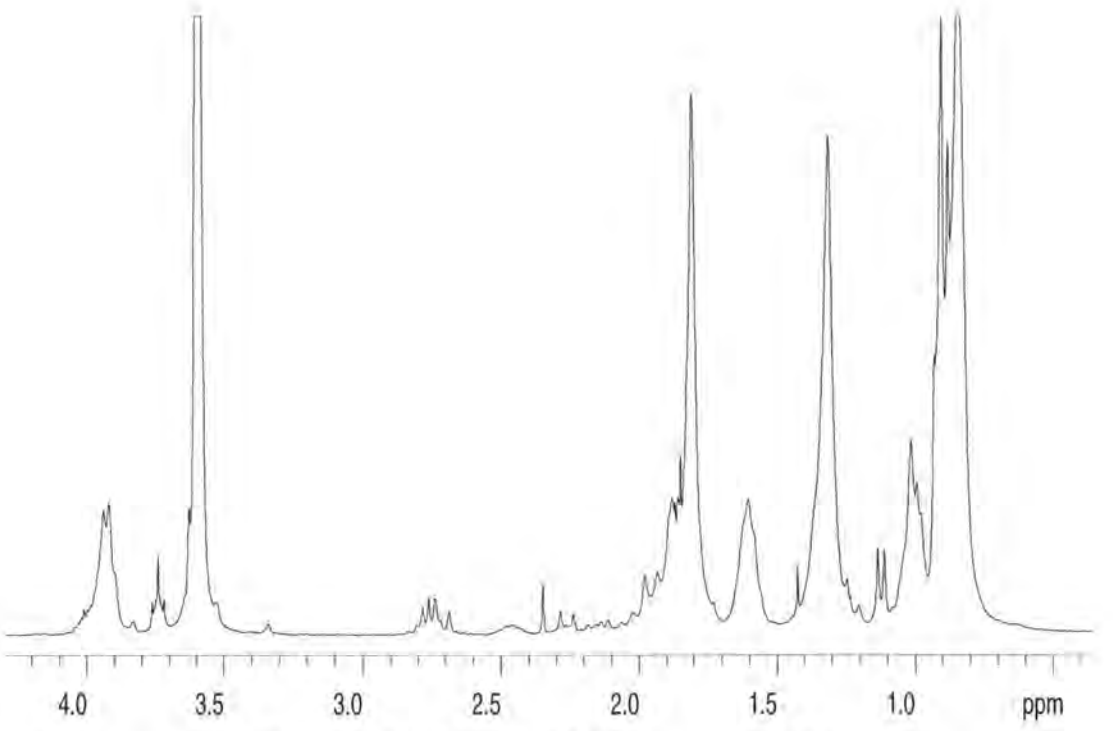

Figure 4.5.2. Proton NMR spectrum of *38*.

The carbon NMR spectrum of *38* (Figure 4.5.3) shows eleven major signals due to carbons of both repeat units. Common to both repeat units are the peaks around $\delta = 177$ ppm corresponding to the carbonyl groups, the peaks occurring between $\delta = 16$-20 ppm corresponding to the pendant methyl groups, the signals occurring at $\delta = 54$ ppm corresponding to the backbone methylene groups, and those between $\delta = 44$-46 ppm corresponding to the backbone quaternary carbons. Additionally, the peak at $\delta = 52$ ppm corresponds to the methoxy groups of the PMMA block, while the peaks occurring around $\delta = 65$, 32, 28, 26 and 23 ppm correspond to the α, δ, β, γ, and ε- methylene groups of the hexyl chain of the PHMA block. The peak at $\delta = 14$ ppm corresponds to the methyl groups of the hexyl chains. Peaks corresponding to the end-groups, and initial and ultimate monomer units, of the copolymer were observed at $\delta = 22$, 35, 48, 59 and 68 ppm. All these observations support the conclusion from the proton NMR, *i.e.* the copolymer has a block architecture.

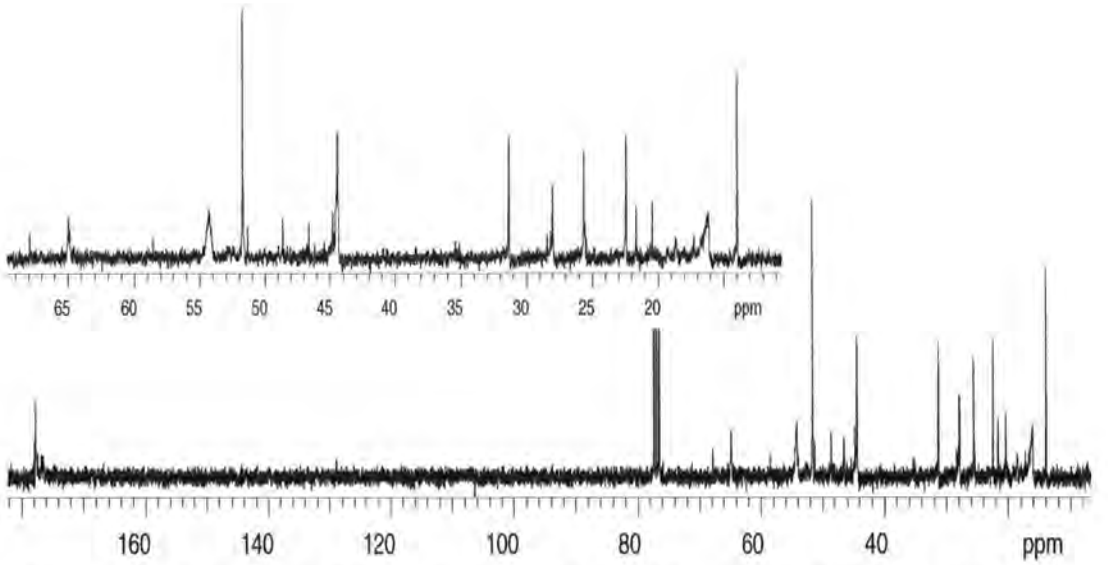

Figure 4.5.3. Carbon NMR spectrum of *38* with expanded higher field region.

The proton and carbon NMR spectra of *39* are shown in Figure 4.5.4. The same signals that were identified and assigned for *38* are found in each spectrum accordingly. The only notable differences are the intensities and integral values for certain peaks. In the proton spectrum for example, the α-methylene:methoxy (peaks occurring at $\delta = 3.9$ and 3.6 ppm respectively) integral ratio is 1:1.57, which is in very close agreement with the expected ratio of 1:1.5, based upon the target copolymer composition. Therefore, the monomer ratio within the sample is approximately 50 mole % for each. With regard

to the carbon spectrum, the fact that the intensities of the peaks at δ = 65, 32, 28, 26, 23 and 14 ppm, due to the hexyl chains, are now greater than that of the peak at δ = 52 ppm, due to the methoxy groups, reflects the increase in HMA contained within the sample.

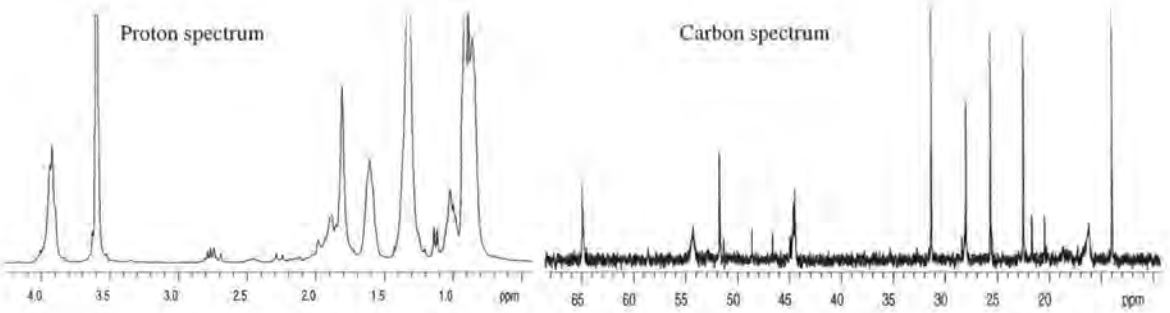

Figure 4.5.4. Proton and carbon NMR spectra of *39*.

Similar observations may be made regarding the proton and carbon NMR spectra of *40* (Figure 4.5.5). The α-methylene:methoxy integral ratio is 2.07:1, which is in very close agreement with the expected ratio of 2:1, based upon the target copolymer composition. Therefore, the monomer ratio within the sample is approximately 25 mole % MMA and 75 mole % HMA. With regard to the carbon spectrum, the fact that the intensities of the peaks due to the hexyl chains are now much greater than that of the peak due to the methoxy groups, reflects the further increase in HMA contained within the sample. Both proton and carbon spectra indicate *38-40* as having the stoichiometric formula given in Figure 4.5.1.

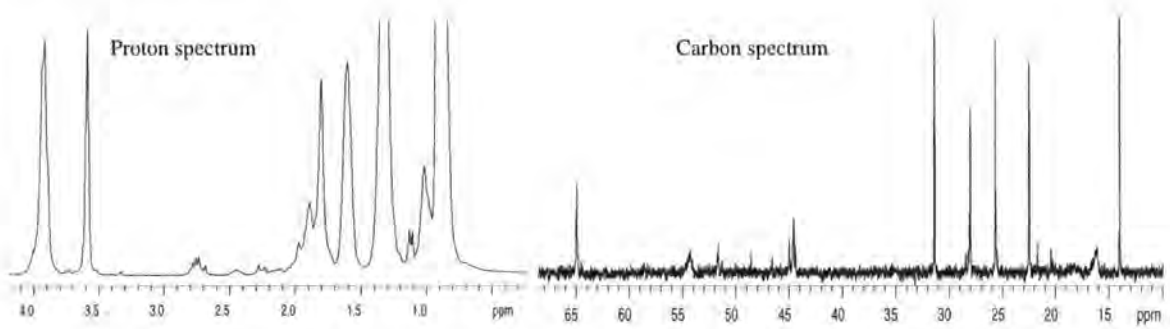

Figure 4.5.5. Proton and carbon NMR spectra of *40*.

The MALDI spectrum of *38* (Figure 4.5.6), again collected using *all-trans*-retinoic acid matrix, is obviously much more complicated than that observed previously for homopolymers. No salt was added to the sample, the intention being to generate

protonated species only, so making the interpretation easier. Thirteen series of peaks were identified within the spectrum and in order to differentiate between them they have been coloured differently. The different series are categorised by how many HMA repeat units are contained in each oligomer, therefore the peak separation within each series will equal the mass of MMA (100 amu). It is unnecessary to consider every peak series, but further details of certain series are given below to illustrate the composition of the sample.

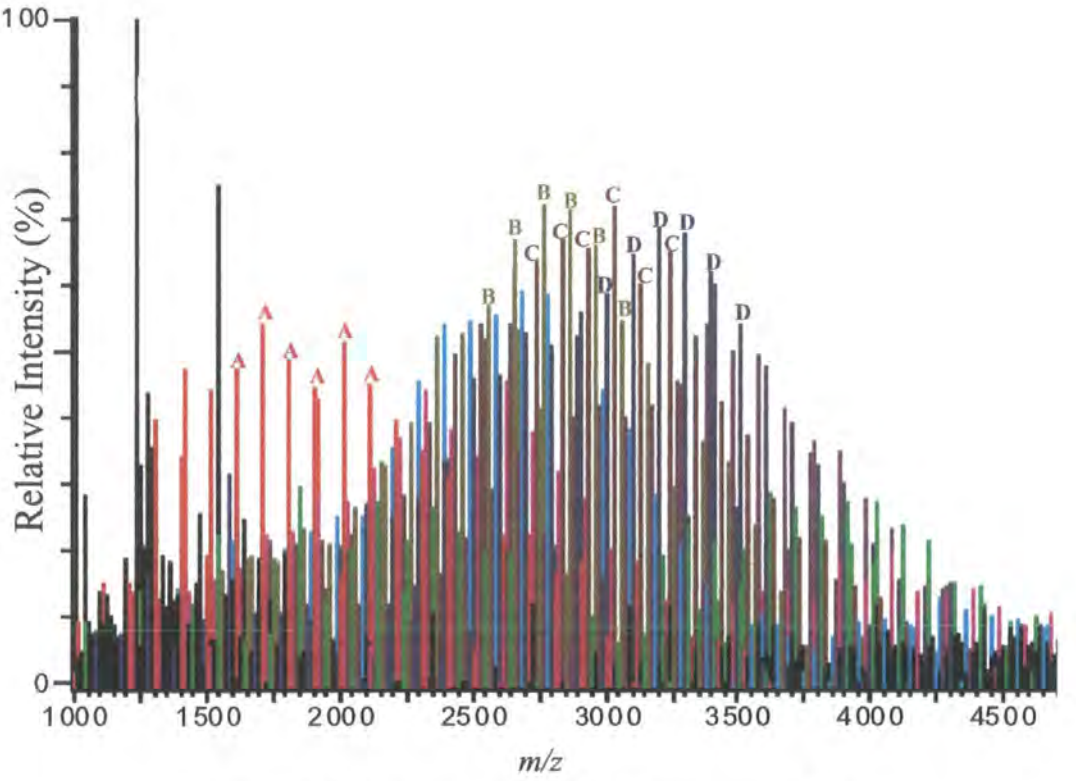

Figure 4.5.6. Reflectron MALDI spectrum of *38*.

Series **A** (red) corresponds to molecule ions that do not contain any HMA units, *i.e.* the $[38(m = 0)+Li]^+$ species, with the Li^+ ions originating from salts remaining in the sample from the polymerisation. This means that the spectrum is overcomplicated, as there will still be series present due protonated species. Average mass comparisons (Table 4.5.2) for the three most intense series, **B** (olive green), **C** (brown) and **D** (dark blue), provide strong evidence that these correspond to $[38(m = 5)+Li]^+$, $[38(m = 6)+Li]^+$ and $[38(m = 7)+Li]^+$ molecule ions respectively. Additionally, series **D** (magenta) and **E** (cyan) are due to $[34(m = 3)+H]^+$ and $[34(m = 4)+H]^+$ molecule ions respectively, and no signals were observed for species containing thirteen or more HMA units. Further proof that these assignments are correct is that the interseries peak

separation between consecutive series for oligomers with equivalent values of n, is approximately 170 amu, *i.e.* the mass of HMA. Similar to the PMMA–P*t*-BMA sample discussed previously, the fact that there are peaks observed due to PMMA homopolymer (series **A**) may point towards the sample being a block copolymer, with the first block being PMMA. Each peak series again possesses something akin to a Poisson distribution that is normally expected for an anionic polymerisation.

B and [*38*(m = 5)+Li]$^+$			**C** and [*38*(m = 6)+Li]$^+$			**D** and [*38*(m = 7)+Li]$^+$		
n	Obs.	Calc.	n	Obs.	Calc.	n	Obs.	Calc.
11	2060.35	2060.70	11	2230.85	2230.95	11	2400.85	2401.21
12	2160.65	2160.82	12	2330.91	2331.07	12	2500.99	2501.33
13	2260.74	2260.94	13	2430.97	2431.19	13	2601.11	2601.44
14	2360.98	2361.06	14	2531.05	2531.31	14	2701.32	2701.56
15	2461.05	2461.17	15	2631.30	2631.43	15	2801.37	2801.68
16	2561.21	2561.29	16	2731.22	2731.55	16	2901.51	2901.80
17	2661.30	2661.41	17	2831.39	2831.66	17	3001.78	3001.92
18	2761.32	2761.53	18	2931.42	2931.78	18	3101.84	3102.04

Table 4.5.2. Average observed and calculated mass comparisons for *38*.

Similar to that carried out for *34*, taking the comonomer composition and percentage area for each oligomer, profile distributions may be plotted for each comonomer within the sample. This was done for *38*, with the resultant plots shown in Figure 4.5.7, and they help visualise the composition of the copolymer. Visualisation of the copolymer composition may be aided further by producing a 3D-plot of both comonomer profile distributions, as illustrated for *38* in Figure 4.5.8. The different series have been given the same colours as the corresponding series in the original spectrum.

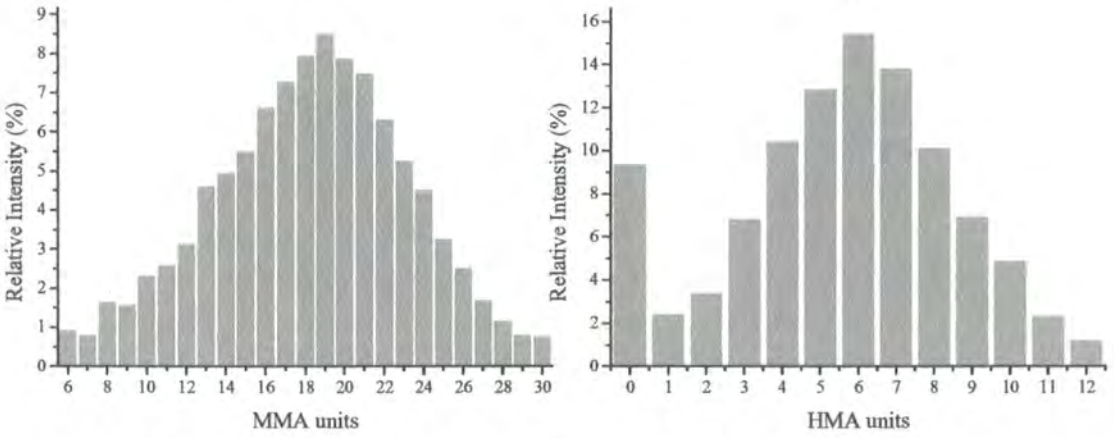

Figure 4.5.7. Distribution profiles of MMA and HMA composition for *38*.

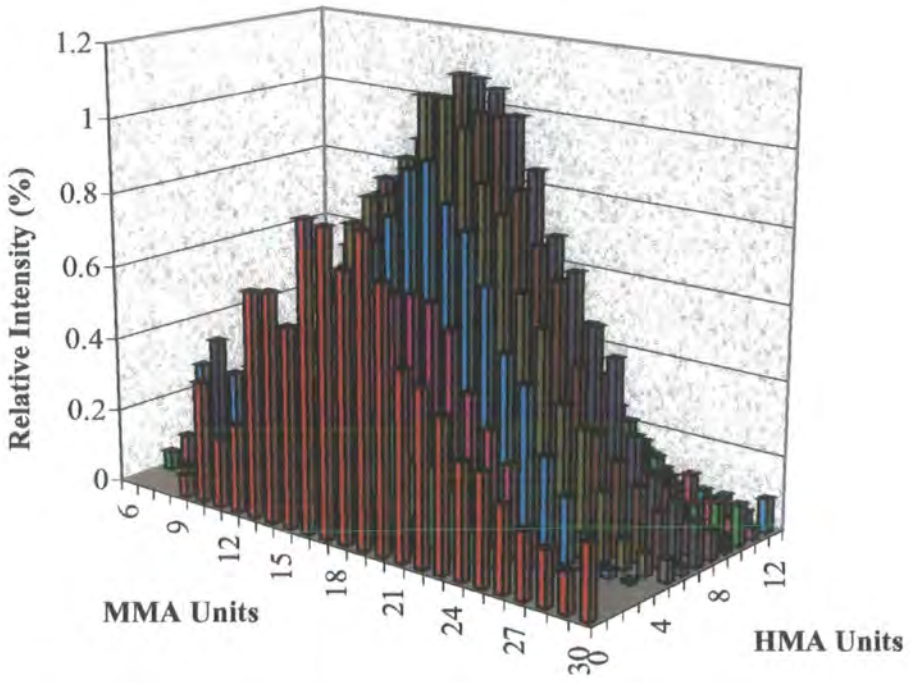

Figure 4.5.8. 3D-plot of MMA and HMA composition distributions for *38*.

The MALDI spectra of *39* was expected to be much more complicated, owing to the equimolar content of each comonomer within the sample. However, no spectrum could be obtained using the standard sample preparation procedure, utilising the *all-trans*-retinoic acid matrix. Making similar alterations to this procedure as described above for *33* made little or no improvement to the results obtained. The same situation was observed for *40*. Unlike the cases of *33*, *35* and *36*, interference from the bulky hexyl ester groups of *39* and *40* leading to a lowering of the molecule ion yield, thus a lowering of the signal:noise ratio, cannot be used as an explanation for these results, as *37* and *38* were analysed without hindrance. In addition to there somehow being

prevention of metal ion cationisation involving both ends of the molecule, large molecular size may explain why peaks corresponding to protonated species are not observed. With the initial block being PMMA, there are no bulky groups to interfere with a proton binding to the nitrogen of the initiator residue. The highly complex nature of the *39* means that a lower signal:noise ratio would be expected for individual peaks, this should not totally prevent a spectrum from being recorded. Therefore, with increasing the HMA content of the copolymer still further, *i.e. 40*, the complexity of the sample would decrease, so this spectrum should be easier to obtain. One possibility is that the samples are of too high a molecular weight, but though the samples have a slightly higher molecular weight than that anticipated, this is still well within the operating range of the spectrometer. Even though the samples were prepared in the normal fashion, another possibility is that the samples may not have dissolved fully, leading to aggregation of molecules during sample preparation and co-crystallisation with the matrix, hence a lack of desorbed and ionised material resulting in low signal detection. Therefore, the lack of spectra cannot be explained satisfactorily at this time.

In conclusion, three PMMA–PHMA copolymers (*38-40*) were synthesised anionically, using LDA initiator and terminating with CH_3OH. The samples contained increasing amounts of HMA. The MALDI spectra of *38*, which contained the least amount of HMA, were obtained with relative ease, and showed that molecules could contain between 0-12 HMA units (m = 0-12) and are most likely to contain between 5-7 HMA units. Graphical representations of the sample composition were obtained from the comonomer composition and percentage peak area for each oligomer. Spectra could not be obtained under various conditions for *39* and *40*, and this observation was rationalised in part, in terms of lower sensitivity due to a slightly higher sample molecular weight, and lower sample solubility resulting in sample aggregation and poor desorption/ionisation processes.

4.6 Experimental

The details of the analytical equipment and protocols were given in Section 2.8 of Chapter 2.

The purification procedures for MMA monomer (Aldrich) and solvents are detailed in Sections 2.9.1 and 2.9.2 of Chapter 2 respectively. The same procedure was also used to purify *t*-BMA and HMA monomers (both Aldrich). However, neither monomer was treated with triethylaluminium, or even dibutylmagnesium, immediately before being added to the reaction vessel. With such an addition *t*-BMA polymerised, while an amount of HMA thermally polymerised during vacuum-distillation, due to its' high boiling point. All solvents were purchased from either Fisher or BDH.

LDA initiator solution (Aldrich) was used as received. Standard high vacuum techniques were used to synthesise all polymers.

4.6.1 Synthesis of P*t*-BMA (*33*) homopolymer (aim = 2000 g mol^{-1})

The polymerisation was performed in the usual way; a detailed description of the process was given in Section 2.9.4. Once the THF solvent had reached the polymerisation temperature of –78°C, **2.30 ml (2.01 g, 1.42×10^{-2} mol)** of *t*-BMA were added to the reaction vessel via syringe. The amount of LDA (2.0 M) required was **0.50 ml (1.00×10^{-3} mol)**. The polymerisation was terminated after 2 hours with N_2-sparged CH_3OH. The polymer was precipitated into distilled water, filtered, and dried overnight in a vacuum oven at 60°C. The polymer was an off-white, flaky solid and the yield was **1.56 g**.

4.6.2 Synthesis of 75:25 PMMA–P*t*-BMA (*34*) block copolymer (aim = 1500 g mol^{-1})

The polymerisation of the initial PMMA block was performed in the normal manner. The amount of MMA was **2.54 g (2.54×10^{-2} mol)**, therefore **1.27 ml (2.54×10^{-3} mol)** of LDA (2.0 M) was required to produce a PMMA block of approximately 1000 g mol^{-1}. The polymerisation of MMA was judged to be complete after 30 minutes, then **1.50 ml (1.31 g, 9.21×10^{-3} mol)** of *t*-BMA were added to the reaction vessel via syringe. The polymerisation was left to proceed for a further 1.5

hours; then it was terminated with N_2-sparged CH_3OH. The polymer was precipitated into cold hexane, filtered, and dried overnight in a vacuum oven at room temperature. The polymer was a white powder and the yield was **2.36 g**.

4.6.3 Synthesis of 50:50 PMMA–P*t*-BMA (*35*) block copolymer (aim = 2500 g mol^{-1})

The preparation of the block copolymer was performed as described above. The amount of MMA was **1.99 g (1.99×10^{-2} mol)**, therefore **1.00 ml (2.00×10^{-3} mol)** of LDA (2.0 M) was required to produce a PMMA block of approximately 1000 g mol^{-1}. The polymerisation of MMA was judged to be complete after 30 minutes; then **3.25 ml (2.83 g, 1.99×10^{-2} mol)** of *t*-BMA were added to the reaction vessel via syringe. The polymerisation was left to proceed for a further 2 hours, then it was terminated with N_2-sparged CH_3OH. The polymer was precipitated into distilled water, filtered, and dried overnight in a vacuum oven at 60°C. The polymer was an off-white, flaky solid and the yield was **4.10 g**.

4.6.4 Synthesis of 25:75 PMMA–P*t*-BMA (*36*) block copolymer (aim = 2500 g mol^{-1})

The block copolymer polymerisation was performed in the usual way. The amount of MMA was **1.31 g (1.31×10^{-2} mol)**, therefore **1.31 ml (2.62×10^{-3} mol)** of LDA (2.0 M) were required to produce a PMMA block of approximately 500 g mol^{-1}. The polymerisation of MMA was judged to be complete after 15 minutes; then **6.39 ml (5.59 g, 3.93×10^{-2} mol)** of *t*-BMA were added to the reaction vessel via syringe. The polymerisation was left to proceed for a further 4 hours, then it was terminated with N_2-sparged CH_3OH. The polymer was precipitated into distilled water, filtered, and dried overnight in a vacuum oven at 60°C. The polymer was an off-white, flaky solid and the yield was **7.31 g**.

4.6.5 Synthesis of PHMA (*37*) homopolymer (aim = 2000 g mol^{-1})

The polymerisation was performed in the normal manner. The amount of HMA was **2.25 ml (1.99 g, 1.17×10^{-2} mol)**, which were added to the reaction vessel via syringe. The required amount of LDA (2.0 M) was **0.50 ml (1.00×10^{-3} mol)**. The polymerisation was terminated after 2 hours with N_2-sparged CH_3OH. The polymer was collected by evaporation of the volatile substances present, the majority of which were removed by rotary evaporation. The polymer was dried overnight in a vacuum oven at room temperature. The polymer was a clear, straw-yellow, syrup-like, viscous liquid and the yield was **1.73 g**.

4.6.6 Synthesis of 75:25 PMMA–PHMA (*38*) block copolymer (aim = 2000 g mol^{-1})

The block copolymer polymerisation was performed in the usual way. The amount of MMA was **2.67 g (2.67×10^{-2} mol)**, therefore **0.89 ml (1.78×10^{-3} mol)** of LDA (2.0 M) was required to produce a PMMA block of approximately 1500 g mol^{-1}. The polymerisation of MMA was judged to be complete after 30 minutes, then **1.71 ml (1.51 g, 8.90×10^{-3} mol)** of HMA were added to the reaction vessel via syringe. The polymerisation was left to proceed for a further 1.5 hours and then it was terminated with N_2-sparged CH_3OH. The polymer was collected by evaporation as described above and dried overnight in a vacuum oven at room temperature. The polymer was an off-white, flaky solid and the yield was **3.60 g**.

4.6.7 Synthesis of 50:50 PMMA–PHMA (*39*) block copolymer (aim = 2500 g mol^{-1})

The block copolymer polymerisation was performed in the usual way. The amount of MMA was **2.60 g (2.60×10^{-2} mol)**, therefore **1.30 ml (1.88×10^{-3} mol)** of LDA (2.0 M) were required to produce a PMMA block of approximately 1000 g mol^{-1}. The polymerisation of MMA was judged to be complete after 30 minutes; then **4.99 ml (4.42 g, 2.60×10^{-2} mol)** of HMA were added to the reaction vessel via syringe. The polymerisation was left to proceed for a further 2 hours, then it was terminated with N_2-sparged CH_3OH. The polymer was collected by evaporation as described above and

dried overnight in a vacuum oven at room temperature. The polymer was a clear, colourless, sticky, glassy solid and the yield was **7.86 g**.

4.6.8 Synthesis of 25:75 PMMA–PHMA (*40*) block copolymer (aim = 3000 g mol^{-1})

The block copolymer polymerisation was performed in the usual way. The amount of MMA was **1.53 g (1.53×10^{-2} mol)**, therefore **1.53 ml (3.06×10^{-3} mol)** of LDA (2.0 M) was required to produce a PMMA block of approximately 500 g mol^{-1}. The polymerisation of MMA was judged to be complete after 30 minutes; then **8.82 ml (7.80 g, 4.59×10^{-2} mol)** of HMA were added to the reaction vessel via syringe. The polymerisation was left to proceed for a further 4 hours, then it was terminated with N_2-sparged CH_3OH. The polymer was collected by evaporation as described above and dried overnight in a vacuum oven at room temperature. The polymer was a clear, colourless, sticky, glassy solid and the yield was **10.41 g**.

4.7 References

1. Antoun, S.; Teyssié, P.; Jérôme, R. *J. Polym. Sci. Pol. Chem.* **1997**, *35*, 3637-3644.
2. Antoun, S.; Teyssié, P.; Jérôme, R. *Macromolecules* **1997**, *30*, 1556-1561.
3. Danis, P. O.; Karr, D. E.; Simonsick, W. J., Jr.; Wu, D. T. *Macromolecules* **1995**, *28*, 1229-1232.
4. Lloyd, P. M.; Scrivener, E.; Maloney, D. R.; Haddleton, D. M.; Derrick, P. J. *Polym. Prepr. (Am. Chem. Soc., Div. Polym. Chem.)* **1996**, *37*, 847-848.
5. Jackson, A. T.; Yates, H. T.; Scrivens, J. H.; Green, M. R.; Bateman, R. H. *J. Am. Soc. Mass Spectrom.* **1997**, *8*, 1206-1213.
6. Kukulj, D.; Davis, T. P.; Suddaby, K. G.; Haddleton, D. M.; Gilbert, R. G. *J. Polym. Sci., Part A: Polym. Chem.* **1997**, *35*, 859-878.
7. Haddleton, D. M.; Maloney, D. R.; Suddaby, K. G. *Macromolecules* **1996**, *29*, 481-483.
8. Suddaby, K. G.; Hunt, K. H.; Haddleton, D. M. *Macromolecules* **1996**, *29*, 8642-8649.

9. Montaudo, M. S.; Montaudo, G. *Macromolecules* **1999**, *32*, 7015-7022.

10. Jackson, A. T.; Scrivens, J. H.; Simonsick, W. J., Jr.; Green, M. R.; Bateman, R. H. *Polym. Prepr. (Am. Chem. Soc., Div. Polym. Chem.)* **2000**, *41*, 641-642.

11. Wilczek-Vera, G.; Danis, P. O.; Eisenberg, A. *Macromolecules* **1996**, *29*, 4036-4044.

12. Wilczek-Vera, G.; Yu, Y. S.; Waddell, K.; Danis, P. O.; Eisenberg, A. *Macromolecules* **1999**, *32*, 2180-2187.

13. Wilczek-Vera, G.; Yu, Y. S.; Waddell, K.; Danis, P. O.; Eisenberg, A. *Rapid Commun. Mass Spectrom.* **1999**, *13*, 764-777.

14. Knochenmuss, R.; Lehmann, E.; Zenobi, R. *Eur. Mass Spectrom.* **1998**, *4*, 421-427.

Chapter 5

Characterisation of Blends of Various End-Functionalised PMMA

5.1 Introduction

The characterisation via MALDI-TOF-MS of equimolar blends of various end-functionalised PMMA samples (*1-3*) is reported. The initial structure determination and MALDI analysis of these has been discussed previously in Section 2.2 of Chapter 2. The aim was to investigate the possible effects that end-group structure might have on MALDI spectra of polymer mixtures. Although this type of investigation does not appear to have been done before, MALDI-TOF-MS analysis of certain polymer blends or mixtures has been attempted. The majority of this work has involved the use of a range of low polydispersity polystyrene (PS),[1-4] poly(ethylene glycol) (PEG)[5] or PMMA[6-8] standards as model systems, in order to study mass discrimination of higher order oligomers in samples with high polydispersities, and how this affects average molecular weight information. Each range of standards had the same stoichiometric formula and they were most likely synthesised by group transfer polymerisation (GTP). Several mixtures of two poly(dimethylsiloxane) standards ($\overline{M}_n = 2200$ and 6140) showed linear desorption/ionisation efficiency from a plot of their peak area ratios against their relative weight ratios.[9] This means that MALDI may prove useful in quantifying the components of a polymer blend. MALDI studies of blends of different types of polymers are scarce, not only because possible mass discrimination effects, but more due to the likelihood of differences in cationisation efficiencies. For a mixture of PS and PMMA samples, the PMMA distribution dominated whether the sample preparation protocol was optimised for PMMA or for PS.[10] A comparison between the dried droplet and electrospray sample preparation techniques has also been performed with mixtures of PEG samples containing various ester functionalities.[11] The latter technique was shown to give more reproducible results.

5.2 Blend of *1* and *2*

Before considering the equimolar blend of *1* and *2*, the different species observed for *1* and *2* were quantified individually. Initiated with LDA, the majority of *1* has been shown to be the proton-terminated species, plus a small amount of self-terminated species. Peaks were observed for both these species cationised by H^+

and Li^+, plus a minute amount of the proton-terminated species cationised by Na^+. Initiated with DPHLi, the majority of *2* has also been shown to be the proton-terminated species, plus a small amount of self-terminated species, and peaks were observed for both these species cationised by Li^+ only. The percentage peak areas for the species of both *1* and *2* are given in Table 5.2.1. The percentage peak areas for each species with a particular cation were calculated for *1* also. For the proton-terminated species, 87.89% was cationised by H^+, Li^+ cationised 9.61%, and Na^+ cationised 2.49%. For the self-terminated species, 96.13% was cationised by H^+, and Li^+ cationised 3.87%. The discrepancies between peak areas are more likely to be due to very low signal:noise ratio for most Li^+ and all Na^+ cationised self-terminated species, rather than being due to the structural difference between the species.

Sample	Species	Cation	% Area	Species %
1	Proton-terminated	H^+	86.35	98.24
		Li^+	9.45	
		Na^+	2.44	
	Self-terminated	H^+	1.69	1.76
		Li^+	0.07	
2	Proton-terminated	Li^+	87.75	87.75
	Self-terminated	Li^+	12.25	12.25

Table 5.2.1. Percentage peak areas for species observed for *1* and *2* individually.

The reflectron MALDI spectrum for the equimolar blend of *1* and *2*, shown in Figure 5.2.1, contains six observable peak series. Labelled **A-F** respectively, these series correspond to both proton and self-terminated *1* species, cationised by H^+ and Li^+, and proton and self-terminated *2* species, cationised by Li^+ only. The percentage peak areas for the series **A-F** are given in Table 5.2.2 below. The % Area values were calculated for that species from the total area observed for either *1* or *2* within the spectrum. There is a fluctuation in these values for the proton-terminated species of *1*, which may be attributed to competing modes of cationisation. It is possible that the presence of an amine end-group interferes with the polymer adopting the preferred U-shaped, horseshoe conformation for binding metal ions.[12] Despite this difference, the relative amounts of proton and self-terminated species (Species %) of either sample

observed in the blend are comparable to those observed for the individual samples. However, the relative total amounts for either sample (Sample %) differ from the expected value for an equimolar mixture of 50% each. This is unlikely to be the result of any mass discrimination, as the samples chosen are of very similar average molecular weights, and mass discrimination is usually observed against higher oligomers, *i.e.* against *2*, contrary to this case. It is possible that this difference is due to the difference in the end-groups of *1* and *2*, as *2* may only be cationised by a metal ion, whereas *1* may be protonated as well. Again, the different modes of cationisation may be competing against each other, in such a way that a proportion of the molecules do not get cationised at all. This would lead to a lower ion yield for *1*, hence it appears that the blend is not equimolar and that end-group structure can have an effect upon the MALDI analysis. Alternatively, the fact that it is energetically more favourable to bind a metal ion over a proton may explain the higher ion yield apparent for *2*.[13]

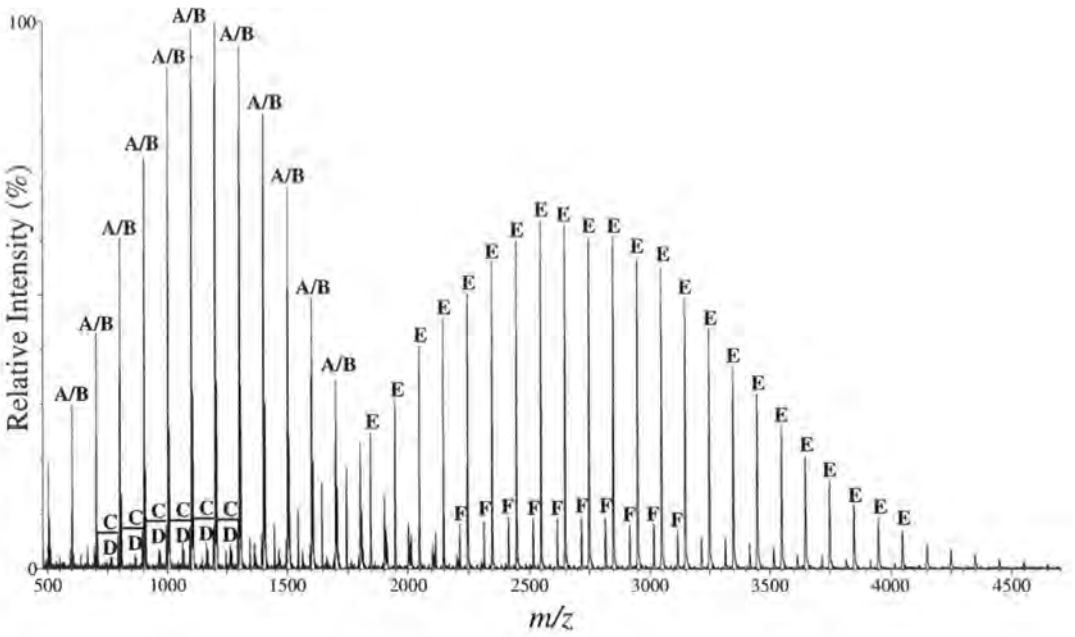

Figure 5.2.1. Reflectron MALDI spectrum of an equimolar blend of *1* and *2*.

Sample	Species	Cation	% Area	Species %	Sample %
1	Proton-terminated	H^+ (**A**)	78.00	98.65	39.71
		Li^+ (**B**)	20.65		
	Self-terminated	H^+ (**C**)	1.26	1.35	
		Li^+ (**D**)	0.09		
2	Proton-terminated (**E**)	Li^+	88.02	88.02	60.29
	Self-terminated (**F**)	Li^+	11.98	11.98	

Table 5.2.2. Percentage peak areas for species observed for an equimolar blend of *1* and *2*.

To summarise, two polymers (*1* and *2*) with different end-groups were mixed together in an equimolar ratio and analysed via MALDI. Generally, the ratios of the different species present in the blend are comparable to the same ratios when each polymer was analysed individually. Competing cationisation modes may possibly account for exceptions to this trend. The total areas of the component samples are not equivalent as expected, instead being slightly biased towards *2*; again competing cationisation modes or ease of cationisation may account for the lower ion yield of *1*. Either of these explanations may be related to differences in end-group structure.

5.3 Blend of *2* and *3*

Initially, the different species observed for *3* were quantified individually, because there are multiple routes to cationisation, analogous with *1*. The individual species observed for *2* have already been presented above. Initiated with LDA, *3* has been shown to consist entirely of the self-terminated species. Peaks were observed for this species cationised by H^+ and Li^+. The percentage peak areas for both cationised species of *3* are given in Table 5.3.1. The ratio of these percentage peak areas was found to be a lot less than that for the corresponding self-terminated species of *1*. This may be due the greater signal:noise ratio for these species in the analysis of *3*. However this ratio is also less than the ratio of the H^+ and Li^+ proton-terminated species of *1*, which may suggest that the cyclic ketone end-group from self-termination has greater cationisation efficiency for Li^+ than the proton-terminated end-group.

Sample	Species	Cation	% Area	Species %
3	Self-terminated	H^+	59.00	59.00
	Self-terminated	Li^+	41.00	41.00

Table 5.3.1. Percentage peak areas for species observed for *3* individually.

The reflectron MALDI spectrum for the equimolar blend of *2* and *3*, shown in Figure 5.3.1, contains four observable peak series. Labelled **A-D** respectively, these series correspond to and the proton and self-terminated *2* species, cationised by Li^+ only, and the self-terminated *3* species, cationised by H^+ and Li^+.

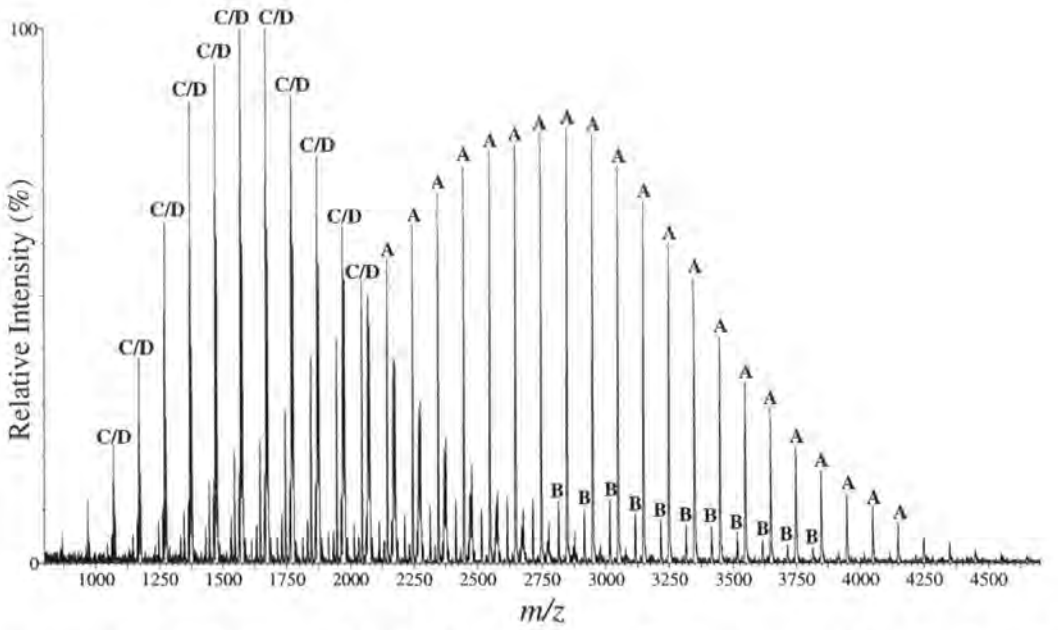

Figure 5.3.1. Reflectron MALDI spectrum of an equimolar blend of *2* and *3*.

The percentage peak areas for the series **A-D** are given in Table 5.3.2 below. The % Area values were calculated for that species from the total area observed for either *1* or *3* within the spectrum. Unlike the blend of *1* and *2*, the relative amounts of both species (Area % and Species %) of either sample observed in the blend are comparable to those observed for the individual samples. This may mean that any fluctuations observed may be random. Again, the relative total amounts for either sample (Sample %) differ slightly from the expected value for an equimolar mixture of 50% each, but the difference is less than that observed for the blend of *1* and *2*. This may mean that the greater cationisation efficiency for Li^+ of the cyclic ketone end-group increases the ion

yield to be more comparable with that of *2*. Once more *2* shows the greater response and similar arguments to those proposed for the blend of *1* and *2*, regarding competing cationisation modes for *3* or ease of cationisation, and not mass discrimination, may explain these observations.

Sample	Species	Cation	% Area	Species %	Sample %
2	Proton-terminated (**A**)	Li^+	89.00	89.00	53.95
	Self-terminated (**B**)		11.00	11.00	
3	Self-terminated	H^+ (**C**)	61.88	61.88	46.05
		Li^+ (**D**)	38.12	38.12	

Table 5.3.2. Percentage peak areas for species observed for an equimolar blend of *2* and *3*.

To summarise, two polymers (*2* and *3*) with different end-groups were mixed together in an equimolar ratio and analysed via MALDI. The ratios of the different species present in the blend are comparable to the same ratios when each polymer was analysed individually, and the competing cationisation modes of *3* do not appear to fluctuate, indicating that fluctuations may be random. The total areas of the component samples are not equivalent as expected, instead being slightly biased towards *2* once more; again competing cationisation modes or ease of cationisation may account for the lower ion yield of *3*.

5.4 Blend of *1* and *3*

The reflectron MALDI spectrum for the equimolar blend of *1* and *3*, shown in Figure 5.4.1, contains what appear to be four, but is actually six, observable peak series. Labelled **A-F** respectively, these series correspond to both proton and self-terminated *1* species, cationised by H^+ and Li^+, and the self-terminated of *1* and *3* species, cationised by H^+ and Li^+, which are the same species.

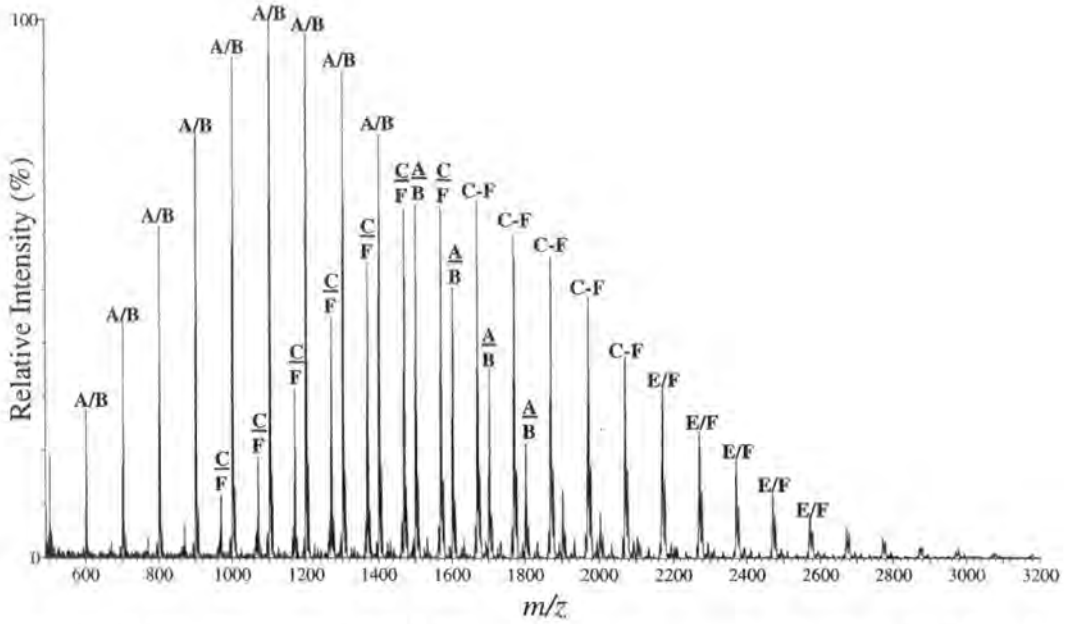

Figure 5.4.1. Reflectron MALDI spectrum of an equimolar blend of *1* and *3*.

By grouping the self-terminated species as being derived from *3* solely, the Sample % values are 46.37% for *1* and 53.63% for *3*. These values follow the trend for the sample with the greater cationisation efficiency for Li^+ having the greater ion yield, *i.e. 3*, but a proportion of the value for *3* is actually due to the same self-termination species of *1*. It is possible to introduce a correction factor, provided certain assumptions are made. Average values for all species of *1* may be calculated from the species ratios already observed. From these values it is possible to calculate the an average area value for the proportion of self-termination species due to *1*, which can then be subtracted from the total area of *3*, added to that of *1*, and new percentage values calculated. The corrected percentage peak areas from such calculations for the series **A-F** are given in Table 5.4.1 below.

The Sample % values are now closer to being equal, but there is still a bias towards *3*, which would still follow the trend of the sample with the greater having the greater ion yield. However, the Species % ratio has increased compared with previous results. This may be due to the invalid assumptions being made for performing the correction or that the competing modes of cationisation do indeed give random value fluctuations.

Sample	Species	Cation	% Area	Species %	Sample %
1	Proton-terminated	H^+ (**A**)	85.45	98.45	47.10
		Li^+ (**B**)	13.00		
	Self-terminated	H^+ (**C**)	1.47	1.55	
		Li^+ (**D**)	0.08		
3	Self-terminated	H^+ (**E**)	76.02	76.02	52.90
		Li^+ (**F**)	23.98	23.98	

Table 5.4.1. Percentage peak areas for species observed for an equimolar blend of *1* and *3*.

In conclusion, two polymers (*1* and *3*) with different end-groups were mixed together in an equimolar ratio and analysed via MALDI. The total areas of the component samples are not equivalent as expected, instead being biased towards *3*. The greater cationisation efficiency of *3* for Li^+ may account for the lower ion yield of *1*, but also the proportion of self-termination species of *1* had to be taken into account. A correction factor was proposed and the calculated ratios of the different species of *3* present in the blend differed from the same ratios observed previously, indicating that fluctuations may be random.

5.5 Experimental

The details of the analytical equipment and protocols were given in Section 2.8 of Chapter 2. Sample solutions were made to 5×10^{-3} M concentrations. Firstly smoothing the spectrum heavily, in order to obtain only one or two peaks per oligomer species, and then centring the peaks by area obtained the peak area values for each spectrum.

The details for the synthetic procedures involved in the polymerisation of *1-3* were given in Section 2.9 of Chapter 2. The specific parts relevant to *1-3* are Sub-Sections 2.9.4-2.9.6 respectively.

5.6 References

1. Domin, M.; Moreea, R.; Lazaro, M. J.; Herod, A. A.; Kandiyoti, R. *Rapid Commun. Mass Spectrom.* **1997**, *11*, 1845-1852.
2. Schriemer, D. C.; Li, L. *Anal. Chem.* **1997**, *69*, 4169-4175.
3. Schriemer, D. C.; Li, L. *Anal. Chem.* **1997**, *69*, 4176-4183.
4. Whittal, R. M.; Schriemer, D. C.; Li, L. *Anal. Chem.* **1997**, *69*, 2734-2741.
5. Vitalini, D.; Mineo, P.; Scamporrino, E. *Rapid Commun. Mass Spectrom.* **1999**, *13*, 2511-2517.
6. Byrd, H. C. M.; McEwen, C. N. *Anal. Chem.* **2000**, *72*, 4568-4576.
7. McEwen, C. N.; Jackson, C.; Larsen, B. S. *Int. J. Mass Spectrom. Ion Processes* **1997**, *160*, 387-394.
8. Spickermann, J.; Martin, K.; Räder, H. J.; Müllen, K.; Schlaad, H.; Müller, A. H. E.; Krüger, R. P. *Eur. Mass Spectrom.* **1996**, *2*, 161-165.
9. Yan, W.; Ammon, D. M., Jr.; Gardella, J. A., Jr.; Mariarz, E. P., III; Hawkridge, A. M.; Grobe, G. L., III; Wood, T. D. *Eur. Mass Spectrom.* **1998**, *4*, 467-474.
10. Nielen, M. W. F. *Mass Spectrom. Rev.* **1999**, *18*, 309-344.
11. Haddleton, D. M.; Waterson, C.; Derrick, P. J. *European Mass Spectrometry* **1998**, *4*, 203-207.
12. Gidden, J.; Jackson, A. T.; Scrivens, J. H.; Bowers, M. T. *Int. J. Mass Spectrom.* **1999**, *188*, 121-130.
13. Knochenmuss, R.; Lehmann, E.; Zenobi, R. *Eur. Mass Spectrom.* **1998**, *4*, 421-427.

Chapter 6

Conclusions and Future Work

6.1 Synthesis and Characterisation of End-Functionalised PMMA

Two proton-terminated PMMA samples (*1* and *2*), synthesised using LDA and DPHLi initiators respectively, and a third sample (*3*), initiated by LDA and allowed to self-terminate, were discussed initially. MALDI results further confirmed the stoichiometric formulas of all three samples, already proven by other analytical techniques. The spectra for LDA initiated samples were found to contain extra peaks, 1 and 2 amu lower than those expected, as the dominant species, and were suspected to originate from an elimination process associated with the amine end-group of the initiator, as this is the most likely protonation site. MALDI-CID data failed to reveal more information regarding the origin of these extra peaks. Analysis with a different matrix at lower laser energies produced a spectrum that mostly contained peaks of intact species, which indicates that the elimination is an effect of the MALDI analysis. A mechanism involving the loss of $H_2(g)$ was proposed for their origin, based upon what could be fitted to the observations. The mechanism utilises the quaternary amine proton together with the methine proton from either of the initiator-derived isopropyl groups. However, a similar mechanism involving a proton from the methylene of the initial repeat unit may be proposed also. A similar sample synthesised with deuterated MMA could be used to differentiate between these two mechanisms. If the mechanism involves the methine proton, the same extra peaks would be anticipated, but if the other mechanism is correct, then a further peak 3 amu lower than those expected should be observed. Alternatively, if suitable initiators or capping agents could be found, a range of samples containing various amine end-groups could be synthesised and analysed, in order to discover the origins of the elimination. Gas-phase conformation studies may give an insight into the cationisation mode, and hence the elimination.

A PMMA polymerisation was divided into three aliquots (*4a-c*), with the capping of each aliquot with a different end-group, DPE + $CO_2(g)$, DPE, and $CO_2(g)$, being attempted. The aim was make direct end-group comparisons, without the added complexities and ambiguities of variances in molecular weight distribution. NMR and MALDI analysis proved that the first two of these reactions were unsuccessful, the third being only partially successful. Difficulties involving the division of the living solution at the reaction temperature of –78°C were highlighted and these may be overcome by: i) designing a reaction vessel that may be totally submersed and manipulated in a

acetone/CO_2(s) bath, *i.e.* does not contain any rubber septa or Young's taps *etc.* ii) employing a polymerisation technique that operates at ambient temperatures. Capping with DPE was attempted (*5* and *6*) but without success and might only prove successful when performed at higher temperatures.

The analytical evidence of MALDI and other techniques confirms that neither the quaternisation (*7*) nor sulphonation (*8*) reactions attempted were completed. When considering the quaternisation reaction, the reason for failure may be that the nitrogen is too sterically hindered, due not only to the amine being tertiary, but also because the amine substituents themselves have substituents. The amine group of the DMPLi initiator used with PS was primary; thus more success may be achieved with PMMA samples containing primary or secondary amine end-groups. Reaction temperature, as with reactions considered previously, may also not be high enough to encourage the reaction and this could be true for the reaction with 1,3-propanesultone as well. Additionally, although methacrylic anions are comparable in reactivity to diphenylmethyl anions, as with the reaction with DPE, their reactivity may not be sufficient to ring-open the sultone.

An effective capping reagent for methacrylate anions was CO_2(g), with functionalisation being $\geq$ 95% for all samples (*9-11*). MALDI analysis showed that these samples were all of the acid form, rather than the lithium carboxylate salt. In continuing to achieve samples of identical molecular weight with various functionalities, attempts to interconvert the acid to other functional groups were made. Conversion of the acid to an acid chloride (*12* and *13*) or acid imidazolide (*14*) and further from the acid imidazolide to a benzyl (*15*) or *n*-propyl ester (*16*) were all shown to be unsuccessful by data from MALDI analysis, as well as that from other techniques. Further investigation revealed that rapid decarboxylation of the acid upon heating, facilitated by the proximity of a keto moiety, provided a reasonable explanation for the results observed. The mechanism for decarboxylation is given and the stoichiometric formula of the polymer product of decarboxylation fits with the recorded data. This problem may be overcome by capping the living PMMA chains with ethylene oxide (EO) instead of CO_2(g). With a lithium counter-ion, only a single EO unit should react, which could be protonated to give an alcohol end-group. If it is possible to selectively oxidize the alcohol to the acid, it may be removed far enough from the pendant ester groups to allow interconversion reactions to proceed.

Neither ($ClSi(CH_3)_3$) (*17* and *18*) nor ($BrSi(CH_3)_3$) (*19-21*) proved useful as end-capping reagents for methacrylic anions at –78°C, as determined via data from both NMR and MALDI. The analogous iodosilane was not tested as an effective capping reagent, but with a still weaker Hal-Si bond, a successful reaction might be achieved. The electron-donating methyl groups of the silane stabilise the Hal-Si bond, which may account for the unreactivness of the silanes used in these experiments. Replacement of one or more of the methyl groups with an electron-withdrawing group, *i.e.* methoxy groups, might increase the reactivity of the silane enough to allow the capping reaction to progress.

MALDI data complemented that from other analytical techniques in corroborating the successful capping reactions of active anionic PMMA chains with both allyl iodide (*22*) and 1-naphthoyl chloride (*23*). Moreover, the MALDI analysis of both these samples was shown to be relatively straightforward, *i.e.* without any observed fragmentation or elimination.

6.2 Characterisation of Non-Classically Synthesised PMMA

Polymerisations of MMA (*24-26*) were performed at 0°C using a novel initiating system that involved *s*-BuLi ligated by a lithium silanolate. The molecular weights of these samples were much higher than anticipated. The reported literature of the system was investigated further to try to ascertain the factors that control the formation of the initiator. Even with certain factors kept constant the amount of initiator formed appears to be fairly random, therefore it would not seem possible to produce polymers of controlled molecular weight with this system. The inventor's claims that monomodal distributions are produced under certain conditions were refuted by SEC data. No further work with this system is planned.

Several PMMA samples (*27-31*) were synthesised via RAFT using $PhCS_2CH_2CO_2H$ (RA′). SEC data revealed that these polymerisations were poorly controlled, so it can be concluded that RA′ should not be used in conjunction with MMA. $PhCS_2C(CH_3)_2Ph$ (RA″) was synthesised and used to produce a well-controlled PMMA sample (*32*), which was well characterised by NMR and UV/Vis spectroscopies. MALDI analysis of *32* revealed discrepancies between the observed and theoretical mass values, thought to be the result of an *in situ* elimination of the dithioester end-group. A mechanism for the elimination was proposed, and is supported

by the comparison of peak isotope distributions and peaks series from MALDI-CID studies. The exact nature of the elimination and the condition required for it to occur are as yet unknown. RA″ and similar reagents are appropriate for RAFT polymerisations of several monomers. A range of different polymers could be synthesised and evidence of similar eliminations looked for in the MALDI spectra, which may help to improve our understanding of this elimination. A similar observation has already been reported for a sample of poly(*N*-isopropylacrylamide) (PNIPAM), which was synthesised using benzyl dithiobenzoate.

6.3 Synthesis and Characterisation of Methacrylate Block Copolymers

Prior to copolymer work, a sample of P*t*-BMA (*33*) was synthesised anionically, using LDA as the initiator and terminating with CH_3OH. In contrast to PMMA samples analysed previously, it was only possible to obtain poorly resolved spectra of *33*, despite making several alterations to aspects of sample preparation, which included the laser power, the type of matrix, solvent and metal salt, and the matrix:sample:salt ratio. These observations have been rationalised in terms of a low molecule ion yield resulting from possible interference in ion-molecule binding processes by the bulky pendant ester groups. Gas-phase conformation studies may give an insight into the cationisation mode, and hence the low molecule ion yield. Three PMMA–P*t*-BMA copolymers (*34-36*) were synthesised anionically, using LDA initiator and terminating with CH_3OH. The samples contained increasing amounts of *t*-BMA. The MALDI spectra of *34*, which contained the least amount of *t*-BMA, were obtained with relative ease, and showed that molecules could contain between 0-4 *t*-BMA units (m = 0-4) and are most likely to contain 2 *t*-BMA units. Graphical representations of the sample composition were obtained for the comonomer composition and percentage peak area for each oligomer. Spectra could not be obtained under various conditions for *35* and *36*, and this observation was rationalised in part in terms of a low molecule ion yield resulting from possible interference in ion-molecule binding processes by the bulky pendant ester groups, combined with an inherently lower signal:noise ratio, due to increased sample complexity. Copolymers synthesised with DPHLi, thus being able to bind metal ions

only, may simplify subsequent MALDI spectra. Lower molecular weight samples may be targeted, also with a view to decreasing the complexity of their spectra.

Prior to copolymer work, a sample of PHMA (*37*) was synthesised anionically, using LDA as the initiator and terminating with CH_3OH. A MALDI spectrum was recorded with relative ease and showed three distinct peak series. Two of these series have been assigned to typical molecule ion species, but the origins of the third series remain somewhat elusive. MALDI data collected with different matrices or metal ions may provide further information about this series. Three PMMA–PHMA copolymers (*38-40*) were synthesised anionically, using LDA initiator and terminating with CH_3OH. The samples contained increasing amounts of HMA. The MALDI spectra of *38*, which contained the least amount of HMA, were obtained with relative ease, and showed that molecules could contain between 0-12 HMA units (m = 0-12) and are most likely to contain between 5-7 HMA units. Graphical representations of the sample composition were obtained from the comonomer composition and percentage peak area for each oligomer. Spectra could not be obtained under various conditions for *39* and *40*, and this observation was rationalised in part, in terms of lower sensitivity due to a slightly higher sample molecular weight, and lower sample solubility resulting in sample aggregation and poor desorption/ionisation processes. Similar future work to that suggested for the PMMA–P*t*-BMA copolymers might be performed also.

6.4 Characterisation of Blends of Various End-Functionalised PMMA

Two component equimolar blends of polymers *1*, *2* and *3* were analysed via MALDI. For a blend of *1* and *2*, the ratios of the different species present are comparable to the same ratios when each polymer was analysed individually. Competing cationisation modes may possibly account for exceptions to this trend. The total areas of the component samples are not equivalent as expected, instead being slightly biased towards *2*; again competing cationisation modes or ease of cationisation may account for the lower ion yield of *1*. Either of these explanations may be related to differences in end-group structure. Similar observations were made regarding the blend of *2* and *3*. However, the competing cationisation modes of *3* do not appear to fluctuate, indicating that such fluctuations may be random. For a blend of *1* and *2*, the total areas of the component samples are not equivalent as expected, instead being biased towards

3. The greater cationisation efficiency of *3* for Li^+ may account for the lower ion yield of *1*, but also the proportion of self-termination species of *1* had to be taken into account. A correction factor was proposed and the calculated ratios of the different species of *3* present in the blend differed from the same ratios observed previously, indicating that fluctuations may be random. These measurements need to be repeated several times in order to assess their reproducibility, and hence the conclusions drawn from them.

6.5 Concluding Remarks

MALDI-TOF-MS and MALDI-CID have been shown to be powerful tools in the characterisation of synthetic polymers. Much has been learned about this technique, but there is much to still be learned, for example, about ionisation mechanisms, sample preparation and end-group and backbone structure. Improvements in instrumentation, *i.e.* resolution up to 24000 FWHM, means that we are limited to very low molecular weight samples no longer. With further improvements in resolution and with mass discrimination issues being addressed, MALDI analysis may one day supersede SEC in providing accurate molecular weight information, but with regard to structure determination, it will always be utilised best when in conjunction with other analytical techniques, *i.e.* NMR. Fragmentation may be rare in standard MALDI analyses, but eliminations are shown to be relatively common, hence care must be taken when interpreting MALDI spectra.